ELECTROCHEMICAL BEHAVIOUR OF TI(C,N) AND TIC CERMETS

by

Melanie Holmes

Submitted in partial fulfillment of the requirements
for the degree of Master of Applied Science

at

Dalhousie University
Halifax, Nova Scotia
August 2012

DALHOUSIE UNIVERSITY

DEPARTMENT OF PROCESS ENGINEERING AND APPLIED SCIENCE

The undersigned hereby certify that they have read and recommend to the Faculty of Graduate Studies for acceptance a thesis entitled "ELECTROCHEMICAL BEHAVIOUR OF TI(C,N) AND TIC CERMETS" by Melanie Holmes in partial fulfillment of the requirements for the degree of Master of Applied Science.

Date: August 14, 2012

Co-Supervisors: _____

_____

Readers: _____

_____

DALHOUSIE UNIVERSITY

DATE: August 14, 2012

AUTHOR: Melanie Holmes

TITLE: ELECTROCHEMICAL BEHAVIOUR OF TI(C,N) AND TIC CERMETS

DEPARTMENT OR SCHOOL: Department of Process Engineering and Applied Science

DEGREE: M.A.Sc. CONVOCATION: October YEAR: 2012

_____

Signature of Author

TABLE OF CONTENTS

LIST OF TABLES

LIST OF FIGURES

Abstract

Three samples of Ti(C,N) were fabricated with 40 vol.% Ni_3Al: Ti($C_{0.3}N_{07}$), Ti($C_{0.5}N_{0.5}$) and Ti($C_{0.7}N_{0.3}$), as well as TiC with 10, 20, 30 and 40 vol.% Ni_3Al binder addition by means of melt infiltration and sintering. Each sample was evaluated for density and microstructure before being placed in a flat cell for electrochemical testing. Open circuit potential was evaluated, followed by the application of a cathodic potential, whereby the response was tracked using Corrware corrosion software throughout the duration of potentiodynamic testing. Following corrosion testing, each sample was reevaluated for changes in microstructure and chemical composition. Ti(C,N) samples were found to have adequate resistance to corrosion, with increased resistance with increasing carbon content, however these samples demonstrated a greater frequency of breakdown and repassivation, suggesting a greater susceptibility to corrosion, despite the initial improved resistance. SEM imaging demonstrated significant crevice corrosion throughout. TiC-cermets demonstrated similar results in terms of SEM evaluation of microstructure. TiC-cermets with the lowest binder content (10 vol.% Ni_3Al) demonstrated greater initial resistance to corrosion but also had the greatest potential for breakdown.

List of Abbreviations Used

CIP	Cold isostatic press
CRC	Carbothermal reduction – carbonitridation
CVD	Chemical vapour deposition
E_{corr}	Corrosion potential
EDS	Energy-dispersive x-ray spectroscopy
HIP	Hot isostatic pressing
HP	Hot pressing
HV	Vickers hardness
i_{corr}	Corrosion current density
ICP-OES	Inductively coupled plasma optical emission spectrometry
LPS	Liquid phase sintering
MIS	Melt infiltration/sintering
OCP	Open circuit potential
PS	Pressureless sintering
PVB	Polyvinyl butyral
PVD	Physical vapour deposition
SEM	Scanning electron microscope
SCE	Saturated calomel electrode
SHS	Self-propagating high temperature synthesis
SPS	Spark plasma sintering
TRS	Transverse rupture strength
TZP	Tetragonal zirconia polycrystal
XRD	X-ray diffraction
ZCP	Zero current potential

Acknowledgements

I would like to thank and acknowledge the support and guidance from my supervisor Dr. Kevin Plucknett throughout this project, specifically for his direction and feedback at all stages of the research. Furthermore I would like to acknowledge his help and guidance in learning proper laboratory techniques, and training on each piece of equipment. I would like to thank Dr. George Kipouros for the knowledge he provided throughout this project, as well as his aid with lab equipment and training. A great thank you to all those within the PEAS department for their support, drive and motivation.

I would like to thank the Natural Sciences and Engineering Research Council (NSERC), as well as the Petroleum Research Atlantic Canada (PRAC) for the provision of funding. The support of the Canada Foundation for Innovation, the Atlantic Innovation Fund, and other partners who helped fund the Facilities for Materials Characterisation, managed by the Dalhousie University Institute for Materials Research, are also gratefully acknowledged. I would also like to thank both Dean Grijm and Patricia Scallion for their technical assistance, without which none of this would have been possible.

1 Introduction

Ceramic metal composites, or cermets, combine a ceramic hard phase with a ductile metal phase, commonly referred to as a metallic binder. A wide variety of cermet systems exist, made from both oxide and non-oxide ceramics, with the later particularly widely used in applications requiring high strength and wear resistance. Among the many non-oxide examples, titanium carbonitride (Ti(C,N)) and titanium carbide (TiC)-based materials have been studied at length for over a century. However, it was not until the concept of metal binder metal alloy additions was introduced that they become prolific in modern industry, notably as cutting tools and in coating applications. As cutting tools, cermets have begun to overtake their closest comparative materials, cemented carbides and more specifically tungsten carbide-cobalt (WC-Co), in their ability to withstand harsh environments and high-speed milling operations.[1] The metallic binders can range both in chemical compositions as well as volume fraction depending on the application, and can be tuned to achieve the desired properties of the cermet. Both Ti(C,N) and TiC are known to possess high hardness, strength, wear, and oxidation resistance over a very broad range of temperatures, as well as having high thermal conductivity, while managing to remain an economically viable option for industrial applications.[2]

The present study addresses the basic methods of consolidating a family of novel Ti(C,N) and TiC cermets, the influence of varying both cermet composition and binder volume fraction, and finally the electrochemical behaviour and response of Ti(C,N) and TiC. The samples used for electrochemical testing are developed using a process known as melt infiltration/sintering (MIS), whereby pressed Ti(C,N) and TiC samples are infiltrated, through capillary action, by a molten Ni_3Al metal binder in a high-temperature vacuum furnace sintering process. Each sample is then ground and polished using a series of diamond pads and pastes, prior to electrochemical testing. The tests require each sample be affixed to a flat unit cell while both open circuit potential and potentiodynamic polarization tests are conducted. Results of each stage of processing and electrochemical testing are compared using a variety of characterization equipment, including scanning electron microscopy (SEM), x-ray diffraction (XRD), energy dispersive x-ray

spectroscopy (EDS), as well as inductively coupled plasma optical emission spectrometry (ICP-OES).

This thesis addresses each area of focus through seven chapters, beginning with a literature review to briefly outline the key points of development and research in this area. Chapter 3 continues with describing the consolidation process, followed by Chapter 4 where results and discussion are provided for the information given thus far. Chapters 5 and 6 focus specifically on the electrochemical testing, results and discussion for Ti(C,N) and TiC samples, respectively. Finally, Chapter 7 concludes the study by providing key pieces of research and discussing potential for further development.

2 Literature Review

Ceramic-metal composites, or cermets, are composite materials that combine the hardness and wear resistance of a ceramic, with the ductility and toughness of a metal binder, which bonds the ceramic phase particles together. They are widely recognized for their high melting points, thermal conductivity, high hardness, resistance to oxidation and wear, as well as relatively high electrical conductivity.[3] The most common applications of cermets are in the cutting tools industry, where the properties of the material allow for increased cutting speeds and improved wear resistance.[4] The term cermet is used to describe a variety of composites typically known for their use as having good electrical properties and thermal conductivities, however is often used to describe titanium-based composites. This is in contrast to tungsten-based 'hardmetal' tools that have been overtaken by industry-driven cermet tools in recent years. A historical review of the development of carbide-based cermets is listed in Table 2–1.

Table 2–1 Historical development of cermets[5]

Year of Establishment	Composition
1930-31	WC-Co
1930	TiC-Mo_2C-(Ni, Mo, Cr)
1930	TaC-Ni
1933	TiC-TaC-Ni
1938-45	TiC-VC-(Fe, Ni, Co)
1949-55	TiC-(NbC)-(Ni, Co, Cr, Mo, Al)
1952-54	TiC-steel binder
1960	TiC-(Ni, Mo)
1970	Ti(C, N) – (Ni, Mo)
1974	(Ti, Mo) (C, N) – (Ni, Mo)
1975	TiC-TiN-WC-Mo_2C-VC-(Ni, Co)
1977-80	TiC- Mo_2C – (Ni, Mo, Al)
1980-83	(Ti, Mo, W) (C, N) – (Ni, Mo, Al)
1988	(Ti, Ta, Nb, V, Mo, W) (C, N) – (Ni, Co) – Ti_2AlN

The original obstacle to increased industrial usage of these carbides was their brittleness. With the development and incorporation of binder metals into a composite cermet structure, such as nickel, molybdenum or cobalt, the brittleness was significantly reduced while still maintaining the strength, hardness and wear resistance. The past two decades have shown significant development in binder research, and a new focus on methods of coating deposition, which has increased the areas of application for most commercial and industrial cermets.[6] A challenge has recently been recognized regarding the resistance to corrosion of modern cermets. Specifically, TiC and Ti(C,N) have been shown to be susceptible to corrosion which can make the material unsuitable for some applications, despite their outstanding mechanical properties. Titanium is known to resist oxidation through the development of a passive oxide film layer, titanium oxide (TiO_2), which forms and protects the bulk material from further oxidation. Studies on titanium-based ceramics have found a strong resistance to corrosion with no binder phase present,[7] while another study suggests the addition of a nickel binder allows for a secondary passivation to occur, which is attributed to passivation of nickel taking place at higher potentials.[8] The following review will address this topic and explore literature pertaining to the oxidation and resulting corrosion of cermets in a variety of circumstances.

2.1 Titanium Carbonitride

Titanium carbonitride (Ti(C,N)) cermets have been studied for their mechanical and magnetic properties, wear and corrosion resistance, as well as thermal conductivity, for over 80 years.[9] Table 2–2 depicts the historical development of cermets since their first appearance in the 1930s.

Table 2–2 Historical development of Ti(C,N) cermets[9]

Year of Establishment	Hard Phase	Binder Phase
1931	Ti(C,N)	Ni(Co, Fe)
1970	Ti(C,N)	Ni-Mo
1974	(Ti,Mo)(C,N)	Ni-Mo
1980-1983	(Ti,Mo,W)(C,N)	Ni-Mo-Al
1988	(Ti,Ta,Nd,V,Mo,W)(C,N)	(Ni,Co)-Ti_2AlN

Year of Establishment	Hard Phase	Binder Phase
1988	(Ti,Ta,Nd,V,W)(C,N)	Ni-Co
1991	(Ti,Ta,Nd,V,Mo,W, etc.)(C,N)	Ni-Cr

Ti(C,N), an alloyed combination of TiC and titanium nitride (TiN), is a strong, hard, wear and corrosion resistant ceramic with a high melting temperature and high electrical and thermal conductivity.[10] Often used in the cutting tools industry, Ti(C,N) outperforms WC-Co hardmetals in cutting speeds and wear resistance.[11] Titanium-based cermets have begun to overtake the more conventional tungsten 'hardmetals' as they are proving to outlast and outperform them over extended periods of time in the cutting tool applications.[12] They have exceptional edge strength and sharpness (i.e. cutting edge retention), are effective at high cutting speeds and produce products with high surface qualities after cutting.[13] Ti(C,N) cermets, however, exhibit somewhat disappointing results with respect to the transverse rupture strength and fracture toughness in comparison with common WC-Co hardmetals. Therefore much attention has been paid to refining the consolidation techniques, binder phase selection, and the addition of grain growth inhibitors to improve the materials in these areas.[14] For example many of the mechanical properties of the Ti(C,N) system, such as microhardness, are dependent on the ratio of [C]:[C + N], which increases as the ratio increases; electrical and thermal conductivities on the other hand decrease with increasing nitrogen.[15] Ti(C,N) is a promising material in terms of the applications it is suited to, a function of its inherently high hardness, flexural strength, thermal conductivity, and very high wear-resistance.[3]

The crystal structure of Ti(C,N) had been an issue for debate until recently. The previously accepted theory was that the crystal structure of Ti(C,N) was similar to that of NaCl, as shown in Figure 2–1 (a), and, unlike pure TiC and TiN, all components (i.e. Ti, C and N) were considered completely disordered.[16] However, further research revealed that this is not in fact the case, and that the structure of Ti(C,N) was more suited to model (b) and model (c) in Figure 2–1, which, after sintering, were indistinguishable.[16] Model (b) depicts a Ti-ordered C-N-disordered FCC NaCl type structure, with model (c) being

similar except that it is tetragonal in orientation and has interchanging carbon and nitrogen disorder. An example of the morphology of Ti(C,N) particles is shown in Figure 2–2. Studies have also established that, due to the face centered cubic (f.c.c) lattice structure of TiC, the addition of nitrogen into TiC can result in decreased hardness of the final Ti(C,N) cermet. However, adding TiN into TiC results in increased plasticity of the TiC component.[17] The simplest form of the compound is $TiC_{1-x}N_x$ with $0 < x < 1$, in which the C and N atoms are randomly positioned throughout the non-metallic sublattice.

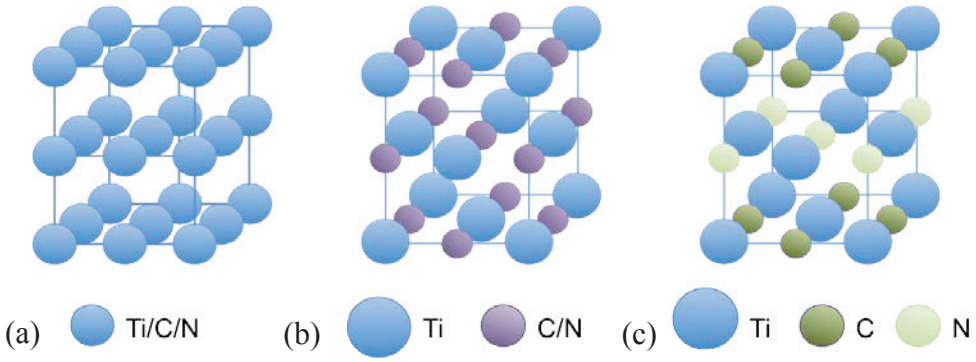

Figure 2–1 Structural model of Ti(C,N)[16]

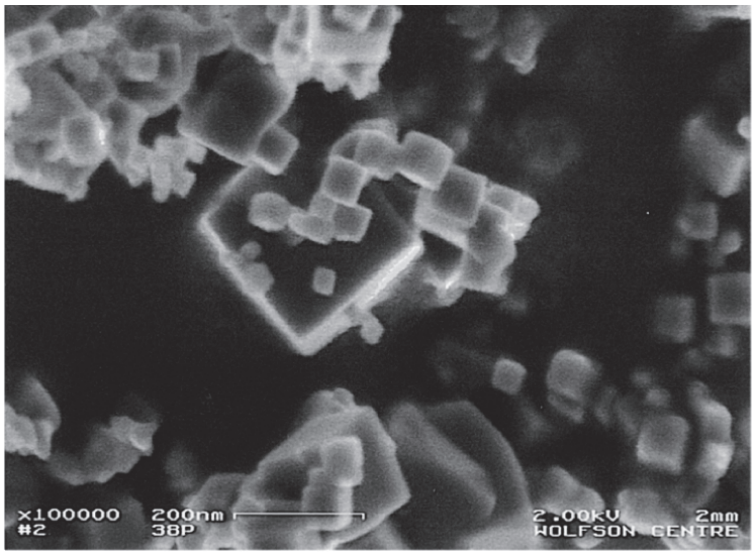

Figure 2–2 SEM micrograph of $TiC_{0.5}N_{0.5}$[16]

2.1.1 Consolidation of Ti(C,N)

Ti(C,N) cermets can be synthesized by several methods, the majority of which develop a complex core-rim structure, as shown in Figure 2–3. The core is comprised of undissolved raw powders, while the rim often has both inner and outer sections: heavier elements combine as a result of solid state sintering to form the inner rim and precipitated elements within the liquid phase sintering medium form the outer rim.[11] The formation of a core-rim structure primarily depends upon the alloying elements within the metallic binder.

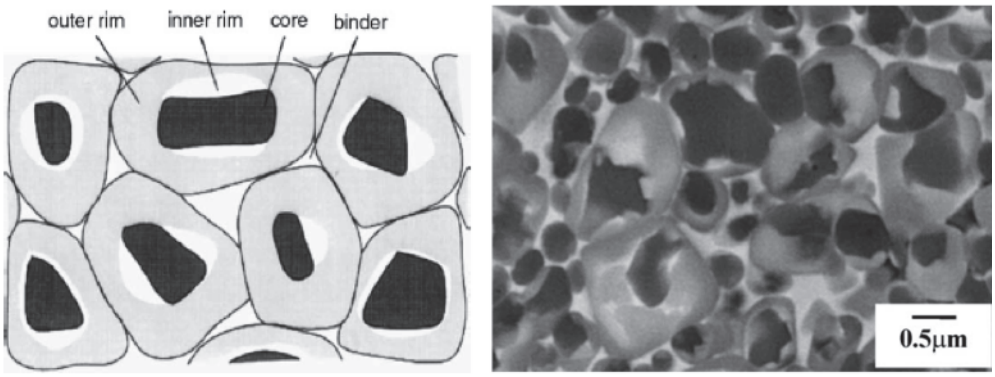

Figure 2–3 Schematic and micrograph ($TiC_{0.5}N_{0.5}$) showing typical cermet core-rim microstructure[18,3]

Common methods of producing Ti(C, N) include: high-temperature (1000-1500°C) solid-state diffusion of C, N or both into Ti; carbothermal reduction-carbonitridation (CRC) from TiO_2; self-propagating high-temperature synthesis (SHS) of TiC, TiN, and Ti(C,N); and thermal decomposition of $TiCl_4$-amine. With each method, increasingly smaller particle sizes will yield higher hardness levels, and, as a consequence, considerable emphasis has been placed on the development of nanosize powder consolidation. Increasingly smaller powder sizes do not, however, demonstrate any increase in strength and toughness.[19] Production of the most homogeneous product to date, was conducted using ultrafine and nanosize powders; in that instance solid-state diffusion mechanisms and CRC were applied.[19] The most promising outcome was a result of the carburization of TiN under flowing argon; as TiN undergoes carburization, C atoms begin to fill any vacancies within the lattice, as well as diffuse inward to replace N atoms which are consequently diffusing outward.[3]

SHS, often performed in conjunction with spark plasma sintering (SPS), is deemed a cost-effective method of producing high purity Ti(C,N). However, supplementary diluent and nitrogen are often required to sustain the reaction.[20] SHS works by igniting the precursory powders and allowing a self-sustaining combustion reaction to progress through the sample,[20] a method commonly used in the consolidation of TiC. For Ti(C,N), SHS produces a reaction between Ti and C in a N_2 environment.[21] In a study of three different stoichiometric samples of Ti(C,N): $TiC_{0.7}N_{0.3}$, $TiC_{0.5}N_{0.5}$ and $TiC_{0.3}N_{0.7}$, it was found that combustion temperature is directly proportional to nitrogen pressure, as seen in Figure 2–4. Optimal results were obtained using a TiN diluent at more than 0.6 MPa N_2 pressure, with the combustion temperature inversely proportional to carbon content[21]. SPS has been shown to produce cermets with higher density, reduced porosity, and improved dissolution of TiN; however SPS can produce a notable increase in denitrification and reduced transverse rupture strength (TRS).[22] The combustion synthesis of Ti(C,N) is a two-step process and proceeds as follows: within seconds of the propagating wave travelling throughout the sample, the first step is the formation of non-stoichiometric $TiC_{0.5}$, followed by nitridation:

$$Ti + C_{0.5} \rightarrow TiC_{0.5} \qquad \text{Equation 2.1}$$

$$TiC_{0.5} + N_2 \rightarrow TiC_{0.5}N_{0.5} \qquad \text{Equation 2.2}$$

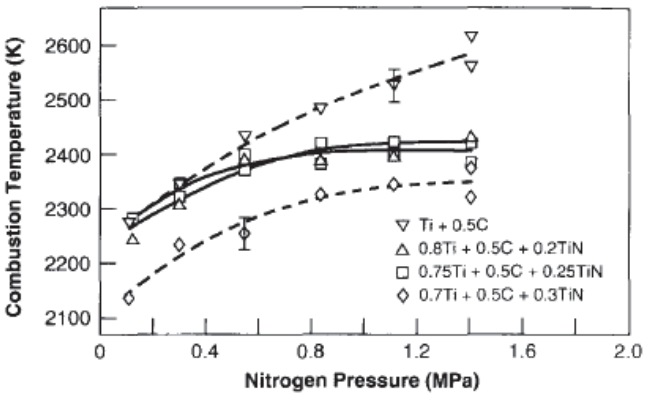

Figure 2–4 Effect of nitrogen pressure on combustion temperature of diluted and undiluted Ti + 0.5C samples[16]

High-energy ball milling is yet another common method of producing Ti(C,N), proving to be competitive in achieving small particles sizes and cost effective.[23] As

demonstrated in Figure 2–5 there are a number of ways of arriving at Ti(C,N) from various starting raw powders through ball milling.

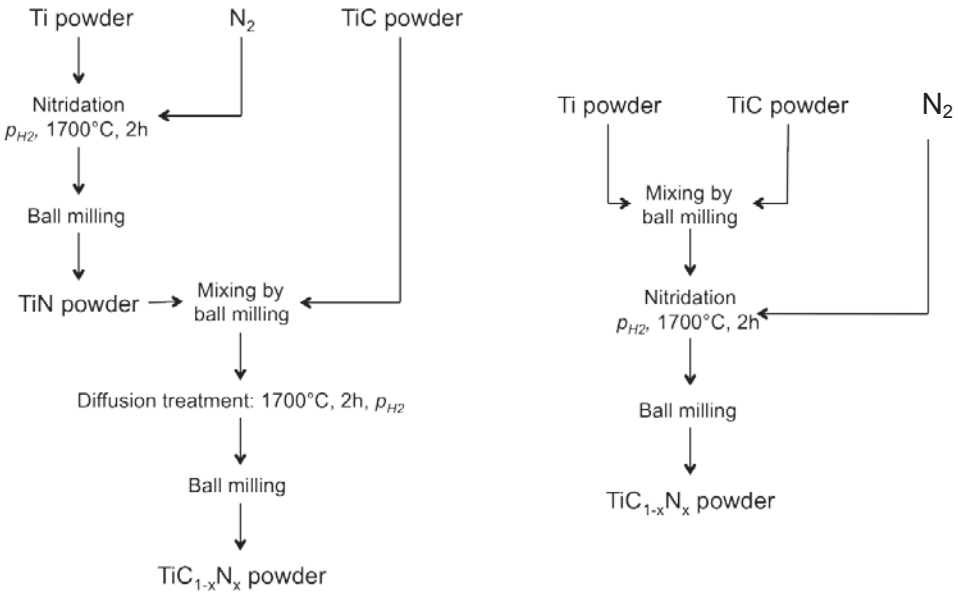

Figure 2–5 Synthesis of $TiC_{1-x}N_x$ from (a) TiC plus TiN, (b) Ti plus TiC[24]

Ball milling as a form of synthesis provides reduced grain size and increased flexural strength with increased milling time.[25] Mechanical properties improve as a result of the breakdown of particles occurring through the high-energy process, resulting in improved final products while maintaining the ability to alter variables and tailor the product to the desired outcome.[26]

2.1.2 Liquid Phase Sintering

Sintering is a common method of producing high density Ti(C,N) cermets. Sintering takes place following powder compaction; the temperature is ramped up to promote melting of the powder particles followed by coalescence. This sequence leads to a notable reduction in overall porosity, beginning with the initial compaction of the raw powders, then the coalescence of grains during sintering. [23]

Liquid phase sintering (LPS) is a method of consolidation that can produce fully dense Ti(C,N)-based materials. It also allows for the tailoring of several processing conditions such as the environment, temperature and time duration for which the product

is sintered in order to produce unique material traits. Sintering Ti(C,N) cermets under vacuum has been shown to be the most suitable process as it produces uniform, homogenous particles with the most desirable mechanical properties.[27] In contrast, sintering in a N_2 or Ar-environment can lead to increased oxygen content after sintering.[28] Sintering under N_2 and Ar also caused the greatest decrease in C content, with the N_2 atmosphere incurring an additional 20-25% increase in N_2 in the sample after sintering.[28] Stability of Ti(C,N) is important to quantify because falling outside the acceptable limits of sintering temperature and composition may lead to decarburization and general loss of integrity. The stable phases of Ti(C,N) under a nitrogen atmosphere and 1 atm pressure sintering are outlined in Table 2–3.

Table 2–3 Stable phases of Ti(C,N) at varying temperatures[1]

Temp. (°C)	Stable Phases		
	TiN + C	$Ti(C_{1-x}N_x) + C$	$Ti(C_{1-x}N_x)$
1400	no data	no data	$x > 0.60$
1527	$x \leq 0.2$	$0.2 \leq x \leq 0.625$	$x > 0.65$
1800	no data	no data	$x > 0.35$
2027	no data	$x \leq 0.16$	$x > 0.16$

Melt infiltration and sintering is a proven effective method of consolidating Ti(C,N) cermets with associated binder alloys. In this instance the Ti(C,N) pressed preform, upon which is a powder layer of the selected binder metal, is sintered as demonstrated in Figure 2–6. As the temperature is increased through the standard sintering process, the powder binder melts and infiltrates the base powder compact beneath. In the case of Ti(C, N) with a nickel aluminide binder, LPS requires that the melting temperature of the liquid phase (i.e. metal or metallic alloy) is reached (e.g. Ni at 1455°C), therefore it is often carried out with temperatures ranging from 1400-1600°C.

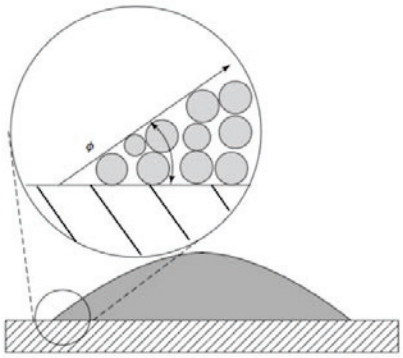

Figure 2–6 Illustration of liquid phase sintering with powder binder metal placed upon pressed powder compact[23]

A noted outcome of LPS under vacuum is the effect of temperature changes on the final Ti(C,N) fabrication. As depicted in Figure 2–7 obvious differences can be noted with varying temperatures. First, it is apparent that at a sintering temperature of 1430°C a core-rim structure has been developed with moderate rim thickness, in conjunction with a fine grain size and little to no aggregation of particles and hence a larger mean free path. Conversely at 1440°C, the rim phase has developed to be quite thick, a result of the grains having grown too large too quickly, which can severely affect mechanical properties, but usually increases the fracture toughness. Similarly, TRS and hardness are affected by sintering temperature, as demonstrated in Figure 2–8, with the highest TRS and hardness occurring at 1430°C. It has been shown that an increasing of rim thickness beyond 5 μm significantly decreases the TRS.[29]

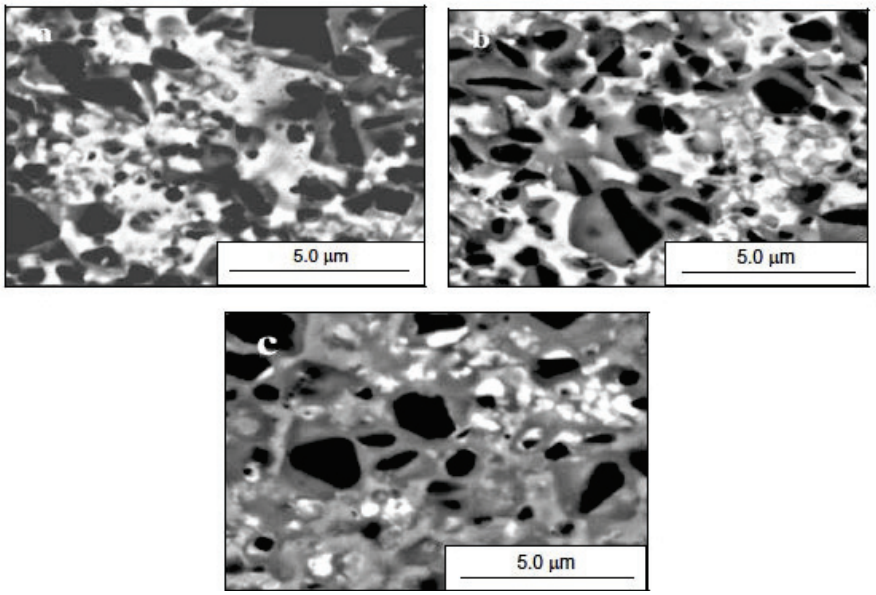

Figure 2–7 Microstructure of Ti(C,N)-based cermets sintered at different sintering temperatures: (a) 1420°C, (b) 1430°C and (c) 1440°C[14]

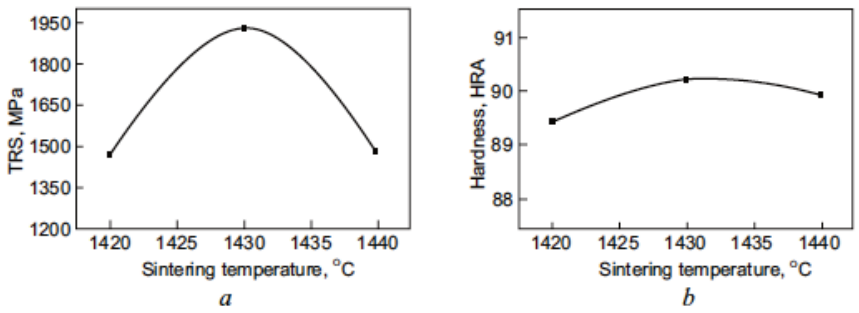

Figure 2–8 Mechanical properties of Ti(C,N)-based cermets (a) TRS vs. Sintering Temp., (b) Hardness vs. Sintering Temp[14]

2.1.3 Ti(C,N) Properties and Effects of Binder Alloying Additions

A number of variables, such as temperature, reaction time, carbon content, amount and type of binder phase chosen and reaction environment (e.g. type and rate of gas flow within the system), can be altered with each method of consolidation to affect the final performance characteristics of the cermet,. For example, varying carbon content from 0-3.5 wt% C in Ti(C,N) cermets demonstrated that carbon content significantly impacts

grain growth, and if the carbon content is too little, or too much, severe deterioration of mechanical properties can be experienced.[30] When carbon content is too high, graphite appears in the microstructure, and conversely when it is too low oxygen is unable to be effectively reduced, hindering wetting.[18] Furthermore, mechanical properties of Ti(C,N) are affected by consolidation methods and composition, as demonstrated in Figure 2–9 whereby microhardness has been found to decrease while thermal conductivity was shown to increase with increasing nitrogen content.[1]

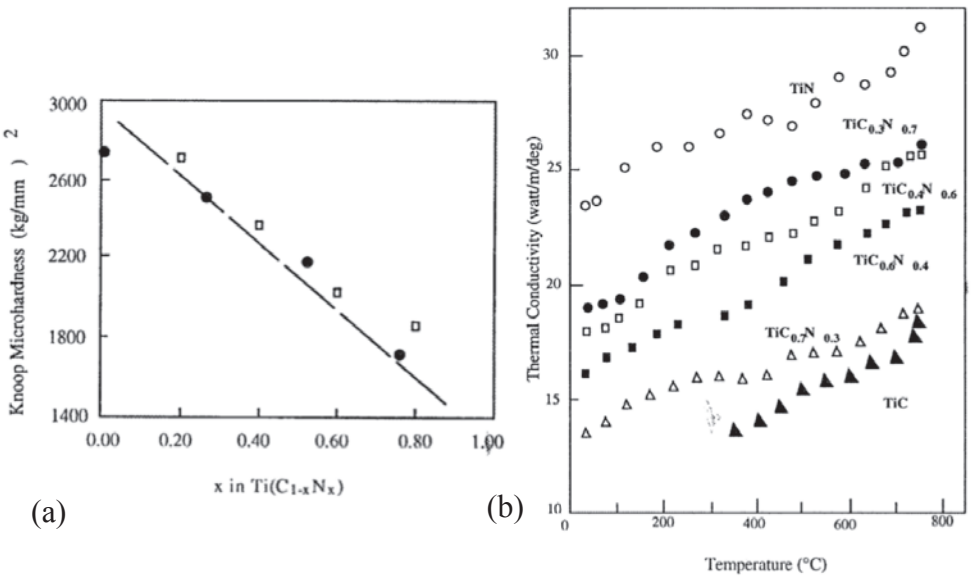

Figure 2–9 Effect of nitrogen content on the microhardness and thermal conductivity of Ti(C,N)-cermets[1]

As with the preparation of both TiC and TiN, an additional phase is required to aid in wetting and overall improvement of mechanical properties (through increased densification). Common additives used in the synthesis of Ti(C,N) are nickel and molybdenum, which can work in conjunction with altering the ratios of nitrogen or carbon within the Ti(C,N) sample. Molybdenum is often used to improve wetting, which in turn improves mechanical properties and contributes significantly to the core-rim structure of Ti(C,N)-Mo after sintering, as it affects the solution reprecipitation of the rim, causing a reduction in overall grain size.[31] As demonstrated in Figure 2–10 there is a variety of consequences generated by altering the composition of the Ti(C,N) cermet. It is important

therefore to tailor the composition to achieve the desired behaviour based on the application.

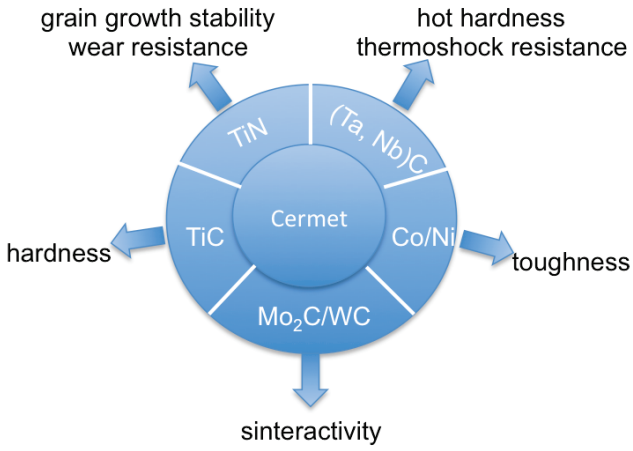

Figure 2–10 Properties of cermet cutting alloys as a function of composition[13]

2.1.4 Corrosion Studies

Ti(C,N) ceramics have shown significant potential with regards to their corrosion resistance, however this diminishes at high temperatures. Unalloyed titanium shows good response to corrosive attack due to its innate ability to passivate, specifically when immersed in seawater and other chloride solutions, hypochlorites, and nitric acid.[32] However it has been found that coupling titanium to metals such as steel often result in hydrogen absorption, increased brittleness, and severe pitting.[32] However, alloying certain materials with titanium, such as Pd or Pt, however, has shown to have produce significant improvement in the resistance to corrosion.[33] Platinum has also been attributed to limiting the breakdown of titanium's passivation layer, which tends to ultimately result in significant pitting.[34] Considerable research has been conducted on the impact of the metallic binder on mechanical properties, grain growth and the final integrity of Ti(C,N) cermets. However, little has been done in terms of identifying the impact a binder component may have on the corrosion resistance of Ti(C,N) cermets. Independent of the nature of the corrosive environment, attack appears to begin at the rim of the Ti(C,N)

grains and proceed inwards, initiating a substitution of carbon by oxygen resulting in progressive transformation of titanium to titania.[35]

High temperature corrosion of Ti(C,N) begins with the formation of oxycarbonitride which then reduces to a rutile scale.[36] This process is governed by the following stages: formation of the oxycarbonitride, followed by atom and/or ion diffusion-based oxidation, and finally an oxidation rate that is considerably lowered and is dependent on the thickness of the rutile scale formation as it behaves as protective barrier to further diffusion.[36] It has been conjectured that the first stage is based on linear-law reaction equations, followed by a parabolic relationship and finally a linear law for the final oxidation mechanisms.[36] However, finite parameters for these equations have yet to be developed and it has been noted that these relationships and kinetic equations have yet to be fully explored and remain varied between studies. The basic reactions for the formation of titanium oxycarbonitride followed by the reduction to rutile are demonstrated through the equations below:[37]

$$TiCN + O_2 \rightarrow TiC_xN_yO_2 \qquad \text{Equation 2.3}$$

$$TiC_xN_yO_2 + O_2 \rightarrow TiO_2 + CO_2 + N_2 \qquad \text{Equation 2.4}$$

During the first stage, the oxidation of Ti(C,N) occurs at temperatures ranging from 400-500°C to form titanium oxycarbonitride, followed by its oxidation between temperatures of 500-850°C, resulting in rutile formation. It has been found that the rates of these reactions and the ultimate rate and volume of oxidation are a function of the carbon and nitrogen content in the Ti(C,N) bulk sample. Specifically, samples with a higher volume of carbon will oxidize more easily than one with higher nitrogen content.[35] This process begins at the rim of the Ti(C,N) grain and proceeds inward until the entire core-rim strucutre of Ti(C,N) has been converted to TiO_2.[35] This is demonstrated in Figure 2–11, which depicts the varying equilibrium composition of $TiC_{0.3}N_{0.7}$ and $TiC_{0.7}N_{0.3}$, oxidized at 1000°C and 1 bar, showing that the rate of release of $CO_{(g)}$ is faster than that of $N_{2(g)}$.

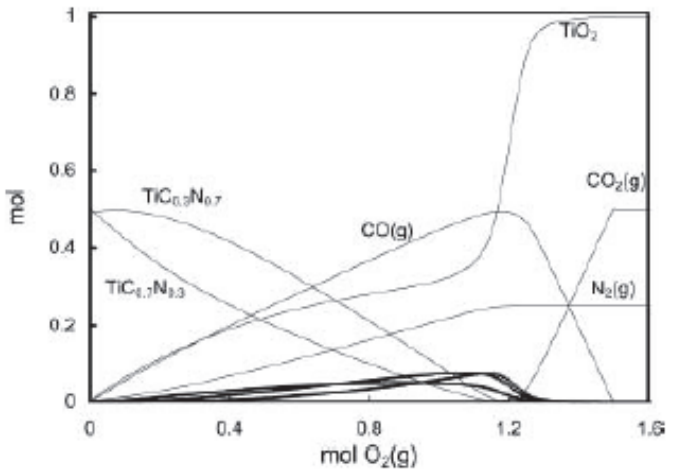

Figure 2–11 Equilibrium composition of TiC_xN_{1-x} at 1000°C and 1 bar, equilibrium amounts of $TiC_{0.3}N_{0.7}$ and $TiC_{0.7}N_{0.3}$ vs. moles of $O_{2(g)}$[35]

The effects of prolonged exposure of Ti(C,N)-based cermets to high-temperature conditions that would encourage oxidation has been studied.[35] The first conclusion to be made was the effect of residual porosity after sintering, which was determined to be a leading factor in the progression of oxidation. With increasing amounts of residual porosity, the likelihood of oxygen ions reaching the bulk materials was increased, which also provided a passageway for the gaseous products to be removed from the bulk material during oxidation.[35] However, as oxidation proceeds, the formation of the rutile scale layer aids in protecting against further corrosion.[35]

Effects of the inclusion of a metallic binder phase on the activation and progression of oxidation on Ti(C,N) has also been studied. It has been found that the resistance is dependent upon both the type and percent composition of the chosen binder, and that at high temperatures the binder may even facilitate sintering of a protective TiO_2 layer on the surface of the sample.[20] Specifically, cobalt, tungsten and molybdenum have been researched, resulting in improved resistance to oxidation with the addition of only Co over the pure Ti(C,N), however resistance improved further with the addition of small quantities of W and Mo.[20] It was demonstrated that the addition of Co allows for the formation of a protective oxide layer, slowing the progression of further attack, with the small amounts of W and Mo slowing oxide solubility into the sample.[20] This is

demonstrated in Figure 2–12, which shows the varying oxide layer formation for three TiC_xN_{1-x} cermets. The inner layer (a) demonstrates no permeation of oxidation, whereas layer (b) and (c) demonstrate damage to the microstructure and continuous rutile layer formation, respectively, for each sample tested.[20]

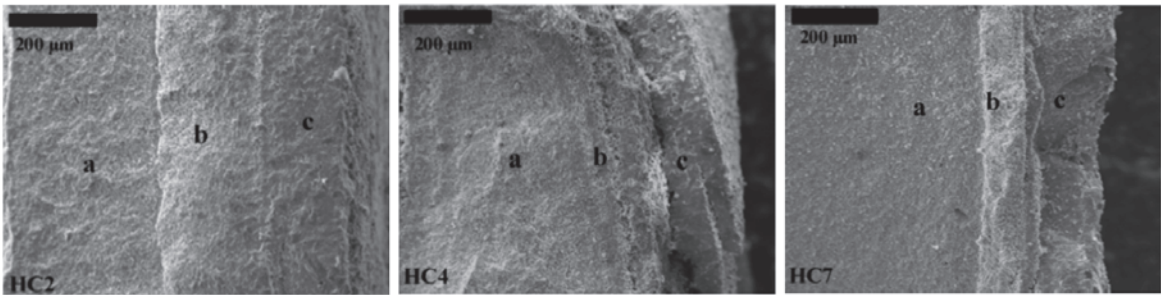

Figure 2–12 SEM micrographs showing cross-sections of oxide scale formation on $TiC_{0.75}N_{0.25}$ + Ni_3Ti, Ni,Ti) (HC_2), $TiC_{0.85}N_{0.15}$ + Co_3Ti (HC_4), and $TiC_{0.74}N_{0.26}$ + CoTi, W(HC_7) cermets[20]

It has been observed that depending upon the type and amount of binder addition, (in this case a comparative assessment was done between WC-Co and Ni/Co additions), the oxidation of the metallic binders will in fact aid in creating a protective oxide layer faster than the pure Ti(C,N) bulk material.[35] This can be slightly offset, however, by the passage of ions from the metallic binder to the reaction zone and oxygen to the bulk, as a result of both a concentration gradient and the capacity to move through intragranular spaces and any existing microporosity,[35] suggesting that achieving highly dense samples with low residual porosity is key to reducing the progression of oxidation through the bulk specimen. This passage through areas of microporosity may ultimately result in a situation whereby a macropore may develop and crack the outer protective layer, as shown in Figure 2–13, allowing for further progression of oxidation reactions. This was observed in trials conducted on $TiC_{0.5}N_{.5}$ + 16.7% (WC-5%Co), which was conjectured to be a result of the oxidation mechanisms of the specific binder alloying phase,[35]

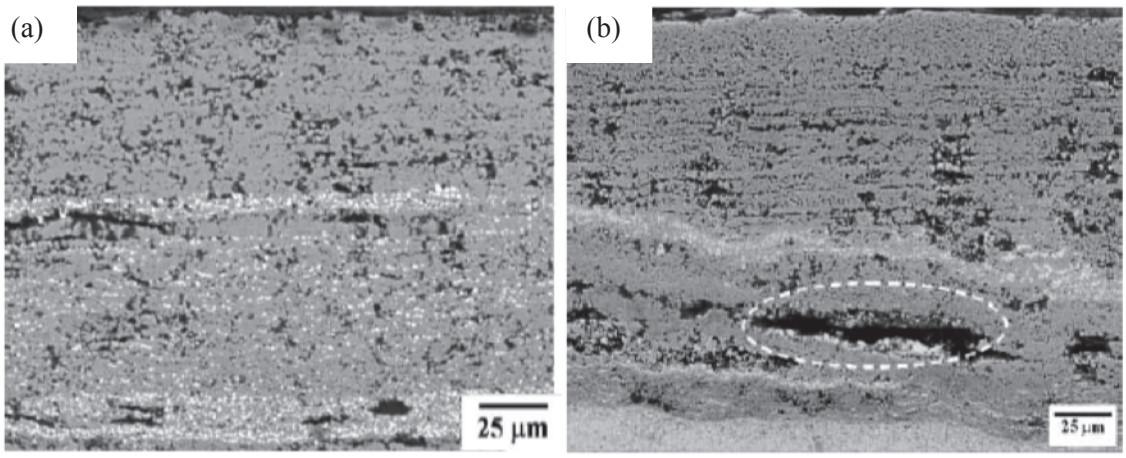

Figure 2–13 SEM micrograph of Ti(C, N) showing (a) the polished reaction scale and (b) the formation of a macropore between reacted scale and bulk material[36]

Further reactions can proceed at temperatures exceeding 850°C, whereby the rutile is in fact sintered.[37] However the comparatively low temperature at which this is observed may be a function of additional alloying elements, such as in the case of a study involving Ti(C,N) with nickel, which showed to drive the reaction forward despite no heat being added to the system.[37] Following from this research it was determined that increasing temperature further, beyond 1100°C, this causes the nickel to oxidize, forming NiO, which resulted in a scale layer that was very resistant to further oxidation.[37]

2.1.5 Common Applications

Ti(C, N)-cermets were not used in industrial applications until after 1968, despite being invented in 1931, and compared to TiC cermets, which were in common use since the mid-1960s, due in large part to a reluctance to include a nitrogen addition to hard metals.[38,39] Ti(C, N)-cermets are predominantly used for high speed milling operations and coatings for carbon alloy and stainless steel cutting tools.[1] The most prolific use of Ti(C, N)-based cermets is in tool coatings and the machining industry, specifically in finishing operations on steel cutting tools, which greatly increased tool life.[1] Ti(C, N) coatings incorporate the high hardness of TiC coatings, the high ductility of TiN coatings, while maintaining impressive adhesion qualities and mechanical properties.[40] They outperform hardmetals and TiC in their ability to maintain high temperature hardness and

withstand much higher cutting speeds, however they do show diminished toughness and thermal shock resistance.[1,41] Table 2–4 demonstrates some of the comparative advantage Ti(C, N)-based cermets have over TiC cermets of similar composition at high temperatures.

Table 2–4 Comparisons of high-temperature properties of TiC and Ti(C, N) cermets[1]

Sample	Microhardness at 1000ºC (kg/mm^2)	Transverse rupture strength (TRS) at 900ºC (MPa)	Weight Gain (oxidation) at 1000ºC ($mg/cm^2 \cdot h$)	Therm. cond. at 1000ºC (watt-deg/m)
TiC-cermet[a]	500	1050	11.8	24.7
Ti(C,N)-cermet[b]	600	1360	1.6	42.3
[a]TiC-16.5Ni-9Mo [b]TiC-20TiN-15WC-100TaC-5.5Ni-11Co-9Mo				

Ti(C,N) coatings exhibit a good resistance to oxidation, however with diminishing resistance at high temperatures above (400°C), its resistance is less than that of TiN which is resistant up to 600°C[40]. One method of improving this property involves the use of multilayer coatings. Multilayer coatings incorporate the concept of applying a metal layer between the Ti(C,N) coating and the surface to aid in chemical bonding and adhesion between the layers, to increase toughness, and to provide a potential stopgap to further pitting corrosion. Figure 2–14 shows a Ti(C,N) coating as well as the TiN/Ti(C,N) multilayer coating. Similar to TiN and TiC, Ti(C,N) most often applied as a coating by the use of either chemical vapour deposition (CVD) or physical vapour deposition (PVD).

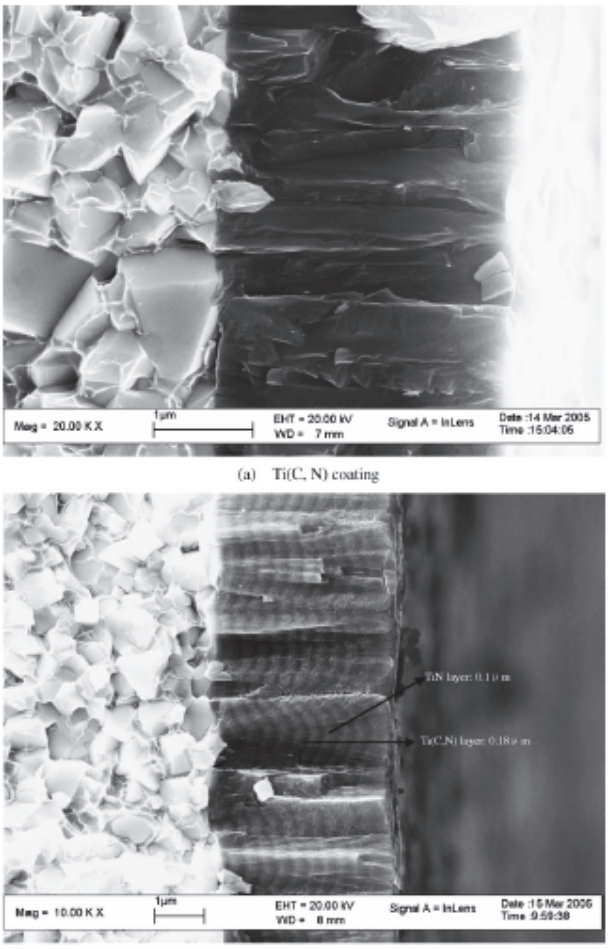

Figure 2–14 SEM images of cross-sections of Ti(C,N) and TiN/Ti(C,N) multilayer coatings[40]

2.2 Titanium Carbide

Titanium carbide (TiC), with a NaCl cubic structure and melting point of over 3000°C,[42] is an extremely hard carbide (Vickers hardness of 19.6-31.4 GPa),[43] often utilized for cutting tools and coatings due to its strength, corrosion resistance, toughness and flexibility. In comparison to Ti(C,N) cermets, TiC has shown slight reduction in some mechanical properties, as demonstrated in Table 2–4. Some basic data for TiC are depicted in Table 2–5.

Table 2–5 Basic properties of TiC[44]

	Melting temp. (°C)	Microhardness (kg_f/mm^2)	Density (g/cm^3)	Lattice parameter (Å)
TiC	3140	3200	4.92	4.322

Further areas of application for TiC include grinding wheels, heat exchangers, magnetic recording heads, turbine engine seals, and bullet-proof vests.[45] In comparison with other familiar ceramics, TiC ranks among the highest in hardness, as demonstrated in Table 2–6.

Table 2–6 Mechanical properties of TiC[1,16]

Material	Hardness (kg/mm^2)
Single-crystal diamond	7000-95000
Polycrystalline diamond	7000-86000
Cubic boron nitride (CBN)	3500-4750
Boron carbide (B_4C)	3200
Titanium carbide (TiC)	2800
Silicon carbide (SiC)	2300-2900
Aluminum oxide (sapphire or polycrystalline)	2000
Tungsten carbide-cobalt (94% WC-6% Co)	1500
Zirconium oxide (ZrO_2)	1100-1300
Silicon dioxide (SiO_2)	550-750

One of the earliest alternatives to tungsten-based hardmetals, TiC proved an effective alternative through the tungsten shortages endured in Germany throughout WWII and could be produced in bulk.[5] The drawback to TiC at the time was brittleness, and research was conducted to include additives such as molybdenum carbide (Mo_2C) and nickel to improve wettability and help curb this disadvantage.[5] The Mo_2C was expected to improve the wettability, as the carbide was able to react with the oxide layer prevalent on the TiC, forming carbon monoxide. Though this was successful it was realized that molybdenum on its own was able to produce this same effect, producing TiC with a core-based structure, with a (Ti,Mo)-C outer rim and mixed Ti-Mo binder phase.[46] In addition to the Mo binder metal, commonly used alternatives include Ni, Co, Al, Cu and more recently Ni_3Al.[5,47,48]

2.2.1 Consolidation of TiC

Standard synthesis of TiC can be grouped into the following three categories: (1) direct carbonization of Ti or TiH_2, or combustion synthesis of TiC, (2) pyrolysis of $TiCl_4$ in carbon and (3) carbothermal reduction of TiO_2, whose starting particles are shown in Figure 2–15. Some industrial-scale methods of production as well as their associated reaction equations are depicted in Table 2–7.

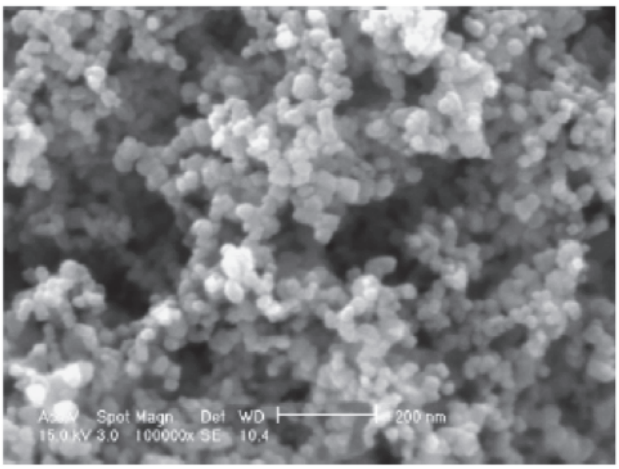

Figure 2–15 SEM micrograph of TiO2 particles[45]

Table 2–7 Typical reactions involved in consolidation of TiC via powder metallurgy[49]

Method	Reaction
Direct reaction between metallic Ti or metallic Ti hybrids and graphite, under vacuum or inert gas	$Ti + C \rightarrow TiC$
Reduction of the Ti oxide by graphite, under vacuum or inert gas	$TiH_2 + C \rightarrow TiC + 2CO$
Reaction of the Ti with carburizing gas	$Ti + C_nH_{1-n} \rightarrow TiC + H_2$
Precipitation from the gas phase by reacting the metallic Ti halide or metallic Ti carbonyl in hydrogen	$TiCl_4 + C_xH_y + H_2 \rightarrow TiC + HCl + (C_nH_m)$ $Ti + carbonyl + H_2 \rightarrow TiC + (CO, CO_2, H_2, H_2O)$

Carbothermal synthesis remains the most widely used method for preparing TiC powders, while remaining relatively efficient and cost effective.[45] Carbothermal reduction of TiO_2 takes places between 1500–2100°C by the following reaction and produces varying particle sizes depending on the length of time at the chosen reaction temperatures, as demonstrated in size stages in Figure 2–16.

$$TiO_2(s) + 3C(s) \rightarrow TiC(s) + 2CO(g) \qquad \text{Equation 2.5}$$

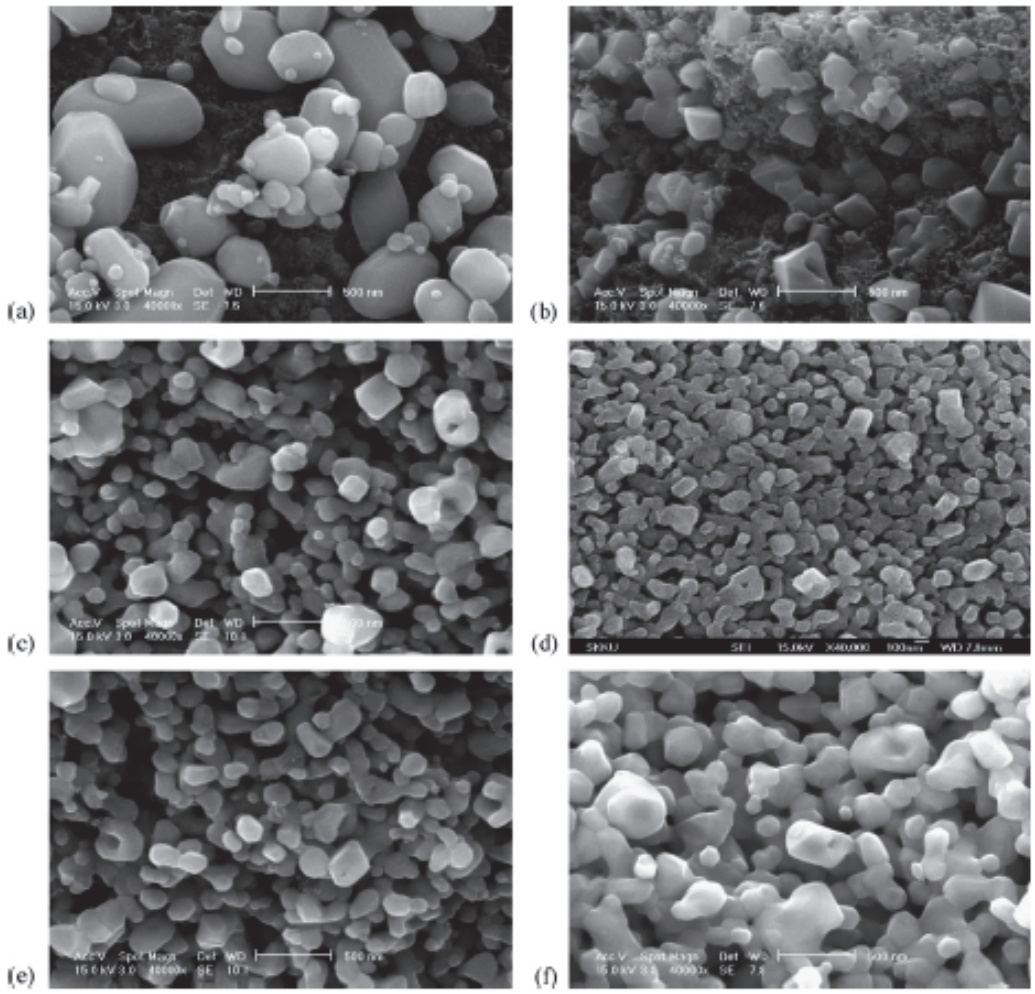

Figure 2–16 SEM morphologies of particles formed by carbothermal reduction, 1500˚C for (a) 0 min., (b) 5 min., (c) 10 min., (d) 15 min., (e) 20 min., (f) 45 min.[45]

However, considering the extremely high reaction temperatures, as well as the prolonged reaction times, carbothermal synthesis can result in significant coarsening and often contamination.[50]

Synthesis of dense TiC ceramics can be performed in several ways, including pressureless sintering (PS), hot pressing (HP), hot isostatic pressing (HIP), spark plasma sintering (SPS), and self-propagating high-temperature synthesis (SHS).[51]

Conventional sintering may take place under a number of different environments, such as in vacuum, argon, or nitrogen. It has been concluded that the best results occur

when sintering in a vacuum, just as in the presence of Ar and N_2, oxygen and nitrogen often affect the carbon content within the system, resulting in degradation of strength, hardness and TRS.[52] Furthermore, studies have been conducted to demonstrate the results of sintering at a specified time and temperature, specifically one hour at 1750°C, over an array of compositions: TiC_x where x = 0.94, 0.84, 0.75, 0.69, 0.63 and 0.58. A number of conclusions were drawn from this analysis, summarized in Table 2–8 and Figure 2–17. The results showed that open porosity and grain size are proportional to increasing titanium content, as was the Mohs hardness. The observed grain growth with increasing titanium content is believed to be a result of the sintering conditions that allow the titanium liquid phase to promote densification and to be the primary mechanism for diffusion.[53]

Table 2–8 Ti-TiC compacts sintered at 1750˚C for one hour[53]

Sample	Bulk (x) TiC_x	Grain Size (μm)	% Open Porosity	Mohs Hardness	Residual Ti (wt %)
A1	0.94	13	32	2	n.d.
A2	0.84	13	30	4.5	n.d.
A3	0.75	14	29	5	n.d.
A4	0.69	13	26	8.5	n.d.
A5	0.63	35	21	9	> 1*
A6	0.58	75	17	8.5	17
*Intragranular texture n.d. = none detected					

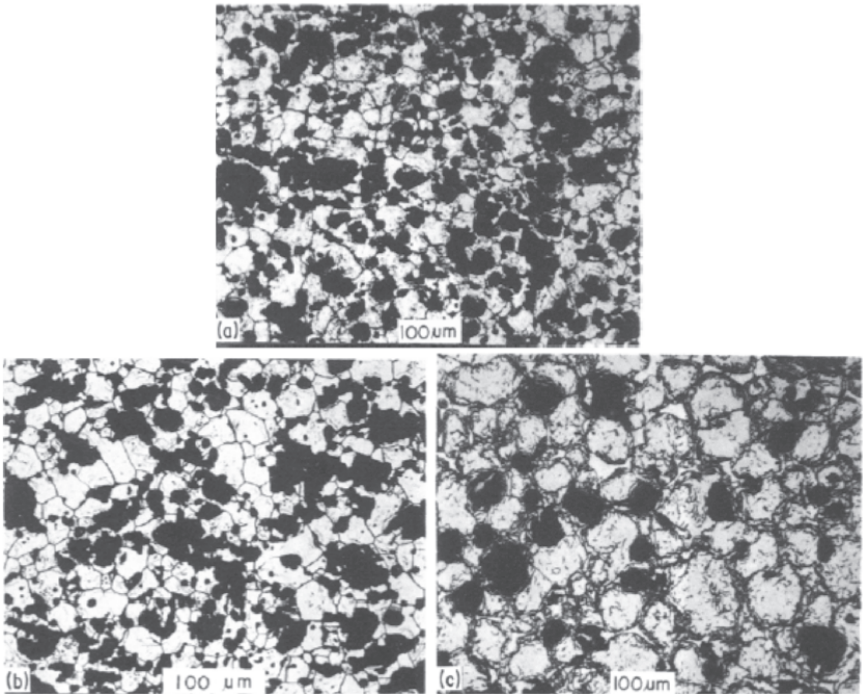

Figure 2–17 Optical micrographs of etched surfaces, sintered in vacuum at 1750 for 1hr. (a) $TiC_{0.69}$, (b) $TiC_{0.63}$, (c) $TiC_{0.5}$[53]

Self-propagating high-temperature synthesis (SHS), or combustion synthesis, is a relatively simple, affordable, and environmentally safe way to effectively and efficiently produce high purity TiC.[54] The basis of SHS is a locally spotted ignition source, followed by a self-propagating combustion wave through the sample, which continues the reaction without any need to provide additional energy to the system. Specifically for TiC synthesis, an igniter is used (such as a tungsten filament) to induce a combustion wave through the sample, melting the Ti and allowing it to spread over the porous C to produce the first TiC crystals without having to supply additional energy; the remaining Ti then melts and reacts with C to form the Ti and C rim surrounding a solid TiC core.[55] Despite the apparent simplicity of SHS, an in-depth analysis of the mechanisms involved has shown there to be a rather intricate sequence of events, from initial melting to complete dissolution of the base metal, and finally the evolution of a complex crystal microstructure as the system is allowed to cool,[56] SHS requires that the reacting temperature is greater than the melting point of pure Ti (1670°C) for the reaction between Ti and C to occur.[42] SHS also makes efficient use of inexpensive, readily found raw

materials such as the oxides, halides and other compounds as well as reducing agents such as Mg, Ca, Al and Zn.[50] The major variables determining the degree of success of combustion synthesis are primarily reactant particle size and microstructure.[57]

As with most consolidation techniques, the addition of additives to aid in synthesis can affect any step of the process. For example, SHS of TiC by means of consolidating Al-Ti-C powders has been shown to have a significant impact on initial ignition temperature, as well as final grain morphology, as can be clearly seen in Figure 2–18, with varying weight percentages of aluminum.

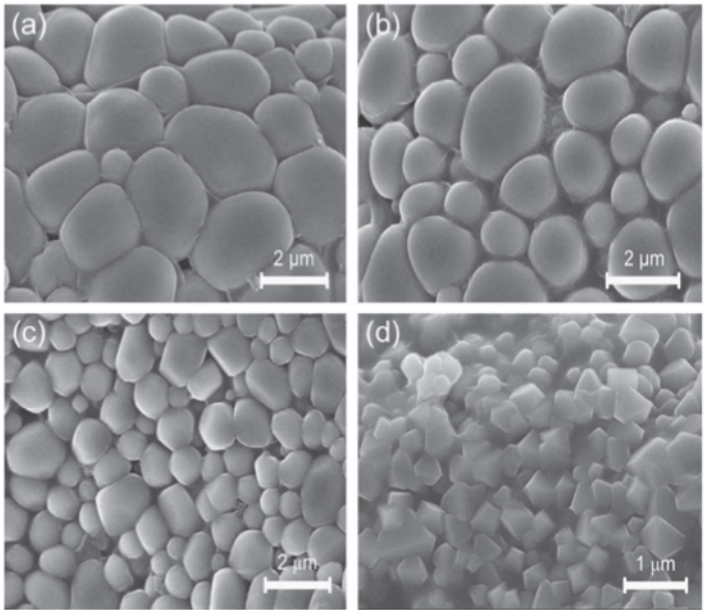

Figure 2–18 SEM microstructure of TiC with varying Al additions: (a) 10, (b) 20, (c) 30, (d) 40 mass%[54]

Similarly, aluminum addition to the SHS process has demonstrated significantly decreased final particle size, as well as increased consistency of particle morphology and rearrangement, as a result of greatly increasing the reaction temperature and shortening reaction time.[54] The effects of some other commonly used additives, their resulting mechanical properties and the standard applications for each are demonstrated in Table 2–9.

Table 2–9 Types of alloys obtained by combustion synthesis, and their applications[58]

Composition	Density (g/cm^3)	Grain Size (μm)	HRD Hardness	Bending Strength (MPa)	Application
(TiC-TiB_2)+Cu	4.94	5-7	93.5	70-800	Cutting inserts
TiC+Ni	5.50	5-7	90	1000-1100	Armouring plates
TiC+(Ni-Mo)	6.40	1-2	87	1600-1800	Press tools
(TiC-Cr_3C_2)+Ni	5.37	3-4	92.5	800-1000	Cutting inserts
(TiC-Cr_3C_2)+steel	5.40	2-4	92.5	700-800	Scale-resistant parts
TiB+Ti	4.20	1-2	86	1200	Thermal-shock resistant articles
(TiC-TiN)+(Ni-Mo)	5.80	1-2	91.5	1200-1400	Cutting inserts

An alternative to SHS processes is using high-energy ball milling to mechanically react Ti and C powders through carburization. Some believe this to be a preferred method for producing nanocrystalline TiC samples, even for industrial scale applications, as it can successfully produce fine, homogeneous particles of uniform size at room temperature.[42] The initial raw precursory materials are irregularly shaped particles which, after increasing milling speed and time became fine, smooth particles averaging approximately 60 nm after consolidation via plasma activated sintering, as shown in Figure 2–19.

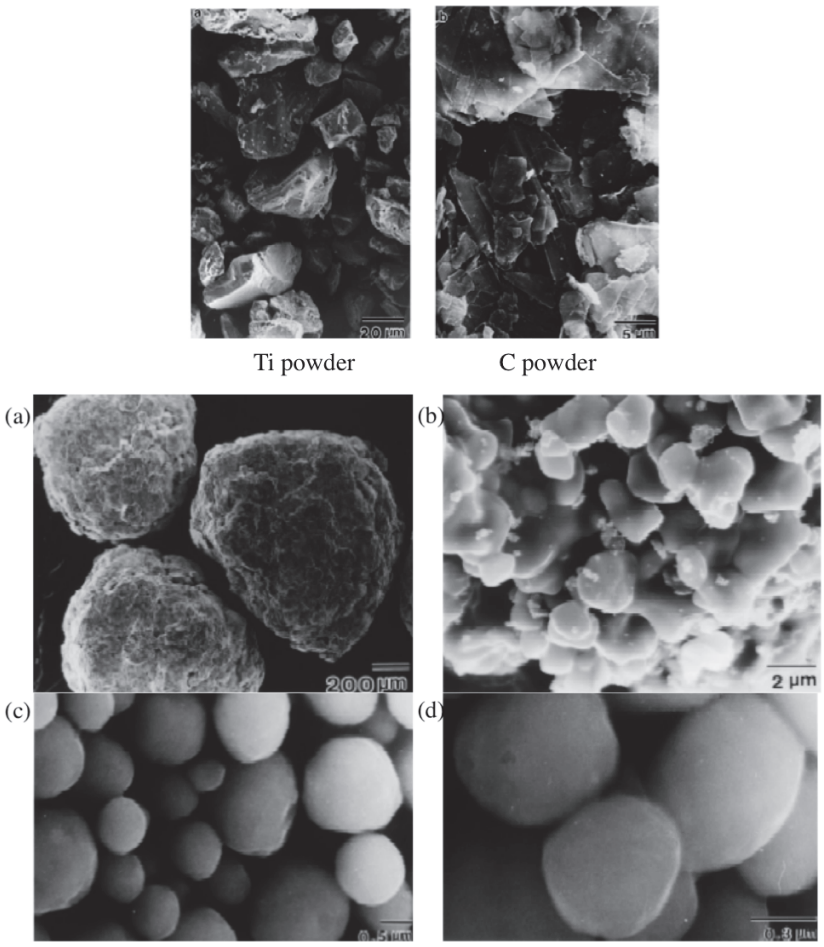

Figure 2–19 SEM micrographs of starting Ti and C powders, followed by mechanically alloyed TiC at (a) 11 ks, (b) 22 ks, (c) 40 ks, (d) 720 ks.[42]

2.2.2 TiC Properties and Effects of Binder Alloying Additions

TiC have been shown to have notably good mechanical properties, specifically low density, a high melting point (3065°C), comparatively high hardness, high compressive strength as well as high wear and abrasion resistance.[59,60] Such properties, as well its comparatively low fatigue sensitivity, lead to the common usage of TiC in industrial applications such as coatings for cutting tools, and any application that endures erosion-wear conditions.[61] Some common mechanical properties of TiC are demonstrated in Table 2–10, and depictions of the grain sizes described are seen in Figure 2–20.

Table 2–10 Properties of TiC[59]

Material	Density (g/cm^3)	% Theor. density	Knoop hardness (GPa)	Grain size (μm)
$TiC_{0.93}$	4.8503	~ 100	17.40 ± 0.74	14
$TiC_{0.83}$	4.6199	97.7	15.14 ± 0.74	20
$TiC_{0.75}$	4.6501	99.8	14.68 ± 0.64	14
$TiC_{0.66}$	4.5983	99.9	12.83 ± 0.42	22

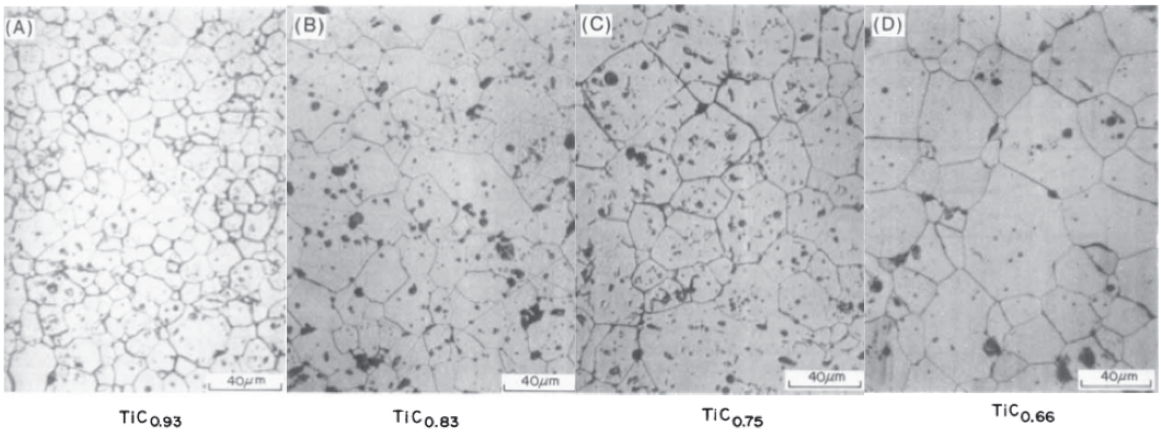

Figure 2–20 Optical micrographs of TiC samples with decreasing carbon content[59]

All of these properties, however, have shown potential for improvement with the addition of various types and volumes of metal binders. Common additives used to improve the mechanical properties of TiC are nickel and molybdenum, due to their promotion of wetting as well as the evolution of the core-rim structure of TiC-Mo rim surrounding a pure TiC core.[62] The mechanism behind this phenomenon is conjectured to be either dissolution-reprecipitation of the TiC-Mo solid solution onto TiC (Ostwald ripening) or the dissolution of Mo into the TiC grain. This evolution throughout the sintering process can be seen in Figure 2–21, alongside a schematic of the same phenomenon. TiC cermets with these types of additives are commonly used for wear applications due to their low friction coefficient, high hardness and high oxidation resistance.[63]

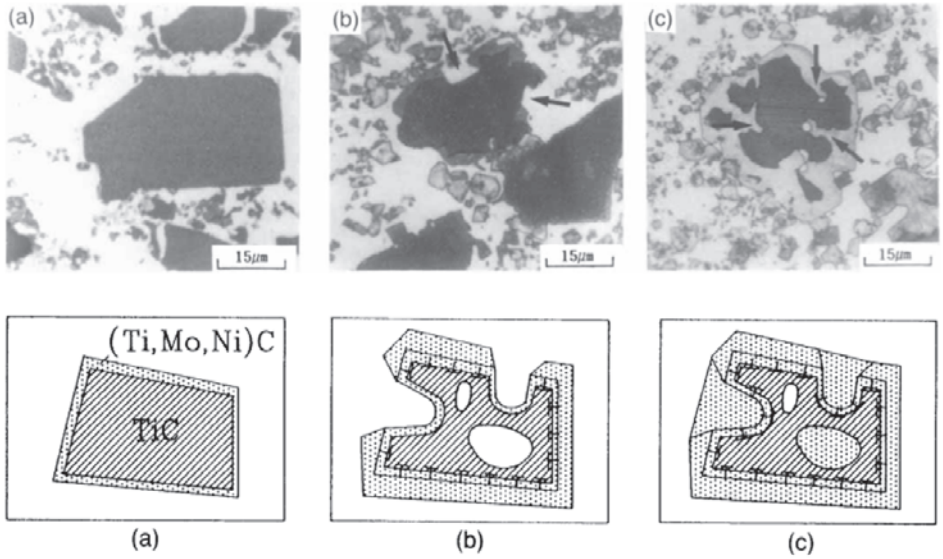

Figure 2–21 Microstructures of TiC-Mo cermets sintered at 1350 for (a) 0 min., (b) 10 min., (c) 60 min., followed by illustrations of TiC grain evolution during sintering[62]

Studies with various types of metal binders have shown improvements in mechanical properties with significant reduction in density for the TiC cermets investigated, as shown in Table 2–11.

Table 2–11 Composition and properties of WC and TiC cermets[64]

Carbide content (wt.%)	Composition and structure of binder	Vickers hardness (HV)	Density (kg/m^3)	Transverse rupture strength, R_{TZ} (GPa)	Modulus of elasticity, E (GPa)
WC (92)	Co	1350	14,500	2.30	650
WC (85)	Co	1200	13,900	2.35	560
TiC (40)	$FeCr_9Si_{1.5}$	1150	6,100	1.83	300
TiC (60)	$FeCr_7Si_{1.5}$	1360	5,800	2.00	380
TiC (60)	$Ni_{26}Mo_{14}$	1190	5,770	1.32	380
TiC (80)	$Ni_{13}Mo_7$	1378	5,500	1.08	400

Further study of Ni-Mo additives was conducted, demonstrating the cermet's ability to withstand different wear conditions. It was found that abrasive/erosive wear resistance is highly dependent on the ratio of binder metal used (Mo:Ni), and that without

improving the strengthening degree of the binder metal, TiC cannot compare with the strength and rigidity of the carbide phase in WC-Co hardmetals.[63]

Nickel aluminide (Ni_3Al) has recently been studied as an alternative metal binder, demonstrating a marked increase in hardness, toughness, and fracture resistance.[65] Using melt-infiltration sintering (MIS) as a method of consolidating the sample, full density can be achieved within very conservative temperatures and times: 1300°C and less than one hour. Furthermore, the addition of Ni_3Al has shown improved yield stress, strength, toughness and resistance to oxidation and corrosion at temperatures exceeding 1000ºC,[48] as demonstrated in Table 2–12.

Table 2–12 Thermal and mechanical properties of TiC composites with Ni_3Al binder[48]

Volume % Ni_3Al	Density (g/cm^3)	Thermal diffusivity (200ºC, cm^2/s)	Vickers Hardness (GPa)	Young's modulus (GPa)
0	4.94	0.0658	21	455
8	5.13	0.0703	17.2	-
12	5.23	-	15.3	430
15	5.31	-	15.3	430
20	5.43	0.0755	14.6	410
25	5.55	-	-	370
100	7.39	0.0343	3	185

2.2.3 TiC Applications

TiC-cermets have been commercially available in the market for industrial applications since the mid-1960s.[38] A primary use for TiC cermets is in erosive and abrasive wear applications. As discussed, the choice of metal binder and TiC stoichiometry used plays an important role in determining the samples' resistance to wear. In addition to this, particle size, grain size and porosity also affect their capacity to withstand wear. Finer particle size and decreased porosity tend to increase wear resistance.[43] As can be seen in Table 2–13, hardness has been shown to be a function of binder type as well as carbon content. This results in improved mechanical properties, as well as improved erosion

resistance and grain boundary microstructure, which increase the overall wear resistance.[43]

Table 2–13 Compositions and properties of TiC-based cermets[43]

TiC (wt. %)	Ni (wt. %)	Additives	Density (g/cm^3)	Vickers Hardness (HV)	Transverse rupture strength (N/mm^2)
80	16	4 wt.% Mo	5.47	1400	1110
80	13	7 wt.% Mo	5.50	1430	1090
60	32	8 wt.% Mo	6.04	990	1400
60	26	14 wt.% Mo	6.02	1190	1320
50	40	10 wt.% Mo	6.40	890	1680
50	54	16 wt.% Mo	6.42	1050	1600

2.2.4 Corrosion of TiC

Titanium carbide is an example of a refractory compound based on titanium metal. Its uses include cutting tool applications, furnace parts, and other applications that warrant high hardness materials coupled with high temperature tolerance and an extremely high melting point.[66] The use of TiC, however, is restricted due to its high susceptibility to oxidation at increased temperatures, and circumventing this problem is therefore a major focus of development and research. The first step during low-temperature corrosion of TiC is the formation of oxycarbide ($TiC_{1-x}O_x$) at approximately 420°C, which is followed by the development of anatase and finally rutile (TiO_2) as temperatures are further increased.[36,67,68] The generalized equations for the oxidation of TiC are shown below:[69]

$$TiC_{1-x} + (2-x)O_2 \rightarrow TiO_2 + (1-x)CO_2 \qquad \text{Equation 2.6}$$

$$TiC_{1-x} + \left({}^{3}/_{2} - {}^{1}/_{2}\,x\right)O_2 \rightarrow TiO_2 + (1-x)CO \qquad \text{Equation 2.7}$$

The initial step involves the formation of a titanium oxide layer, which is used to assess the rate of oxidation as a function of the apparent gain in mass of the tested sample. The formation of a noticeable anatase layer begins to be apparent at temperatures of approximately 600°C. If temperatures are kept in this range or raised, the layers will

expand and often cause cracking of the oxidized surface layer (Figure 2–22), allowing oxygen to pass through and continue to corrode the bulk layer.[67] As temperatures are increased to 700°C there is further development of the anatase layer, followed by the formation of crystalline rutile. As temperatures exceed 700°C, rutile is the dominant crystalline phase formed on the surface layer, with further growth of the anatase crystalline layer ceasing.[69] This sequence was found to be a direct result of the increasing temperature, allowing for sintering of the anatase scale to take place, reducing the amount of residual carbon and causing the reaction rate to now be limited by gas and solid-state diffusion mechanisms.

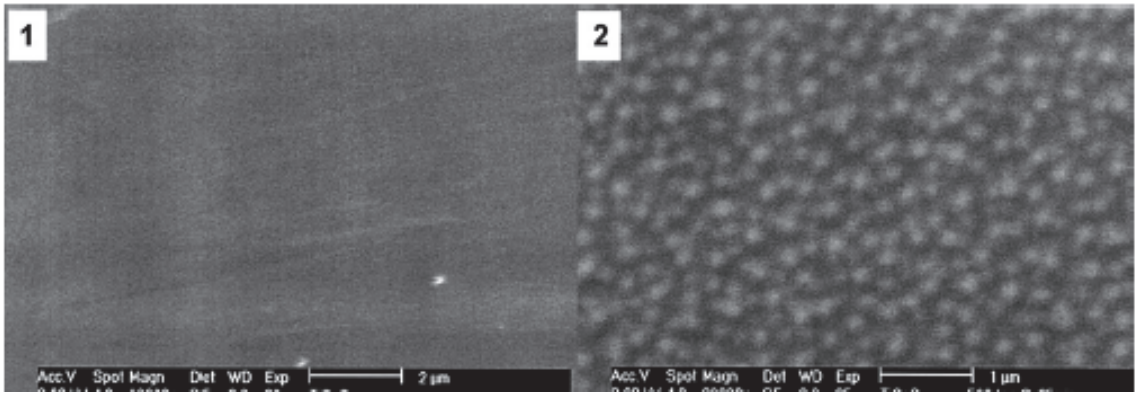

Figure 2–22 SEM micrographs illustrating (1) the oxidizing surface of TiC at 500ºC, (2) and 600ºC[69]

Similarly, varying the particle size has been shown to affect the rate of oxidation; the smaller the particle and grain size, the faster the rate of oxidation.[36] This also revealed an impact on the effects of temperature, as reduced particle sizes demonstrated a limiting effect on increased reaction rates above 800°C. However, with increasing particle size there is an obvious increase in reaction kinetics taking place when temperatures exceed 900°C.[36]

The majority of studies concerning the aqueous corrosion of carbides have been focused on SiC, demonstrating increased reaction kinetics and dissolution with exposure to steam.[70] Aqueous corrosion of TiC has been found to proceed in a similar manner, however results in less residual porosity as well as less frequent observation of interlayer

cracking.[68] This phenomenon is observable in Figure 2–23, which comparatively demonstrates the impact of oxidation in H_2O. Furthermore, it has been found that the presence of water increases the rate of transformation from anatase to rutile, reduces the amount of carbon dissolution when compared to oxidizing in pure O_2, and results in H_2 and CO/CO_2 gas byproducts.[67]

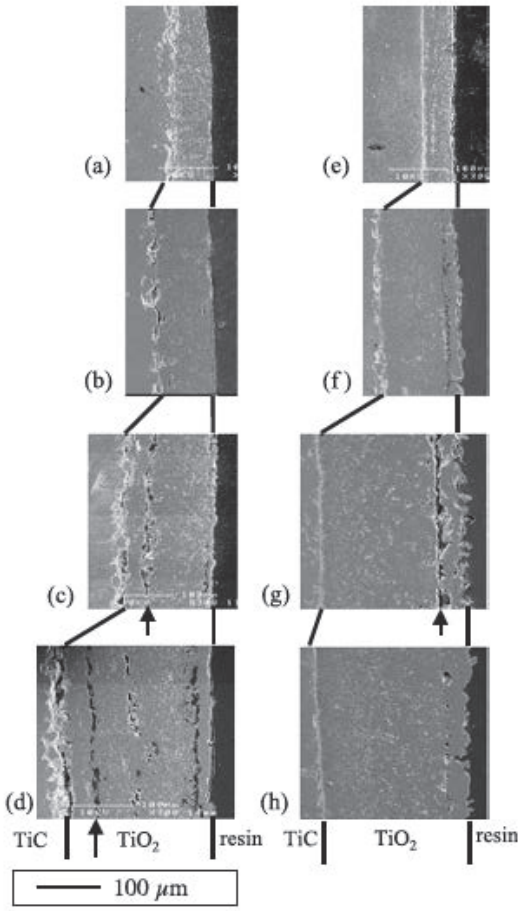

Figure 2–23 SEM micrographs of TiC oxidized at 900°C in dry air at (a) 5 h., (b) 10 h., (c) 26 h., (d) 50 h., and in H_2O at (e) 5h., (f) 20 h., (g) 30 h., (h) 34 h.[71]

Preliminary research conducted on the corrosion resistance of TiC with a Ni_3Al binder phase has shown improved resistance to corrosion with an observable aluminum oxide scale forming as the result of the binder at high temperatures.[48] When immersed in a corrosive environment, it was found that it is significantly more resistant to corrosion in

sulfuric acid than nitric acid, however less resistant in hydrochloric acid, as demonstrated in Figure 2–24.

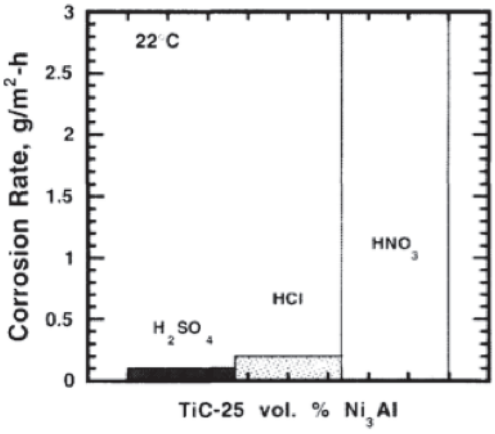

Figure 2–24 Corrosion resistance of TiC-Ni_3Al in acid solutions (1 normal) at 22°C[48]

2.3 Titanium Nitride

Titanium nitride (TiN) is a ceramic material of extreme hardness often used as a coating on either titanium or steel alloys, in medical applications (due to its nonpathogenic nature), as well as in jewelry, as it is gold in colour.[72] In addition, TiN possesses other desirable qualities such as an extremely high melting point (2950°C), chemical stability, high electrical conductivity, as well as excellent wear and corrosion resistance.[25] Some basic properties of TiN are listed in Table 2–14.

Table 2–14 Basic properties of TiN[44]

	Melting temp. (°C)	Microhardness (kg_f/mm^2)	Density (g/cm^3)	Lattice parameter (Å)
TiN	2930	2000	5.22	4.242

It is for these reasons that TiN is often used as an additive for other materials or thin coatings, in order to improve surface properties of materials in applications such as drilling, steel-making, automotive components, diamond coating, plumbing, aerospace and semiconductor production.[73,74,75] The attractiveness of TiN as a coating is highly

dependent on the ability of the substance to adhere to steel alloys, its high hardness and good tribological qualities.[76] Bulk samples of TiN are much more rare, but it has been shown that it can be sintered at extremely high temperatures, upwards of 2000°C, with lower sintering temperatures achieved (1300-1500°C) through the use of nanosized particles.[76] Table 2–15 demonstrates some comparative properties of TiC and TiN.

Table 2–15 Properties of TiC and TiN[1]

	Melting Temp. (°C)	Micro Hardness (kgf/mm^2)	Density (g/cm^3)	Electrical Resistance (μΩ·cm)	Thermal Conductivity (Watt/m/deg)	Lattice Parameter (Å)	Young's Modulus
TiC	3140	3200	4.92	68	10	4.322	491
TiN	2930	2000	5.22	25	23	4.242	600

2.3.1 Consolidation of TiN

There are a number of methods by which TiN is synthesized, the most common of which include reaction synthesis of titanium with nitrogen at high temperatures (1000 - 1500°C) and carbothermal reduction of titanium oxide.[77] Carbothermal reduction of TiO_2 occurs according to the following equation:

$$TiO_2 + 2C + {}^1/_2 N_2 \rightarrow TiN + 2CO \qquad \text{Equation 2.8}$$

TiN has also been synthesized using SHS, driving the reaction by utilizing the innate properties of its own exothermic reactions.[76] It was found that consolidating TiN by this method produces a high enough temperature of combustion (~ 4727°C) coupled with a relatively fast rate of combustion (25 cm/s). For SHS to be viable, the capacity of the raw powders to take up the gases provided must not occur at a faster rate than that required to sustain the reaction itself. As such, the relative density of the sample proves to be the limiting factor in terms of the effectiveness of the process, shown to be unmaintainable at densities greater than approximately 58% theoretical density.[78] As a

result, SHS as a method of producing fine grain size TiN powders has been shown to be relatively simple, efficient and economically viable.[76]

2.3.2 TiN Properties and Applications

Producing TiN as a bulk material has proven to be a generally undesirable objective because of its extremely high melting temperature makes it difficult to obtain fully dense solid components with advantageous mechanical properties. The majority of TiN is used as coatings for cutting tools, intricate circuitry and other areas that would benefit from the notable thermal and electrical conductivity, as well as corrosion resistance.[79] Coatings are a method of extending tool life and application. In the case of TiN coatings, which are often applied by either chemical vapour deposition (CVD) or physical vapour deposition (PVD), the TiN coatings are believed to increase tool life by several hundred percent while maintaining an impressively high degree of ductility.[80] Such coatings have been used to improve cutting tools and machining, as well as in solar energy cell development and silicon circuitry.[80]

2.3.3 Corrosion of TiN

TiN, with titanium being a member of the refractory metals, has behaved well in applications that warrant strength and hardness. However, it has been susceptible to oxidation and resulting degradation due to corrosion at high temperatures.[81] For example, TiN powder has been found to begin pronounced oxidation at 500°C while dense, sintered TiN demonstrates significant oxidation at approximately 700°C.[82] Furthermore, there appears to be little research conducted on this subject, specifically in the area of reaction kinetics and mechanisms that occur during the oxidation of TiN. A number of researchers have conducted their studies based on the theory of oxy-nitride formation, followed by titanium dioxide growth, forming a rutile scale. A mineral composed of titanium dioxide (rutile) begins developing at approximately 600°C, while anatase begins developing at lower temperatures.[82] Similarly, titanium nitride was found to be resistant to oxidation in H_2, N_2 and O_2 at temperatures below 1000°C, however it shows notable and in some cases severe volatilization at temperatures above 1400°C.[81]

Research has shown that typical oxidation of TiN occurs by forming a rutile scale in accordance with the reaction mechanism:[83]

$$TiN_x + O_2 \rightarrow TiO_2 + {}^{x}/_{2}\, N_2 \qquad \text{Equation 2.9}$$

The rate laws are comprised of a rate-determining step followed by a diffusion-limited step dependent upon the diffusion layer that develops after prolonged oxidation.[83] Figure 2–25 illustrates the standard reaction mechanisms behind the oxidation of TiN, showing the progression of O_2 diffusion first through the sintered layer, then through the oxide layers until it reaches the rutile layer (at point E), finishing at the nitride substrate. Meanwhile, concurrent dissolution of N_2 is taking place in the opposite direction.

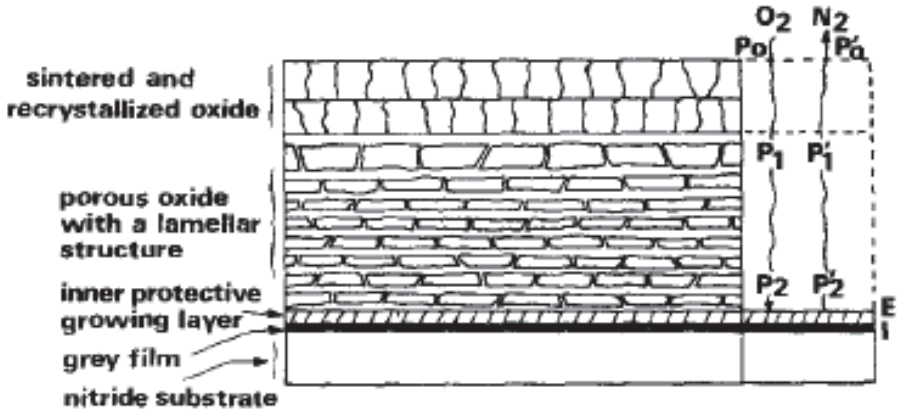

Figure 2–25 Illustration of the reaction mechanisms involved in the oxidation of TiN[83]

The oxidation behaviour of TiN, with varying nitrogen contents in an O_2 atmosphere, demonstrates that the same mechanism is responsible for oxidation, regardless of nitrogen content. More specifically, the rate-limiting step was identified as being the diffusion through the interface between the predominantly oxide layer and that of the nitride. This layer is composed primarily of rutile and acts as a barrier for further oxidation.[83] The varying nitrogen content also plays a role as thicker plates demonstrated a reduction in the rate of diffusion of nitrogen outward, while oxygen diffused inward, which was also shown to be a function of the pressure of the system, increasing with temperature.[83]

As oxidation of TiN takes place, atoms migrate from the bulk material to the oxide film at the surface, leaving vacancies at the boundary that can ultimately cause a void, or cavity, between the TiN bulk and oxidized film. This behaviour is illustrated in Figure 2–26. The migration of ions and vacancies throughout the matrix often can result in the development of internal stresses, which can lead to cracking of the surface film, resulting in an area where renewed oxidation can take place. This cycle is responsible for the formation of lamellar scale development on the surface of the TiN.

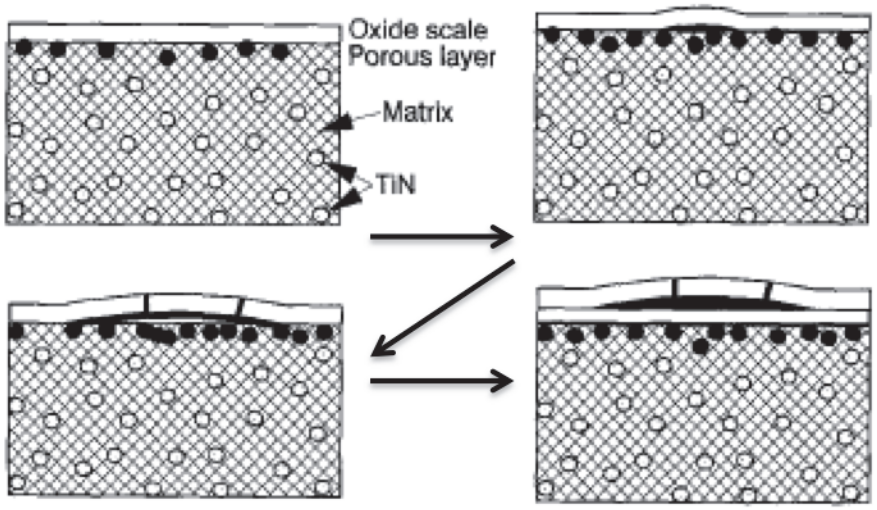

Figure 2–26 Illustration of scale formation and resultant cracking of the oxide layer formed on TiN during oxidation[82]

The effect of varying temperature as it relates to varying particle sizes demonstrates that reaction rates will increase with temperature up to a limit that is a function of the particle size.[36] Small particle sizes will see a limit to the oxidation reaction rates at approximately 600°C, however rates will increase with size up to approximately 900°C for very coarse particles.[36] This would be in accordance with the concept of smaller particle sizes having greater surface areas, which would allow for a greater area for reaction and oxidation to take place.

In preliminary studies on coatings, TiN has been shown to be a very promising material to protect against corrosion, as compared to TiC or TiCN, as well as TiN/Au, TiN/Ni and multilayer coatings.[84] However, if binder contents are exceedingly high, this

may result in the removal of large grains, leaving significant voids that will ultimately increase the sample's susceptibility to corrosion.[85]

3 Materials and Methods

The following chapter will outline the materials and methods used to prepare the samples and conduct electrochemical tests for an array of Ti(C,N) cermets. The outline will include the powder preparation for $Ti(C_{0.3}N_{0.7})$, $Ti(C_{0.5}N_{0.5})$, $Ti(C_{0.7}N_{0.3})$ and TiC, as well as the milling and polishing stages of preparation. Finally, this chapter will address the methods involved in cold isostatic pressing (CIP) as well as the vacuum sintering required to melt infiltrate the associated binder phase to achieve a final highly densified sample.

3.1 Materials

3.1.1 Titanium Carbide and Titanium Carbonitride

All samples were prepared using TiC (Lot #PL20125339) from Pacific Particulate Materials (Vancouver, Canada) and the following Ti(C,N) powders: $Ti(C_{0.3}N_{0.7})$ (Lot #L25747), $Ti(C_{0.5}N_{0.5})$ (Lot #L29865) and $Ti(C_{0.7}N_{0.3})$ (Lot #25809) from Treibacher Industrie AG (Althofen, Austria). Figure 3–1 demonstrates scanning electron microscopy (SEM) images of each powder, and particle size distributions were compared to those given by the manufacturer, as listed in Table 3–1. The SEM analysis showed agreement with the manufacturer's specification of average particle size.

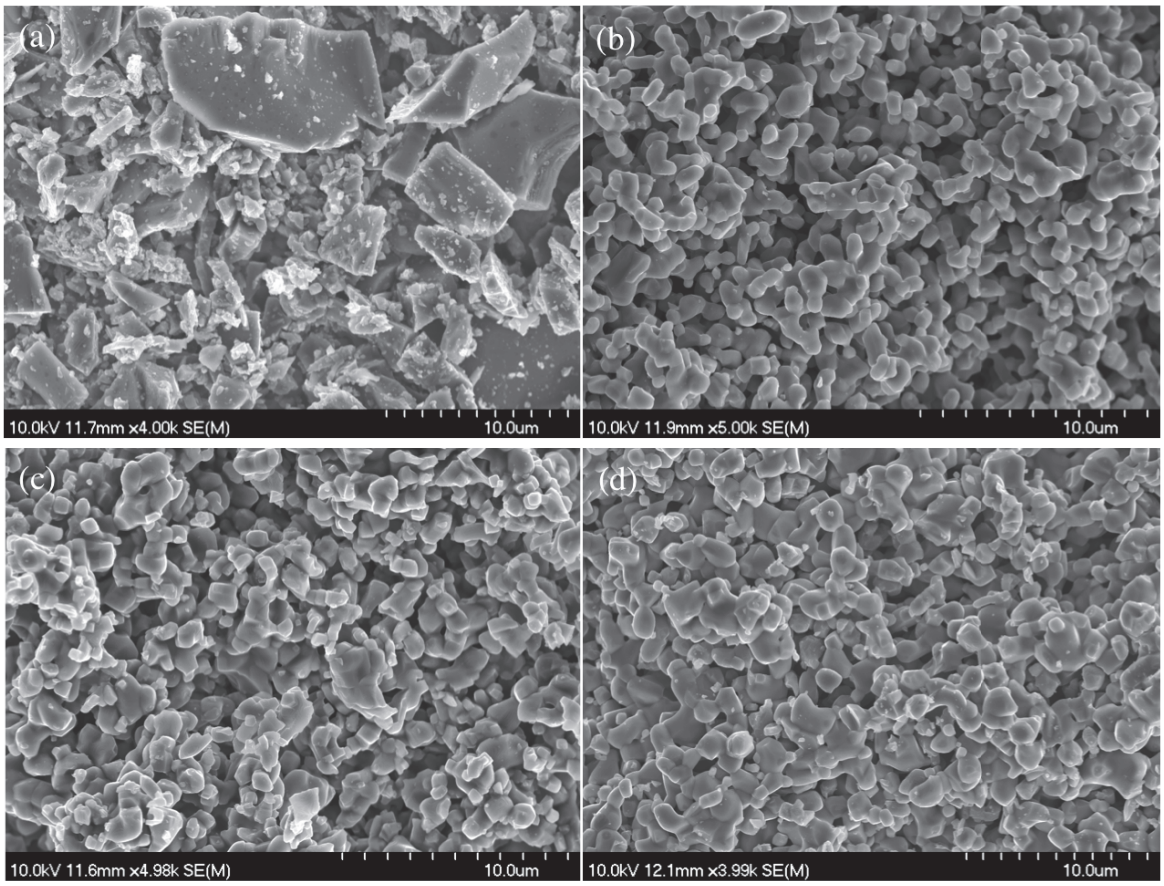

Figure 3–1 SEM micrographs of starting powders, (a) TiC, (b) $TiC_{0.3}N_{0.7}$, (c) $TiC_{0.5}N_{0.5}$, (d) $TiC_{0.7}N_{0.3}$

Table 3–1 Starting powder particle sizes and densities

Powder	Particle Size (μm)	Density (g/cm^3)
TiC	1.25 ± 0.53	4.92
$TiC_{0.3}N_{0.7}$	2.10 ± 0.57	5.13
$TiC_{0.5}N_{0.5}$	1.74 ± 0.49	5.07
$TiC_{0.7}C_{0.3}$	1.72 ± 0.49	5.01

Furthermore, each manufacturer provided a detailed account of each component present within the powders (Table 3–2). Energy-dispersive x-ray spectroscopy (EDS), and x-ray diffraction (XRD) analysis were performed on each of the powder samples, resulting in agreement with the manufacturer's specifications of the average chemical composition.

Table 3–2 Composition of each starting powder from manufacturer

	Composition (wt %)								
Powder	Free C	Total C	Al	Ca	Fe	N	O	S	Ti
TiC	0.12	19.51	-	-	0.06	0.05	0.39	-	79.87
$TiC_{0.3}N_{0.7}$	0.02	6.31	< 0.01	< 0.01	< 0.03	15.53	0.37	< 0.01	77.71
$TiC_{0.5}N_{0.5}$	0.17	10.43	< 0.01	< 0.01	< 0.03	10.89	0.22	< 0.01	78.23
$TiC_{0.7}C_{0.3}$	0.21	13.28	< 0.01	< 0.01	< 0.03	7.50	0.27	< 0.01	78.68

3.1.2 Nickel Aluminide

All samples required the addition of nickel aluminide (Ni_3Al) IC-50 powder, which was obtained from Ametek Specialty Metal Products (Eighty Four, PA, USA) (Lot #0412399). Ni_3Al provided the ductile metal binder phase within each sample, known to have relatively high yield strength, Young's modulus and density. The powder obtained contained the following chemical composition, as listed in Table 3–3, which was also verified using EDS analysis, confirming the information provided. SEM images were taken (Figure 3–2), to further verify the information given by the manufacturer.

Table 3–3 Composition of raw Ni_3Al powder from manufacturer

	Composition (wt %)			
Powder	Ni	Al	Zr	B
Ni_3Al	76.9	22.5	0.5	0.1

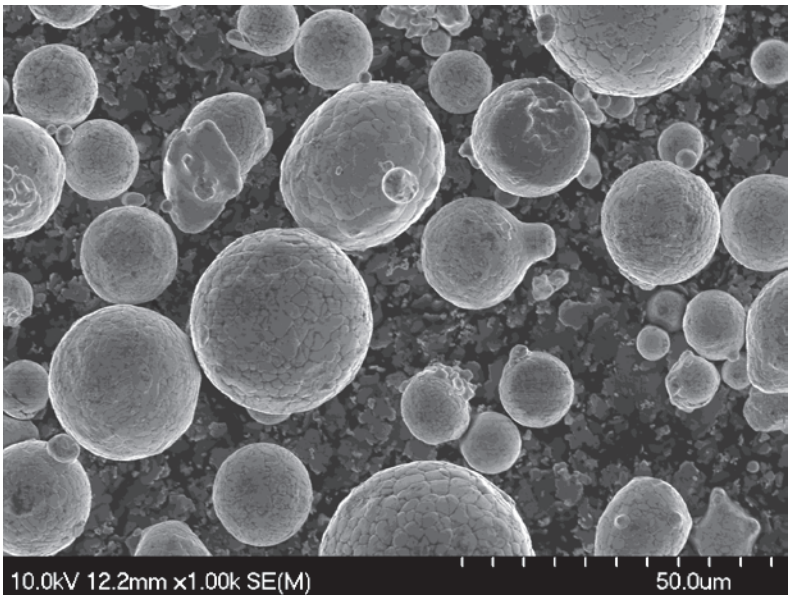

Figure 3–2 SEM image of Ni3Al raw powder

3.1.3 Compaction Binder

Ti(C,N) proved difficult to compact without the aid of an organic binder. Therefore 1 wt.% polyvinyl butyral (PVB) was incorporated into the powder mixtures prior to the ball milling process. The PVB was obtained from Solutia Inc., (St. Louis, MO, USA) and improved the compaction process. The mixture of powder plus PVB was then milled for 24 h followed by a 24 h drying period.

3.2 Experimental Procedure

This section will outline the procedures used to produce each sample, followed by the testing processes involved to analyze the electrochemical behaviour.

3.2.1 Sample Preparation

The Ti(C,N) powders proved difficult to compact, therefore the first step was to introduce 1 wt.% polyvinyl butyral (PVB) binder to the powder. This mixture was then combined with ~500 g of tetragonal zirconia polycrystal (TZP or t-ZrO_2) milling media, as well as

200 mL of acetone and then ball milled for 24 h at 45 rpm. Upon completion of milling the solution was poured into drying pans and left to dry for an additional 24 h. The resultant powder was caked to the drying pan and simply required breaking up and grinding with a mortar and pestle. The powder was then sieved to < 140 mesh. The TiC could be compacted as received and therefore did not require the additional binder.

Each powder sample was uniaxially pressed using a standard tabletop press. The cylindrical die was first coated with steric acid, which acts as a lubricant to ensure easy removal of the sample and no loss of form or integrity. The samples consisted of 7.5 g of powder in the die, as well as ~12 drops of hexane to improve lubrication and ease of compaction. The die was then assembled and a pressure of 45 MPa was applied and held for two minutes. A lever was used to ensure a very slow release of pressure upon completion, and the die was carefully disassembled, leaving the small, fragile disc of pressed powder. A vacuum sealer was then used to cover each sample in a double layer of plastic. Finally, each sample was further compressed by cold isostatic pressing (CIP), whereby a fluid encompasses the plastic-covered samples and applies uniform pressure, up to 220 MPa, for 2-3 min.

Measurements were taken of each green body prior to continuing with sample preparation. In doing so, calipers were used to measure the diameter and height of each sample. A balance was used to measure the sample weight to an accuracy of 10^{-4} g.

Following the CIP, each sample was ready for sintering and melt infiltration. Depending on the weight percent of nickel aluminide (Ni_3Al) to be studied, portions were weighed out accordingly. The Ni_3Al was then poured directly onto each sample immediately prior to sintering. The samples were placed within the vacuum furnace, which was held at ~20 milliTorr throughout the sintering process. The temperature was increased at a rate of 10 °C/min to 1500°C, after which it was held for one hour before cooling at a rate of 25 °C/min.

The fully infiltrated samples were then sent to a diamond grinder to flatten the samples and prepare for finer polishing. The polishing pads used thereafter include 125 μm to 15 μm diamond pads, followed by 9 μm to 1/4 μm diamond paste. Prior to each

corrosion experiment, each sample was placed in an ultrasonic bath to remove any residual debris or contaminants, and then dried.

3.2.2 Electrochemical Testing

The polished samples were affixed to a unit cell used for electrochemical testing, exposing an area of 1 cm^2. The cell was then filled with a freely aerated 3.5 wt% NaCl solution at room temperature. A platinum plate sat opposite the sample, acting as the counter electrode in the electrolytic cell, and a saturated calomel electrode (SCE, Ag|AgCl|KCl), obtained from Accument (SN01094027 P7), was placed in the uppermost portion of the cell acting as the reference electrode (-0.241 V versus the standard hydrogen electrode). Figure 3–3 shows the configuration of the cell, including an affixed sample and electrode connections.

Figure 3–3 Flat cell for electrochemical testing

Electrochemical instrumentation, comprised of a potentiostat (EG & G PARC Model 273A, Princeton Applied Research, USA), was used to perform open circuit potential and potentiodynamic tests concurrently on each sample. The machine utilizes a Xantrex DC power supply (0-100V, 0-28A), which is connected to a Solartron/Schlumberger 1250 Frequency Response Analyzer and interfaces with an associated computer running Corrware corrosion evaluation software supplied by Scribner Associates, Inc.

The first test establishes a state of equilibrium between the sample and the solution, without applying any current to the electrolytic cell, and provides a reading for the open circuit potential (OCP) of the sample. Once equilibrium is established, the potentiodynamic test begins collecting data by polarizing the sample to a cathodic potential of -500 mV, using a scan rate of 0.1667 mV/s, to 3000 mV.

Data obtained from electrochemical testing was analyzed using the Tafel extrapolation method, described as a more accurate method of calculating extremely low rates of corrosion over the conventional weight gain method,[32] as well as the computer software used with the Potentiostat equipment. The Tafel extrapolation method uses the curves developed by the Corrware software, and is reaffirmed through correlation with the raw data obtained, to deduce corrosion potential and corrosion rate, as illustrated in Figure 3–4.

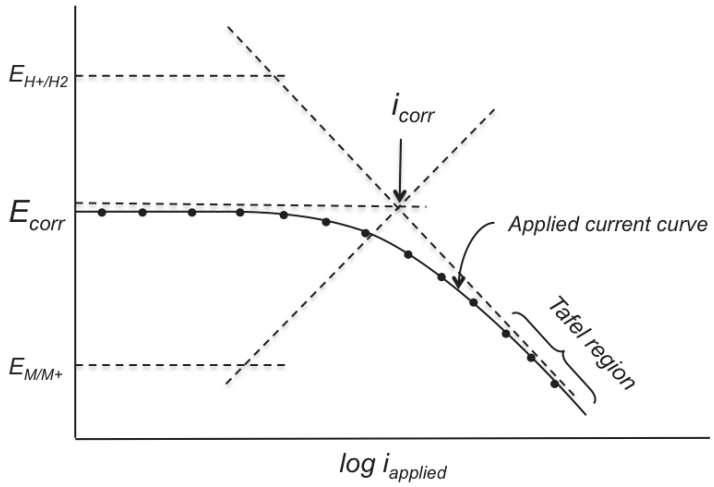

Figure 3–4 Applied current cathodic polarization curve showing Tafel extrapolation[32]

4 Results and Discussion

The following section includes an analysis of the base components of each sample prepared, including powder characterization by means of x-ray diffraction (XRD) and scanning electron microscopy (SEM). Furthermore, a calculation of each sample density following the melt infiltration process was performed. This information is supplemental to results presented in Chapter 5 and 6.

4.1 Powder Characterization

Each powder used was analyzed using SEM, XRD and energy-dispersive x-ray spectroscopy (EDS) to ensure accuracy to within the manufacturer's specifications for particle size, crystallographic structure, as well as chemical composition. SEM images of each powder sample were depicted previously, in Figure 3–3. Figure 4–1, shows the XRD results of each tested sample, confirming the same chemical composition provided by the manufacturers. Similarly, Figure 4–2 focuses on the area between 35 and 45 degrees, showing a slight shift along the x-axis, indicative of the increasing amounts of nitrogen causing expansion of the crystallographic structure.

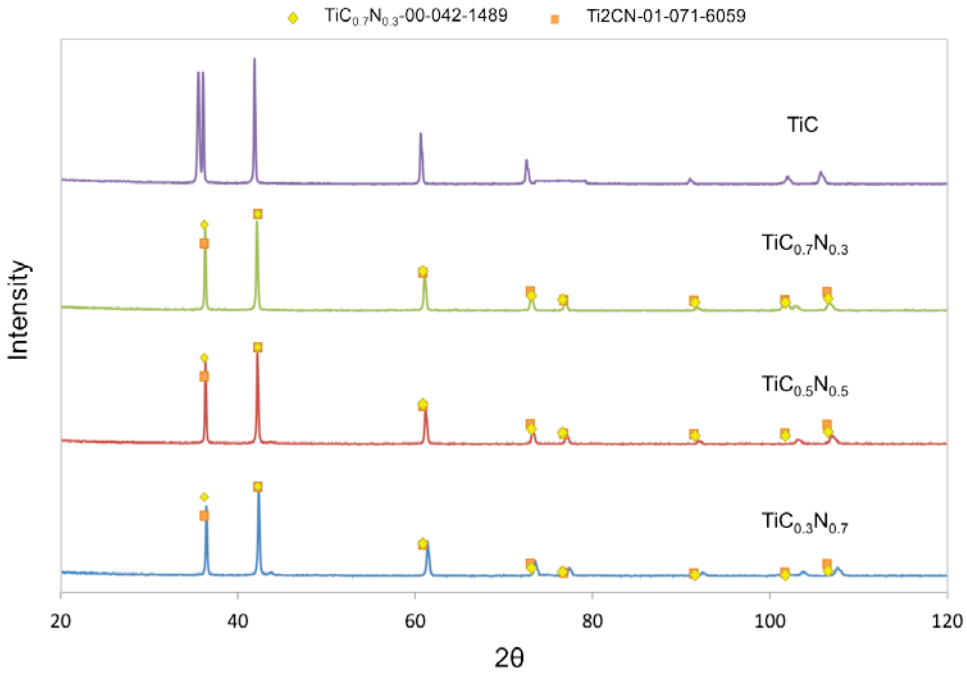

Figure 4–1 XRD results for TiC_xN_{1-x} starting powders

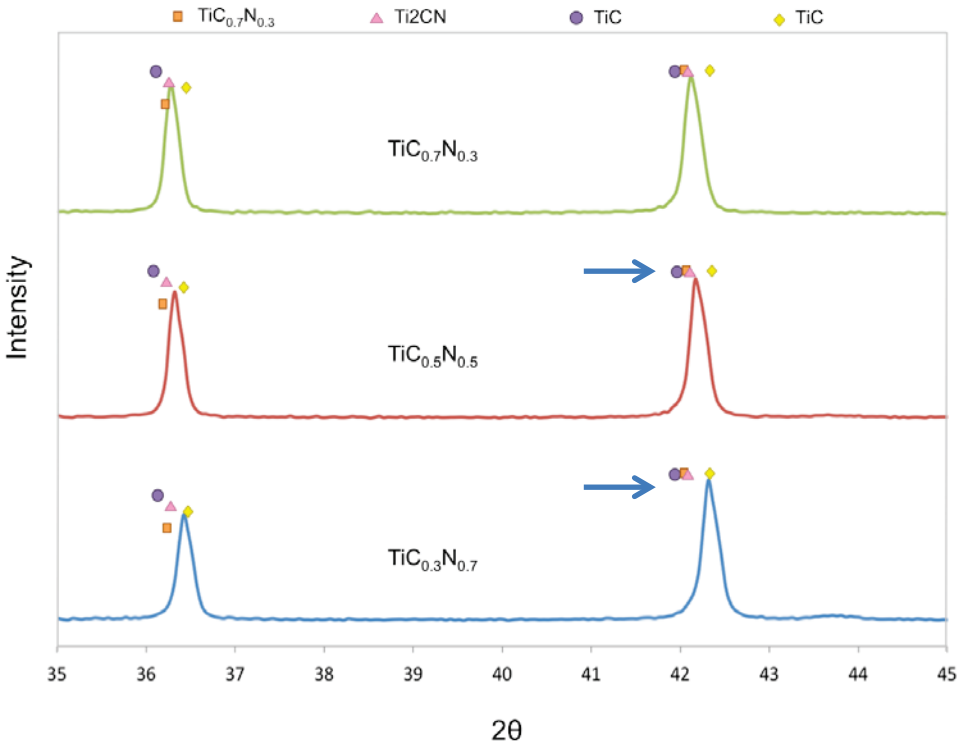

Figure 4–2 XRD results for TiC_xN_{1-x} and TiC starting powders, from 35 – 45 degrees.

4.2 Density Measurements

The density of each sample was determined using the Archimedes principle. Each sample density was then compared to its theoretical density, as demonstrated in Figure 4–3 and Figure 4–4.

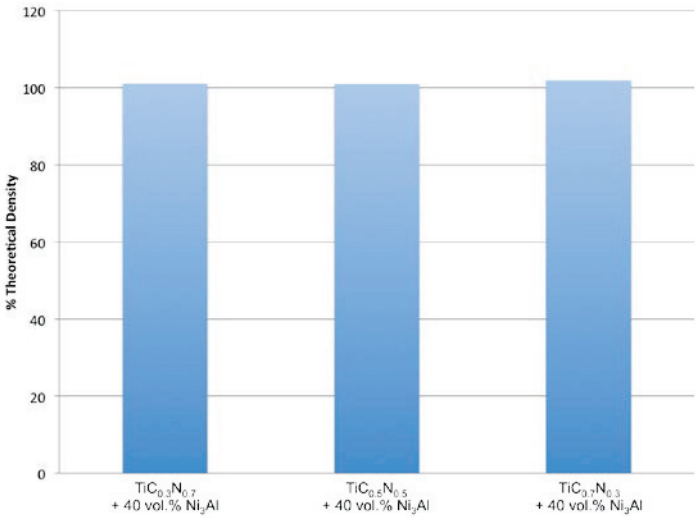

Figure 4–3 Density of TiC_xN_{1-x} samples as a percentage of theoretical density

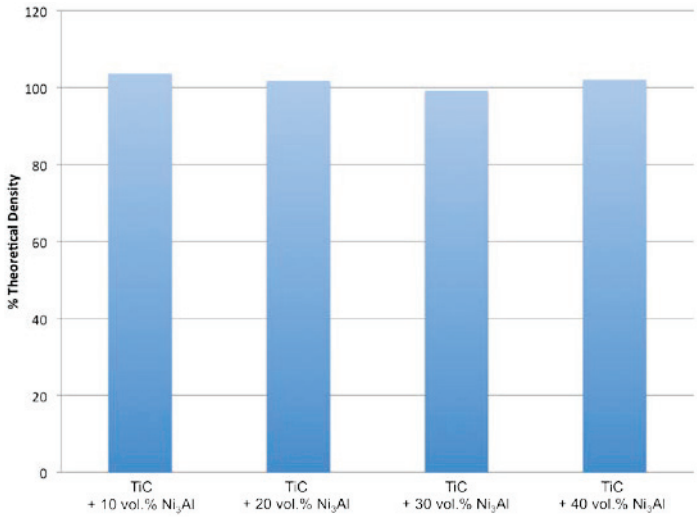

Figure 4–4 Density of TiC samples as a percentage of theoretical density

The majority of densities were in the range of 99% to 102% of theoretical density. The reason for this is conjectured to be the varied stoichiometric quantities of both Ni and B in the Ni_3Al binder powder as received from the manufacturer, having received an alloy (IC-50) and not stoichiometric Ni_3Al.

4.3 Microstructure characterization

Following the sintering process, characterization of each samples' microstructure was conducting, including using the linear intercept method to establish average grain size, with results indicated in Table 4–1. SEM images (depicted in Chapter 5 and Chapter 6 for Ti(C,N) and TiC, respectively) demonstrate the typical intermittent Ni_3Al binder with Ti(C,N) and TiC grains throughout. The average grain size for each sample following the melt infiltration and sintering processes indicate increasing grain size with increasing Ni_3Al in the TiC samples and with increasing carbon content in Ti(C,N) samples. This is in agreement with previous work establishing similar findings both with TiC cermets, as well as WC-Co based hardmetals.[65]

Table 4–1 Mean grain size of TiC and Ti(C,N) samples

Sample	Mean Grain Size (μm)
TiC + 10 vol.% Ni_3Al	4.36 ± 0.74
TiC + 20 vol.% Ni_3Al	4.37 ± 0.71
TiC + 30 vol.% Ni_3Al	5.02 ± 0.93
TiC + 40 vol.% Ni_3Al	5.65 ± 1.25
$TiC_{0.3}N_{0.7}$ + 40 vol.% Ni_3Al	2.47 ± 0.44
$TiC_{0.5}N_{0.5}$ + 40 vol.% Ni_3Al	2.55 ± 0.51
$TiC_{0.7}C_{0.3}$ + 40 vol.% Ni_3Al	3.01 ± 0.66

5 Electrochemical Behaviour of Ti(C,N)-Ni_3Al Cermets

M. Holmes, G.J. Kipouros, Z.N. Farhat and K.P. Plucknett*

Dalhousie University, Materials Engineering Program, Department of Process Engineering and Applied Science, 1360 Barrington St., Halifax, Nova Scotia, CANADA

Abstract

TiC_xN_{1-x} (with x = 0.7, 0.5 and 0.3) cermets were successfully prepared with 40 vol.% Ni_3Al metallic binder, using a simple melt-infiltration sintering process. In order to assess their susceptibility to electrochemical corrosion, the polished cermets were then evaluated immersed in a 3.5 wt.% NaCl solution. An increasing corrosion current density was observed with increasing carbon content. However, there also appear to be greater areas of passivation/repassivation with increasing carbon content, suggesting that although the lower carbon content samples displayed a predisposition to corrosive attack, they were more suited to withstand that attack, conjectured to be a result of protective titanium oxide formation. Crevice corrosion was observed with each sample, demonstrating an increasing degree of formation of crevices with rising carbon content.

5.1 Introduction

Titanium carbonitride ($Ti(C_xN_{1-x})$) based ceramic-metal composites, or cermets, have found numerous industrial applications due to their notable properties, such as high strength, high hardness, good thermal conductivity and strong resistance to both wear and corrosion. TiC_xN_{1-x} cermets have been extensively developed during the past 40 years, especially as cutting tools,[1] and have proven to significantly prolong tool life and outperform WC-based hardmetals in ongoing research into their application as coatings.[2] Specifically, as compared with commonly used WC-based hardmetals, $Ti(C_xN_{1-x})$ cermets have shown increased hardness and toughness, as well as better resistance to corrosion, while offering significantly lower densities.[2]

Considerable research has surrounded the potential for $Ti(C_xN_{1-x})$ cermets to be fabricated with tailored properties, such as the percent composition of TiC and TiN within the composite, as well as the type and amount of binder alloy additions chosen. For example, it has been shown that the addition of metal binders such as Ni, Co or Fe as well as carbides such as WC, Tac, HfC and NbC can significantly improve toughness.[3] Similarly, experiments have been performed to demonstrate the effects of varying the stoichiometric quantities of TiC and TiN (i.e. the overall C:N ratio), in conjunction with varying binder elements, on the mechanical, tribological and wear properties.[1,2,4-7]

Comparatively little research has been conducted on the corrosion resistance of $Ti(C_xN_{1-x})$ cermets, specifically the aqueous corrosion response at ambient temperature. Studies on the susceptibility of $Ti(C_xN_{1-x})$ cermets to oxidation at high temperature have demonstrated the predicted formation of a protective oxide layer, TiO_2-based scales, however, significant degradation and microstructural changes have also been observed.[3] The limited studies on aqueous corrosion have shown a decreased capacity to withstand corrosion due to the inclusion of metal binders,[3] further demonstrating preferential attack and selective dissolution of the metallic phase, leaving a ceramic skeleton, as noted for other cermet systems.[8,9-13] In comparison, typical WC-Co based hardmetals have demonstrated selective dissolution of the Co component, with significant pullout of WC grains, despite the material's inherent capacity to pseudo-passivate at high potentials.[9]

Being able to tailor the chemical composition of the product with metal binder alloying additions to retain the favourable mechanical properties, while maintaining an acceptable degree of corrosion resistance is a highly anticipated goal in the continued research into these unique cermets.

In the present work, a series of novel $Ti(C_xN_{1-x})$-based cermets, with ductile nickel aluminide (Ni_3Al) binders, have been prepared using a simple melt infiltration process. The cermets were then characterized using a variety of electrochemical tests to assess their potential to corrosion resistance.

5.2 Materials and Methods

5.2.1 Sample Preparation and Characterization

The samples used for electrochemical testing were prepared using three commercially obtained grades of $Ti(C_xN_{1-x})$ powder, namely $Ti(C_{0.3}N_{0.7})$ (lot #L25747; D_{50} = 1.72 μm), $Ti(C_{0.5}N_{0.5})$ (lot #L29865; D_{50} = 1.74 μm) and $Ti(C_{0.7}N_{0.3})$ (lot #L25809; D_{50} = 2.10 μm); all of the $Ti(C_xN_{1-x})$ powders were sourced from Treibacher Industrie AG (Althofen, Austria). The powders were first ball-milled for 24 h with 1 wt. % polyvinyl butyral (PVB) wax, which aided in the subsequent compaction process, and acetone. The powders were then left to dry for an additional 24 h and upon completion were sieved to 140 mesh. Disc-shaped samples (31,75 mm diameter and ~4 mm thick) were then uniaxially pressed to ~45 MPa in a hardened steel die. The samples were vacuum-sealed in plastic and cold isostatically pressed (CIPed) to ~220 MPa. Prior to the melt infiltration and sintering processes, the samples were placed in alumina crucibles on a bed of bubble alumina. Based on the $Ti(C_xN_{1-x})$ pellet mass, an appropriate amount of Ni_3Al powder (325 mesh; alloy IC-50; Ametek, Eighty Four, PA, USA), corresponding to 40 vol.% metallic binder in the final sample, was then placed on top. Each sample was sintered in a vacuum furnace, evacuated to ~20 milliTorr, which is maintained essentially constant throughout the process. The temperature cycle employed included a ramp up to 1500°C, at a rate of 10°C/min, held for 1 h after which the samples were cooled at a nominal rate of 25°C/min

(below ~900°C a natural furnace cool was observed). The final samples prepared include $Ti(C_{0.3}N_{0.7})$, $Ti(C_{0.5}N_{0.5})$ and $Ti(C_{0.7}N_{0.3})$ all with 40 vol.% Ni_3Al.

Following melt infiltration, the density was determined by means of the Archimedes immersion method in water. Prior to the final assessment, each sample was ground using a surface grinder with a diamond peripheral wheel, to ensure that they were suitably flat for electrochemical testing. Subsequent to this they were ground and polished using successively finer grades of diamond embedded pads (125 to 15 μm) and diamond pastes (9 to ¼ μm). Final sample cleaning was performed in acetone within an ultrasonic bath. The microstructure of polished and electrochemically tested samples was analysed using a scanning electron microscope (SEM; Model S-4700, Hitachi High Technologies, Tokyo, Japan). The mean grain size was determined from the polished surfaces using the lineal intercept method.[14]

5.2.2 Electrochemical Testing Procedure

For corrosion testing each of the cermet samples was individually assessed using a standard electrochemical cell, with all testing performed using a potentiostat. The test cell contains a platinum electrode and a saturated calomel electrode is also attached, which acts as the reference electrode (-0.241 V versus a standard hydrogen electrode). To begin, an open-circuit potential (OCP) test is conducted to establish equilibrium between the sample and 3.5 wt% NaCl aqueous solution within which a 1 cm^2 area of the polished sample surface is immersed. The test lasts for 2 h, by which time equilibrium has been reached and each OCP value is recorded. Directly upon completion, the potentiodynamic test begins, which applies a cathodic potential to the cell and reads the resultant current, as the potentiostat scans from -0.5 V to 3 V at a scan rate of 0.1667 mV/s. Each sample is then examined using the SEM to determine the state of the cermet following electrochemical testing. Additionally, samples of the remaining NaCl solution were analyzed for compositional modification using inductively coupled plasma optical emission spectroscopy (ICP-OES; Varian Vista-Pro CCD Simultaneous ICP-OES).

5.3 Results and Discussion

5.3.1 Sample Analysis

The process of melt infiltration was successfully achieved for all the $Ti(C_xN_{1-x})$ samples, as demonstrated by the SEM analysis conducted prior to electrochemical testing, and shown in Figure 5–1. It is evident from the micrographs that the results are generally comparable in terms of grain size and degree of densification; however it is also apparent that grains with a slightly less cubic morphology were developed in samples with a higher carbon content, namely the $Ti(C_{0.7}N_{0.3})$ samples, which also exhibit slightly coarser grain size. These general observations demonstrate that the melt infiltration/sintering process does not drastically alter the cubic particle shape of the original $Ti(C_xN_{1-x})$ particles following the addition of Ni_3Al,[14] which will be dictated by the balance of surface energies,[15] and the Ni_3Al successfully infiltrates the porous aggregate of particles and forms a binding matrix throughout. Immersion density measurements indicated that all samples achieved densities ranging from 98-100% theoretical density.

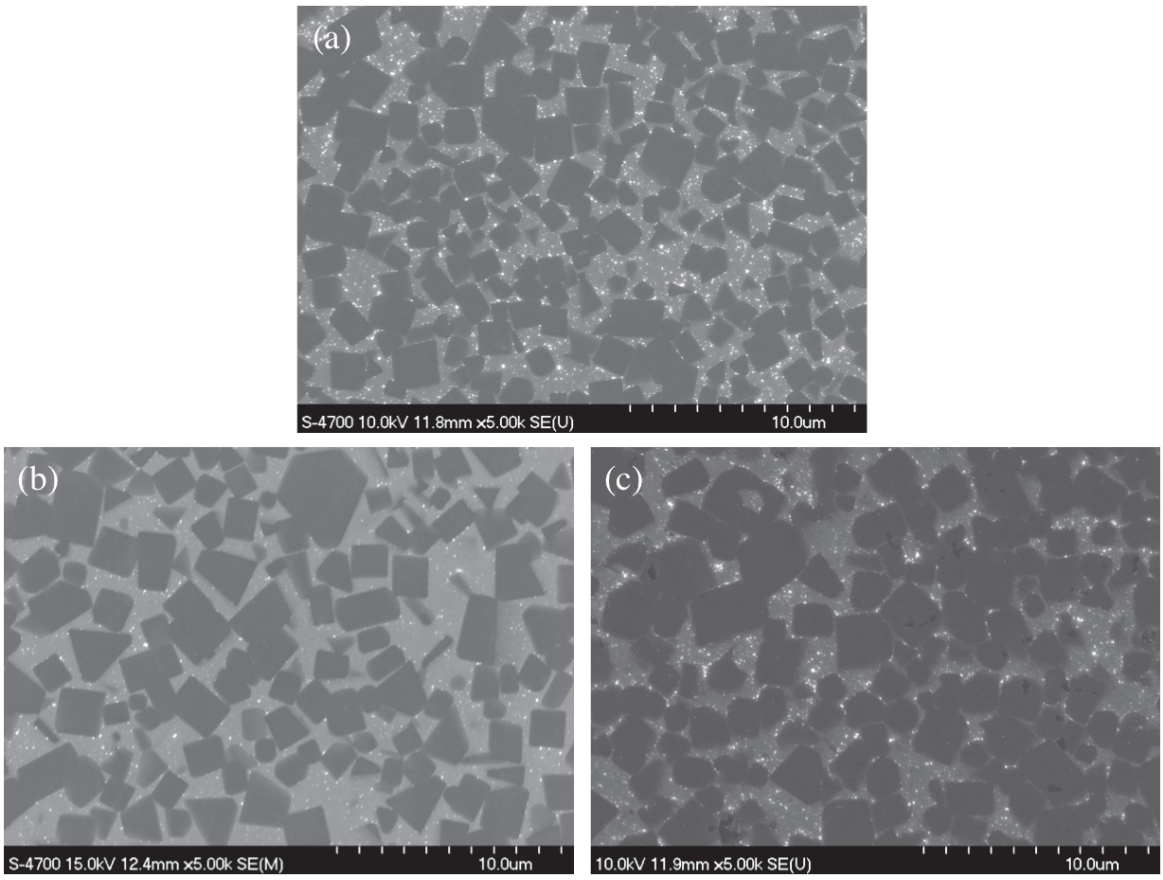

Figure 5–1 SEM micrographs of (a) $TiC_{0.3}N_{0.7}$ (b) $TiC_{0.5}N_{0.5}$, (c) $TiC_{0.7}N_{0.3}$ polished samples

5.3.2 Electrochemical Testing

Prior to any corrosion testing, namely prior to applying a current to the sample, each sample must be evaluated for its OCP, also known as the zero current potential (ZCP). The OCP is a measure of a material's tendency to oxidize in a given corrosive environment. Equilibrium must be established between the two terminals, in this case the working sample and the unit cell electrode, to evaluate the oxidizing power of the aqueous solution in which it is immersed, in this case 3.5 wt.% NaCl. A platinum electrode was used in this three-electrode test representing a stable electrode, meaning that any changes in potential thereafter will be attributed to reactions taking place at the sample and solution interface. The third electrode used was a saturated calomel electrode (SCE) with a potential of -0.241V. Figure 5–2 demonstrates the OCP established for each test sample.

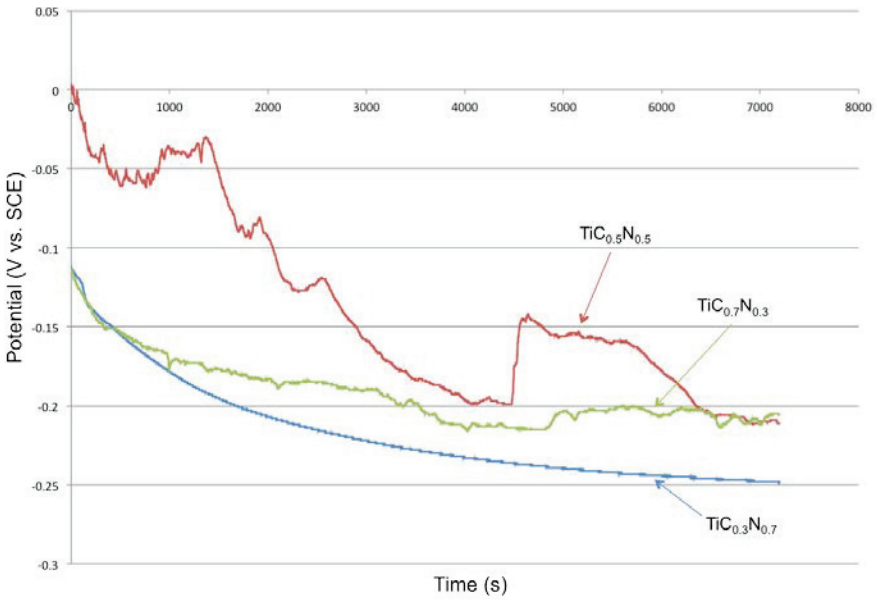

Figure 5–2 Open circuit potential results of Ti(C, N) samples

The gradual decline in potential suggests the working sample may already be undergoing a subtle reaction with the aqueous solution in which it is immersed.[16] In this instance, there is the potential for an early oxide layer, TiO_2, with the possibility of additional metal oxides, to begin forming on the surface. Generally a steady decline in potential indicates a decreasing resistance to corrosion, which based upon the remainder of electrochemical data accumulated, is in agreement with the overall response of the $TiC_{03}N_{0.7}$ sample to corrosion. Although the results of this test were consistent for each sample analyzed, the ability to replicate very similar curves was difficult, suggesting variations among samples, specifically the degree to which polishing as well as the surface finishing may have a relatively large impact on the obtainability of a smooth curve. For this reason the inconsistency within the trending $TiC_{0.5}N_{0.5}$ may be attributed to surface irregularities.

Potentiodynamic polarization curves for each Ti(C,N)-cermet sample are demonstrated in Figure 5–3 and Figure 5–4, depicting the comparative results of all three samples directly. The multiple curves, depicted in Figure 5–3 (a-c), indicate the reproducibility of results for each individual sample and unique composition, as shown by the dotted lines depicting the repeated experiments.

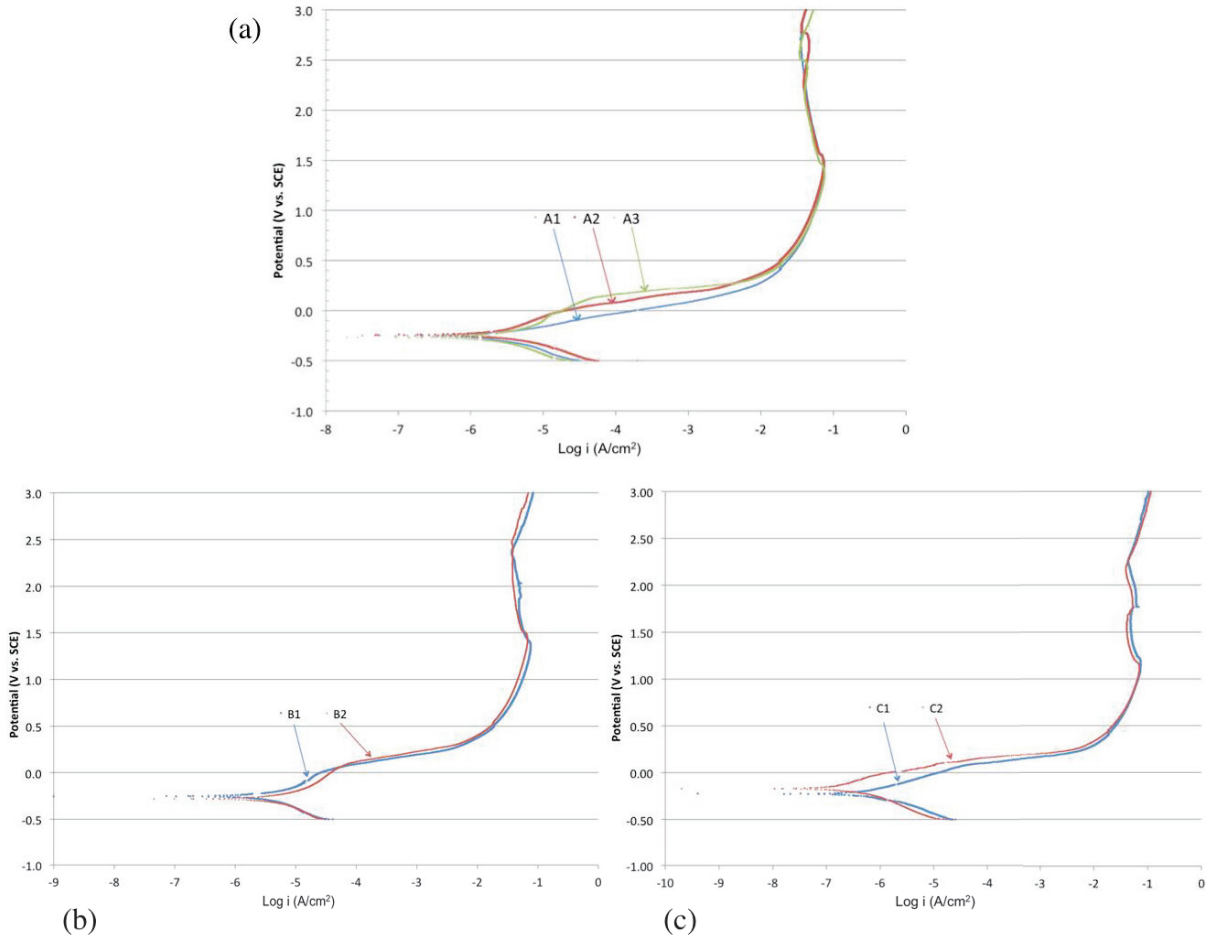

Figure 5–3 Potentiodynamic polarization plots of (a) $TiC_{0.3}N_{0.7}$ samples (b) $TiC_{0.5}N_{0.5}$ samples, (c) $TiC_{0.7}N_{0.3}$ samples.

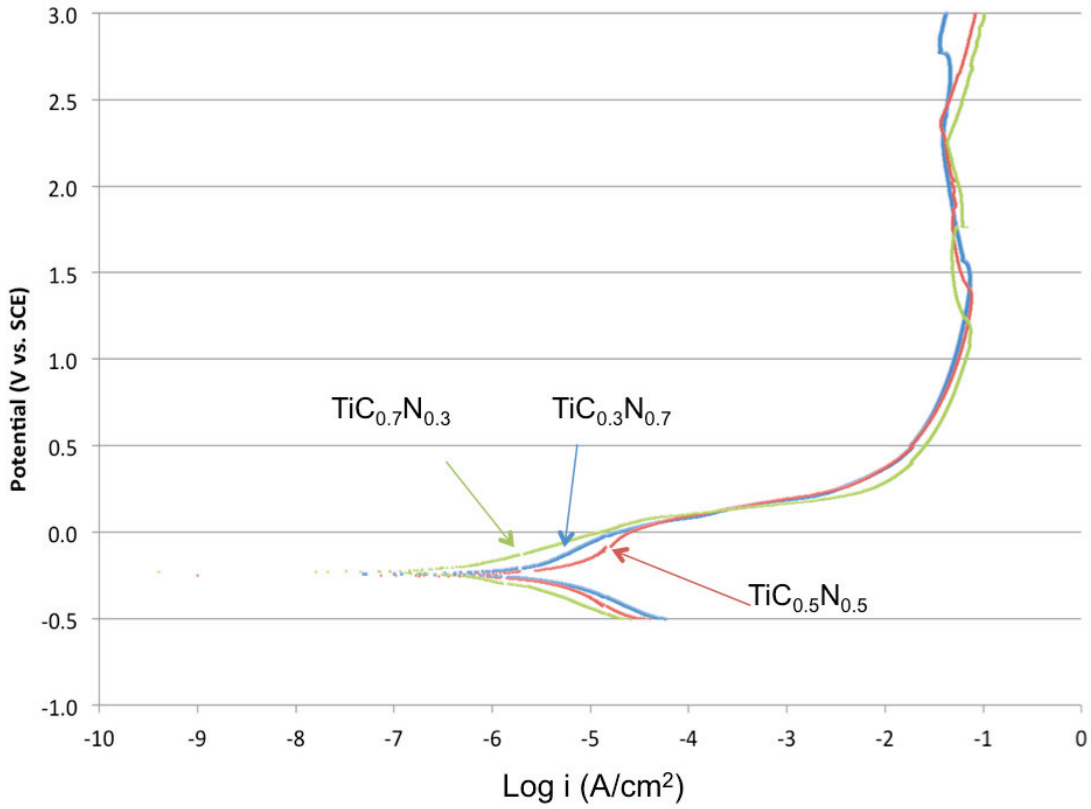

Figure 5–4 Potentiodynamic polarization plot of combined $TiC_{0.3}N_{0.7}$, $TiC_{0.5}N_{0.5}$ and $TiC_{0.7}N_{0.3}$ samples.

Tabulated results of significant values, including open circuit potential (OCP), corrosion potential (E_{corr}), corrosion current density (i_{corr}), are outlined in Table 5–1. These results were obtained using the Tafel extrapolation method, which has been demonstrated to be equal to if not better than the standard method of weight gain measurement.[17]

Table 5–1 Results of electrochemical corrosion testing

Sample	OCP (V vs. SCE)	E_{CORR} (V vs. SCE)	i_{CORR} ($\mu A/cm^2$)
$TiC_{0.3}N_{0.7}$	-0.205 (0.043)	-0.250 (0.005)	1.49 (0.878)
$TiC_{0.5}N_{0.5}$	-0.236 (0.032)	-0.224 (0.018)	1.21 (0.664)
$TiC_{0.7}N_{0.3}$	-0.173	-0.197	0.248
** Values are mean (standard deviation), N=3			

As a general rule, as E_{corr} and E_b decrease there is an increase in corrosion behaviour and associated response.[18] Alternately, as i_{corr} and i_{crit} increase there is accelerated corrosion behaviour. As can be seen in Figure 5–3 and Figure 5–4, as well as Table 5–1, both i_{crit} and i_{corr} decrease with increasing amounts of carbon (and corresponding increasing amounts of nitrogen). Furthermore, E_{corr} values show a tendency to increase with increasing carbon content. This is indicative of an increasing tendency to withstand corrosion, demonstrating that between the three tested samples $TiC_{0.7}N_{0.3}$ shows the greatest potential to withstand corrosion, with $TiC_{0.3}N_{0.7}$ being the most susceptible to corrosion. It should be noted, however, that although there is a tendency to corrode, all samples have demonstrated values of i_{corr} that are significantly low, suggesting the overall ability to withstand corrosion among this group of cermets remains high. As there is no difference between the samples' binder content (40 vol.% Ni_3Al), a conclusion can be made in terms of the effect of varying stoichiometric quantities of both C and N having a direct effect on the material's ability to withstand corrosion. It is speculated that the resistance to corrosion could be in part due to any residual porosity of the sample; for this study, $TiC_{0.7}N_{0.3}$ samples did have the greatest mean density as a percentage of theoretical density, though theoretical densities are such that the inverse is true. A $Ti(C_xN_{1-x})$ sample with low porosity, independent of the type of metal binder and method of fabrication, is believed to limit the potential for infiltration into the sample and ultimately reduce the potential for pitting corrosion.[19-20]

Typical active-passive behaviour, as well as a clearly defined region of passivation, can be seen with each potentiodynamic curve. Results also demonstrate the tendency for each sample to passivate, followed by breakdown of the region of passivation and in some cases repassivation, data for which can be found in Table 5–2. An interesting result of the passivation criteria is that although $TiC_{0.7}N_{0.3}$ displays better response in terms of capacity to resist corrosion, it shows an overall small region within which it undergoes passivation. For all cases, the region of potential greater than 1 V shows multiple areas of passivation, breakdown, and repassivation. This is believed to give rise to the multiple areas of significant crevice and pitting corrosion noted in the SEM analysis that follows.

Table 5–2 Passivation criteria for Ti(C, N) samples

Sample	E_{PP} (V vs. SCE)	$E_{bp}1$ (V vs. SCE)	$E_{bp}2$ (V vs. SCE)	Passive range1 (V vs. SCE)	Passive range2 (V vs. SCE)	Total Passive Range (V vs. SCE)
$TiC_{0.3}N_{0.7}$	0.48	1.51 (0.058)	2.66	1.06	1.12	2.18
$TiC_{0.5}N_{0.5}$	0.52	1.38 (0.057)	2.42	0.93	0.99	1.92
$TiC_{0.7}N_{0.3}$	0.44	1.12	2.22	0.38	1.07	1.45

This demonstrates that the breakdown potential decreases with increasing carbon content, and the range of passivity decreases with increasing carbon content. This shows a greater tendency to transition from transpassivity with increasing carbon content, which can lead to an increasing tendency towards pitting. This also indicates a distinctively overall broader passive region observed in samples with lower carbon content. It is also evident, however, that the increasing carbon content samples demonstrate a greater tendency to repassivate at approximately 2.4 V versus the lowest carbon content Ti($C_{0.3}N_{07}$) samples, which show this occurrence taking place at approximately 2.7 V.

Following the electrochemical testing, all of the samples were analyzed using SEM, with the aim of assessing the associated microstructural changes that have occurred as a result of the testing. The corrosion behaviour exhibited by each sample, namely pitting and/or crevice corrosion, can be seen in Figure 5–5 through Figure 5–8. Figure 5–5 (a) demonstrates the significant corrosion that is taking place in the high nitrogen content samples, with preferential attack of the Ni_3Al binder and apparent crack formation at the interface between the $TiC_{0.3}N_{0.7}$ grains and the binder. Further analysis shows the developing corrosion, resulting in significant attack of the Ni_3Al binder and the creation of nominally loose $TiC_{0.3}N_{0.7}$ particles, as evident in Figure 5–5 (b) and (c). Finally, Figure 5–5 (c) and (d) demonstrate the sample edge being corroded away, leaving the original cubic grains exposed. The images show the remnant sample surface on the left side, with a scale of NaCl solution visible on the surface, and the area of targeted attack clearly visible on the right. These results indicate, as mentioned, a preferential attack on

the binder phase and then what is believed to be targeted dissolution occurring throughout the transpassive regions.

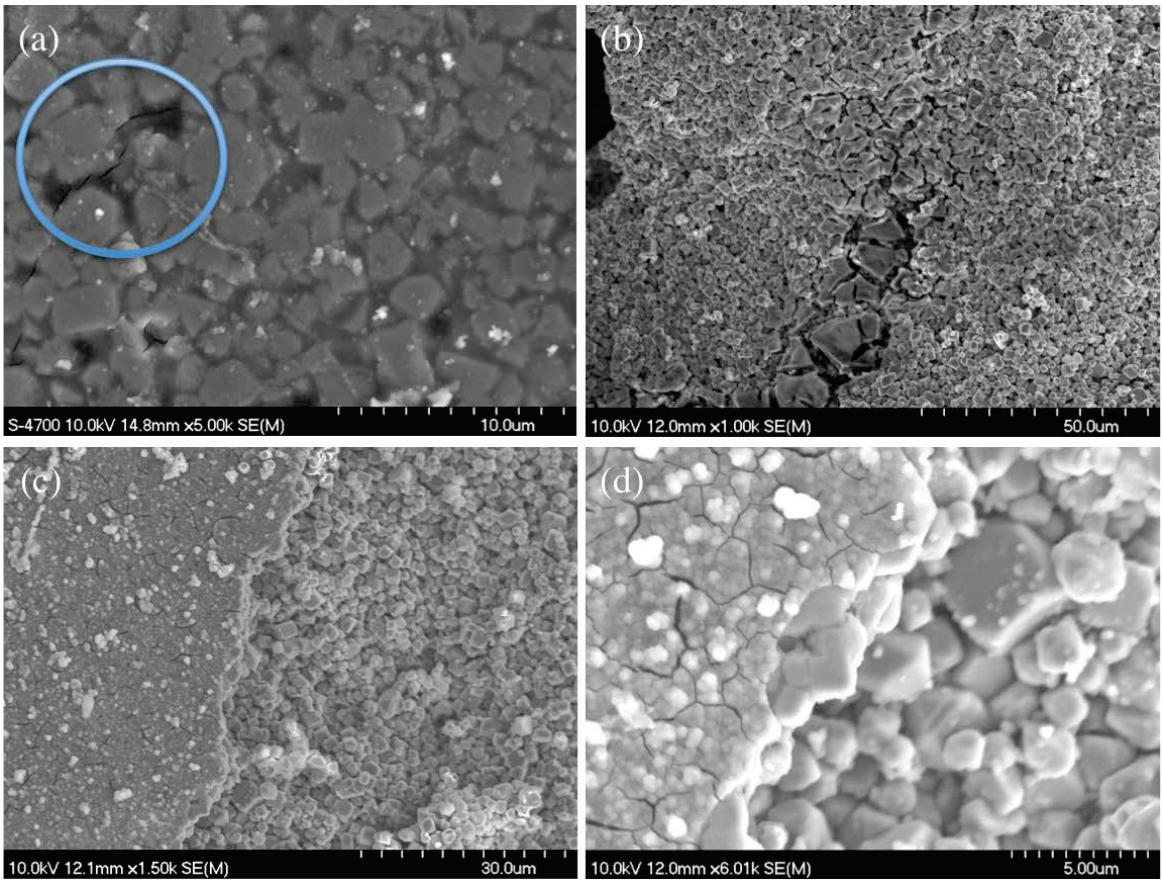

Figure 5–5 Post-corrosion testing SEM micrographs of $TiC_{0.3}N_{0.7}$ samples

Similar results can be viewed in Figure 5–6, for samples with an equivalent atomic ratio (i.e. 1:1) of carbon and nitrogen, as the same pitting and crevice corrosion is giving way to nominally binder-free $TiC_{0.5}N_{0.5}$ grains. Figure 5–6 (a) through (d) all show the development of the preferential Ni_3Al attack, with polished surfaces still visible while the Ni_3Al binder remains intact. This sample demonstrated a reduced appearance of deep crevices; instead revealing numerous pockets of pitting, intermixed amongst regions of untouched polished surfaces. Figure 5–6 (d) shows what appears to be evidence of intragranular remnants of the Ni_3Al binder phase, more notably depicted with increased magnification, shown in Figure 5–7.

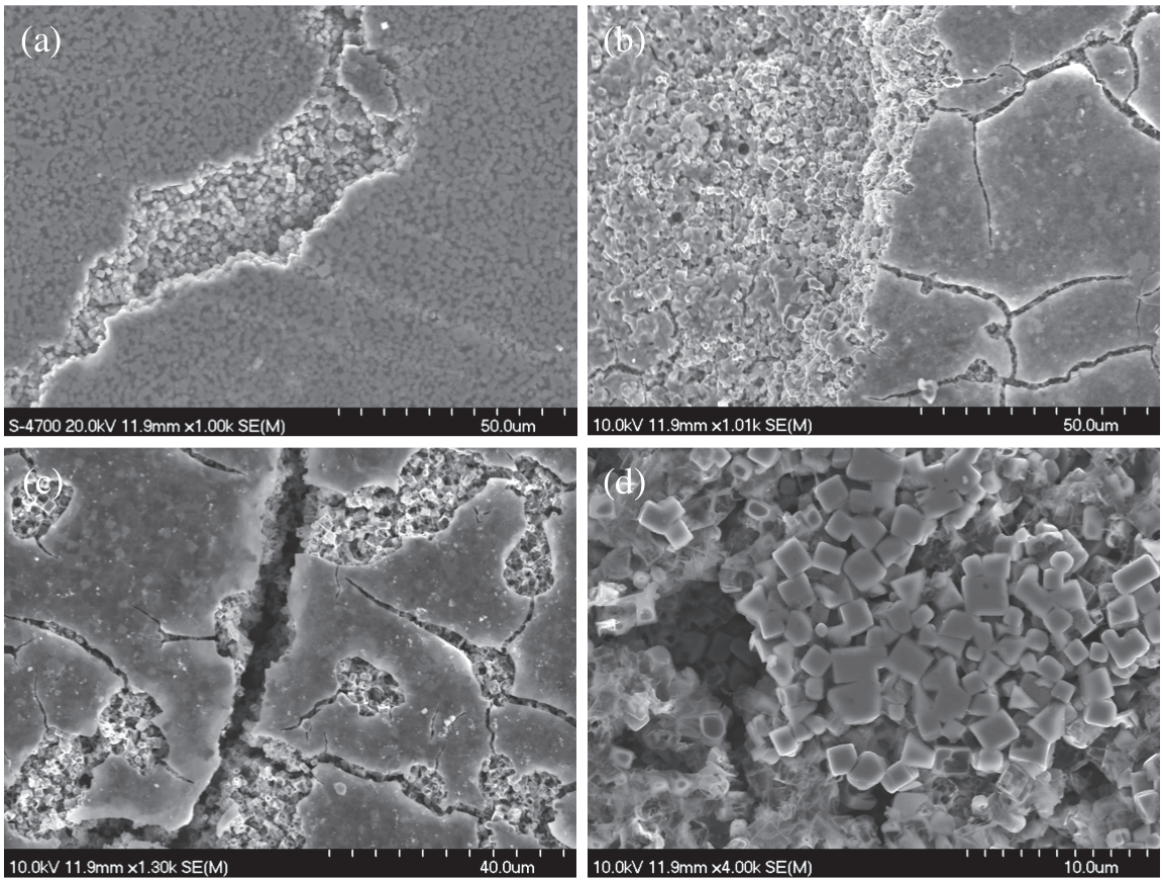

Figure 5–6 Post-corrosion testing SEM micrographs of $TiC_{0.5}N_{0.5}$ samples

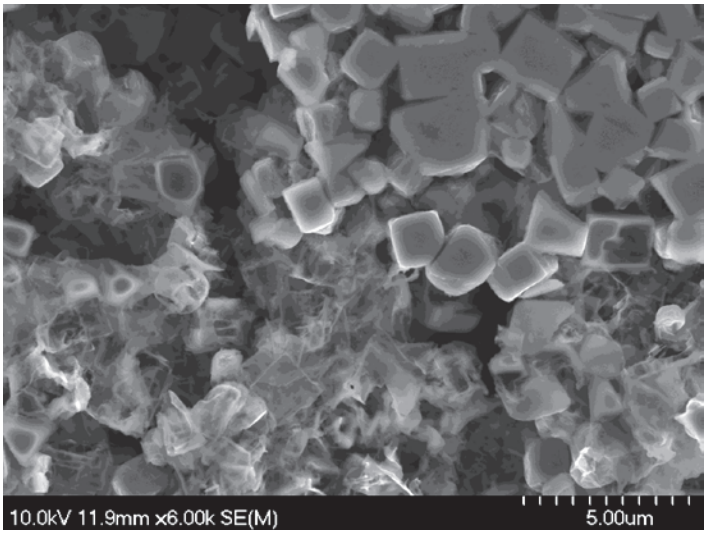

Figure 5–7 SEM micrographs of corrosion surface of $TiC_{0.5}N_{0.5}$ sample.

SEM images of the $TiC_{0.7}N_{0.3}$ samples after corrosion testing, shown in Figure 5–8, demonstrate similar results to the previous samples, with deep crevices appearing intermittent throughout areas of residual polished surfaces. Similar to the observations with the other samples, there appear to be areas of complete degradation, leaving $TiC_{0.7}N_{0.3}$ grains intact throughout. $TiC_{0.7}N_{0.3}$-Ni_3Al cermets, as indicated through the electrochemical testing data, demonstrate a greater ability to resist corrosion. However, this is coupled with a lower total region of passivation and seemingly more regions of breakdown and transpassivation. As evidenced by SEM imaging, specifically Figure 5–8 (b), crevice corrosion appears to be more marked and has significantly greater penetration when compared to the $TiC_{0.3}N_{0.7}$ and $TiC_{0.5}N_{0.5}$ cermet samples. This suggests a greater tendency to achieve repassivation, most probably a result of the recurring breakdown and passivation giving way to subsequent TiO_2 development as the Ni_3Al is preferentially attacked.

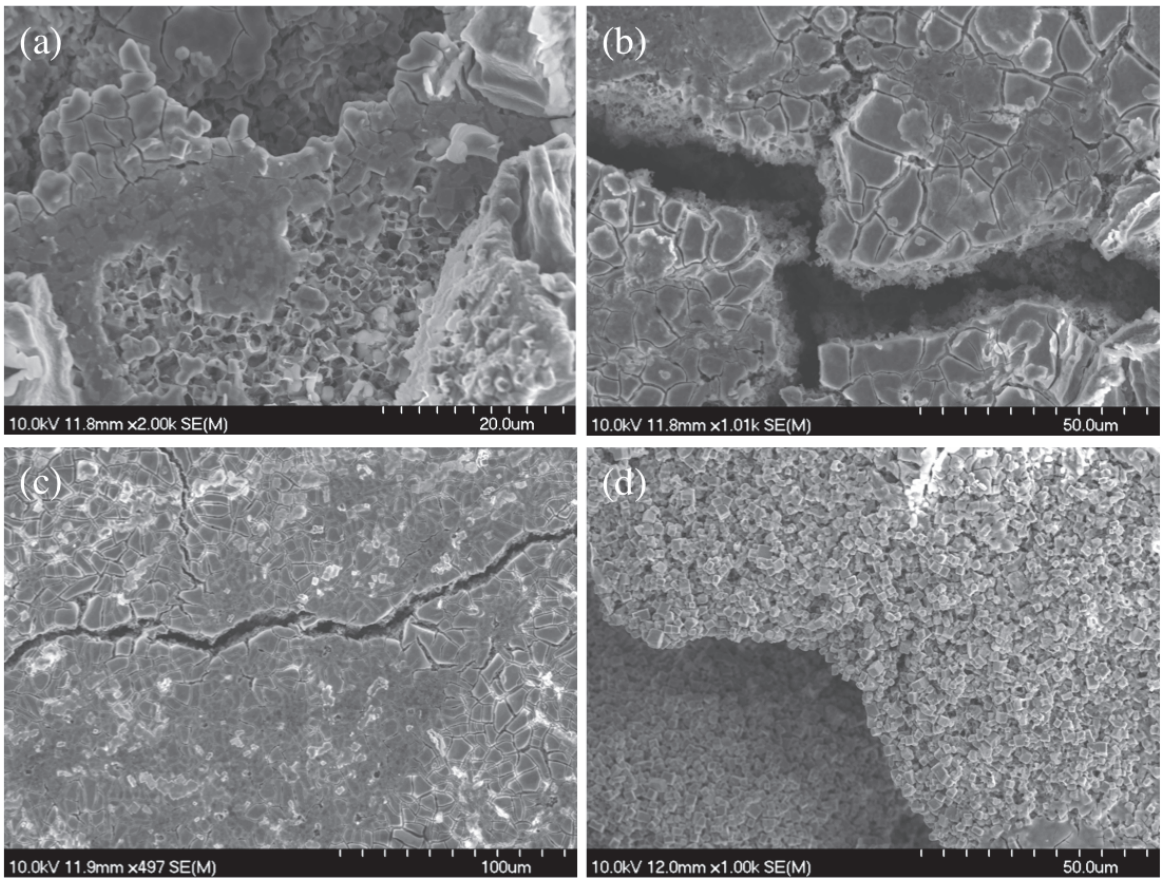

Figure 5–8 Post-corrosion testing SEM micrographs of $TiC_{0.7}N_{0.3}$ samples

Further SEM analysis revealed areas that exemplified the notion of the constant passivation/repassivation, as shown in Figure 5–9. There are clear indications of significant pitting and crevice corrosion taking place.

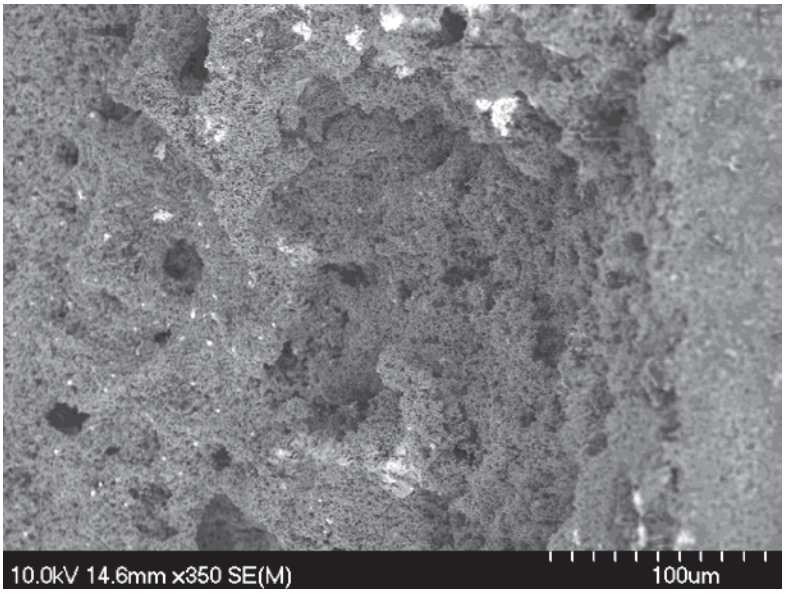

Figure 5–9 SEM image of $TiC_{0.7}N_{0.3}$ sample following corrosion testing, showing unique areas of pitting and crevice corrosion

A notable observation of the $TiC_{0.7}N_{0.3}$ samples following corrosion was the apparent grain pull-out taking place in a few selected areas, as shown in Figure 5–10. There appear to be sections indicating complete removal of the original $TiC_{0.7}N_{0.3}$ grains, however in this instance the Ni_3Al binder matrix phase remains intact. This behaviour is not evident in any of the other compositions tested.

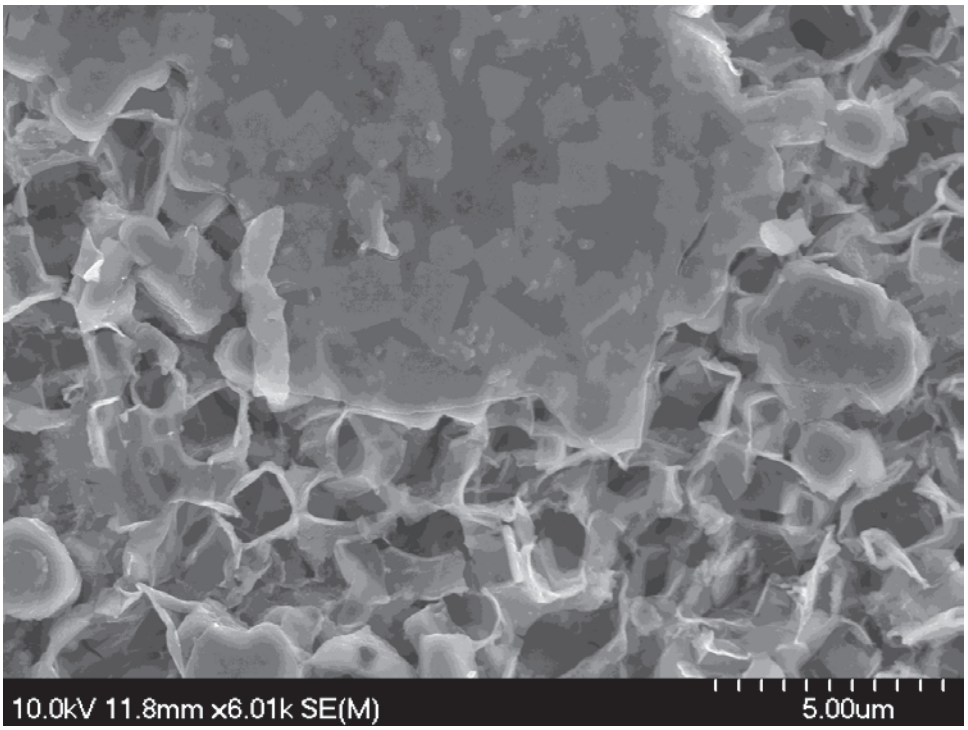

Figure 5–10 SEM image of $TiC_{0.7}N_{0.3}$ following corrosion testing, showing grain removal.

Further analysis of each sample was conducted using EDS. Results, shown in Figure 5–11, indicate a relative increase in titanium content remaining within the sample with increasing carbon content. Furthermore, there is a decrease in Al, Ni, N and C present. This information conflicts with the experimental data, which suggests the $TiC_{0.7}N_{0.3}$ shows better resistance to corrosion, demonstrating instead that there is less metal binder remaining throughout the sample. This information agrees, however, with the suggestion that the repeated passivation and repassivation could lead to reoccurring protective oxide formation followed by significant breakdown leading to dissolution.

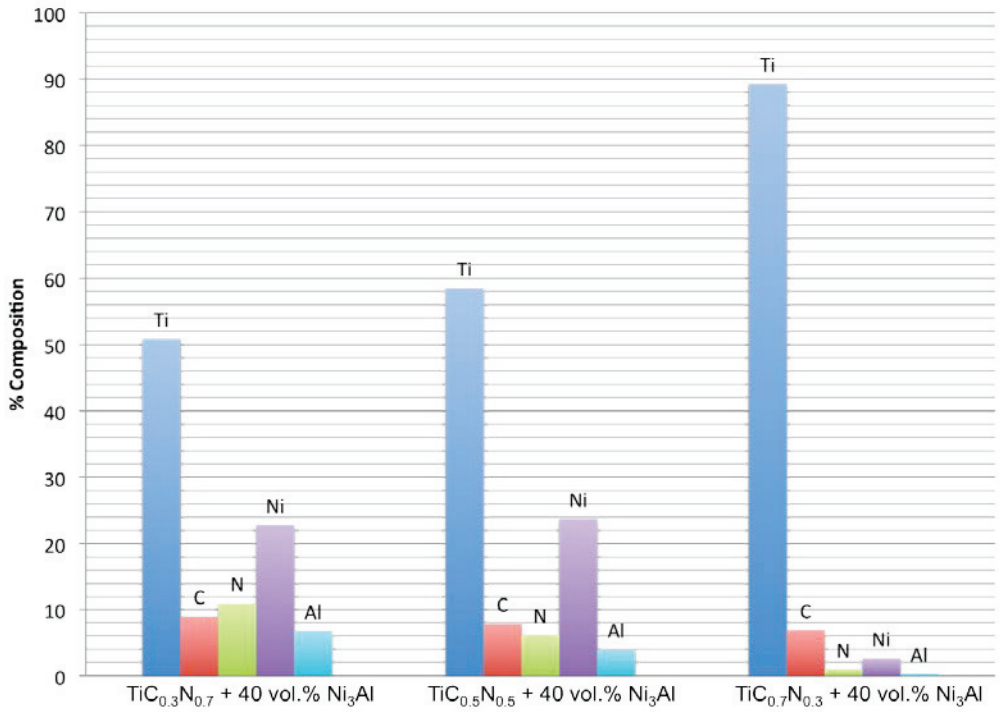

Figure 5–11 EDS analysis on samples following corrosion testing

Solute remaining in the electrochemical cell upon completion of each test was retrieved from the cell, as pictured in Figure 5–12, and analyzed using ICP analysis.

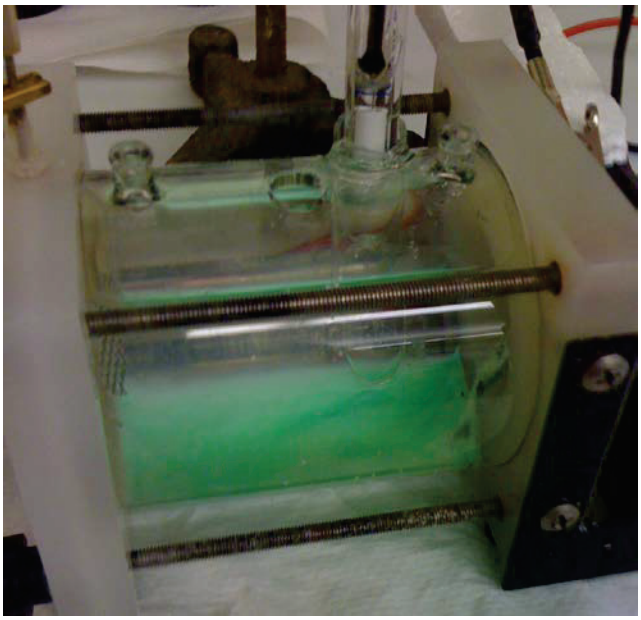

Figure 5–12 Solution remaining in flat cell upon completion of corrosion testing

Figure 5–13 demonstrates a small variation in Ni and Al present in the solution. However, the analyses demonstrate an increasing quantity of Ti with increasing C content releasing into solution throughout the corrosion testing. This confirms the observations noted throughout the SEM analysis, that although the higher carbon content samples demonstrate higher resistance as a function of corrosion current density, the passivation/repassivation may offset this fact. This is believed to contribute to grain removal, demonstrating an increased Ti content in solution.

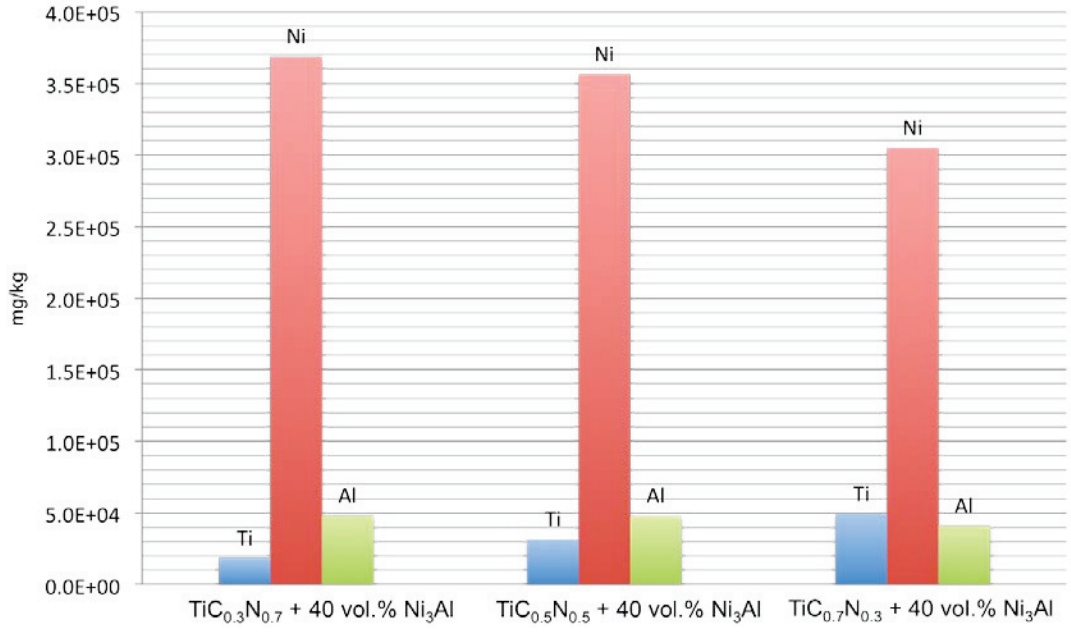

Figure 5–13 ICP results of each tested sample for remaining Ti, Ni and Al within the flat cell solute

5.4 Conclusions

Ti(C,N) cermets with varying C:N ratios were successfully fabricated with 40 vol.% Ni_3Al metal binder content. Each cermet composition was evaluated for its resistance to electrochemical corrosion and analyzed using SEM, EDS, ICP as well as Corrware software to interpret electrochemical corrosion response. The results indicate that although the Ti($C_{0.7}N_{0.3}$) samples demonstrated greater resistance to corrosion, they also

showed fewer regions of repassivation, which can account for the observable degradation through the SEM examination. As indicated by EDS analysis, following the corrosion testing, increasing amounts of Ti were observed with increasing C:N ratio, which indicates an increased tendency for grain pullout and subsequently less Al and Ni in solution.

Generally, the corrosion rate and breakdown potential increase with carbon content. However, it can be conjectured that although the electrochemical response suggests the critical current density to occur at a lower value, instances of passivation/repassivation occur more often for the higher content $Ti(C_xN_{1-x})$ samples. This would indicate that although a greater initial predisposition exists to withstand corrosion for the $TiC_{0.7}N_{0.3}$ samples, there also exists the potential for increased susceptibility to degradation and breakdown of any formed protective oxide layers, and hence an overall increased corrosive attack overall and observable response.

5.5 References

1. Zhang, S., *Titanium carbonitride-based cermets: processes and properties*, Materials Science and Engineering, A163 (1993), 141-148.

2. Ettmayer, P., Kolaska, H., Lengauer, W., & Dreyer, K. *Ti(C,N) Cermets - Metallurgy and Properties*, Int. J. of Refractory Metals & Hard Materials, 13 (1995), 343-351.

3. Kumar, B.V.M., Balasubramaniam, R., Basu, B. *Electrochemical behavior of TiCN-Ni-based cermets.* J. Am. Ceram. Soc*.,* 90 [1] (2007), 205-210.

4. Zhang, S. *Material development of titanium carbonitride-based cermets for machining applications,* Key Engineering Materials, 138 (1998), 521-543.

5. Watanabe, T., Dotsu, T., Nakanishi, T., *Sintering properties and cutting tool performance of Ti(C,N)-based ceramics,* Key Engineering Material, 114 (1996), 189-266.

6. Xingzhong, Z., Jiajun, L., Baoliang, Z., Hezhuo, M., Zhenbi, L., *Wear mechanisms of Ti(C,N) ceramic in sliding contact with stainless steel,* J. Mat. Sci., 32 (1997), 2963-2968.

7. Bologini, S., Feusier, G., Mari, D., Viatte, T., Benoit, W., *High temperature mechanical behaviour of Ti(C,N)-Mo-Co cermets,* Int. J. of Ref. Metals and Hard Mater., 16 (1998), 257-268.

8. Tomlinson, J., Linzell, C.R., *Anodic polarization and corrosion of cemented carbides with cobalt and nickel binders,* J. Mater. Sci., 23 (1988), 914-918.

9. Human, M., Nothrop, I.T., Luyckx, S.B., James, N.M., *A comparison between cemented carbides containing cobalt and nickel-based binders*, J. Hard. Mat., 2 (1991), 245-256.

10. Human, M., Exner, H.E., *Electrochemical behavior of tungsten-carbide hard metals*, Mater, Sci, Eng., A209 (1996), 180-191.

11. Sutthiruangwong, Mori, G., *The relationship between electrochemical behavior and in-service corrosion of WC-based cemented carbides*, Int. J. Ref. Metals and Hard Mat., 15 (1997), 65-71.

12. Tomlinson, J., Ayerst, N.J., *Anodic polarization and corrosion of WC-Co hard metals containing small amounts of Cr3C2 and/or VC,* J. Mat. Sci., 24 (1989), 2348-2354.

13. Sutthiruangwong, Mori, G., Kosters, R., *Passivity and pseudopassivity of cemented carbides*, Int. J. Refr. Metals and Hard Mater. 23 [2] (2005), 129-136.

14. Mendelson, M.I. *Average grain size in polycrystalline ceramics,* J.Am. Ceram. Soc., 52 [8] (1969), 443-446.

15. German, R.M., *Liquid Phase Sintering, 1st Edition,* Plenum Publ. Corp., New York, NY, USA (1985).

16. Jimenez, Y.S., Gil, M. T., Guerra, M. T., Baltes, L.S., Rosca, J.C.M. *Interpretation of open circuit potential of two titanium alloys for a long time immersion in physiological fluid.,* Bulletin of the Trans. Uni. Of Brasov, 2 [51] (2009), 197-204.

17. Fontana, M.G., *Corrosion Engineering, 3rd Edition.* Tata McGraw-Hill (2005).

18. Stern, M., Geary, A.L., *A theoretical analysis of the shape of polarization curves,* Journal of the Electrochemical Society, (1957).

19. Cunha, L., Andritschky, M., Rebouta, K. Pischow, K. *Corrosion of CrN and TiAlN coatings in chloride-containing atmospheres*, Surface and Coatings Technology, 116-119, (1999) 1152-1160.

20. Levi, G., Kaplan, W., & Bamberger, M. *Structure refinement of titanium carbonitride (TiCN)*, Materials Letters, 35 (1998), 344-350.

6 Electrochemical behaviour of TiC

Abstract

TiC cermets were successfully prepared with varying amounts of Ni_3Al binder, ranging from 10 vol.% to 40 vol.% through melt infiltration and sintering. To assess their susceptibility to electrochemical corrosion, each sample was polished and affixed to a flat cell for testing, and immersed in a 3.5 wt.% NaCl solution. Results indicate that although the lowest binder content results in greater potential to resist corrosion, it is conjectured that the higher metal binder content samples (30-40 wt.%) display a lower frequency of breakdown and passivation/repassivation, and hence an overall greater resistance to corrosive attack in terms of overall sample degradation potential.

6.1 Introduction

Titanium carbide (TiC) based ceramic-metal composites, or cermets, are widely used due to their combination of high strength, fracture toughness, extremely high hardness, low friction coefficient and oxidation resistance.[1-3] In addition, owing to the fact that TiC is significantly lower density than materials with comparatively noteworthy mechanical properties (i.e. approximately three times less dense than WC), it is frequently used as an alternative to more conventional tungsten-based hardmetals.[4,7] Significant research has been performed on of refining the processing of TiC cermets, and tailoring their properties through increasingly smaller particle sizes, and also the use of modified metallic alloying additions.[1,3,8] As a result it has been possible to obtain TiC-based cermets that outperform, outlast the commonly used WC-Co materials in industrial settings, at comparatively lower cost to the consumer.[6,9,10]

TiC is often associated with industries involved with high-speed cutting tools, coatings, inserts, and environments associated with high stress and wear.[3,11] As such, a variety of binders have been developed to further improve performance, the most common of which are alloys based on Ni, Mo, and Fe.[3,11] Furthermore, the methods by which the TiC-cermets are synthesized, specifically the sintering temperature and time, have a significant effect on grain growth and the fabrication of the typical core-rim microstructure that contributes to the resulting good mechanical properties. It has been demonstrated that decreasing the final grain size leads to improved mechanical and tribological properties.[12]

However, while the mechanical and tribological properties of these materials have been relatively widely studied, limited research has been conducted to evaluate the ability of TiC-cermets to withstand corrosion. It has been shown that TiC behaves similarly to pure titanium, in that there is formation of a titanium dioxide (TiO_2) protective oxide layer, which aids in slowing the progression of corrosion.[13] Most research has focused on the ability of TiC to resist corrosion at high temperatures (i.e. oxidation), a quality of interest due to the increasing usage of TiC-cermets in such environments, of which several have shown discouraging results.[0] Corrosion of Ti-alloys tends to follow the same

progression: adsorption of anions onto the TiO_2 layer, reaction of the anions with titanium cations or titanium hydroxide, weakening of the oxide layer, and finally localized attack on the underlying metal.[15] At high temperatures, this progressively gives way to localized pitting, complete degradation of oxide layer(s) and eventual cracking of the specimen.[14] The present study will aim to determine the susceptibility of TiC, with varying volume percentage additions of nickel aluminide (Ni_3Al) binder, to corrosive attack in an aqueous chloride solution.

6.2 Materials and Methods

6.2.1 Sample Preparation and Characterization

All TiC-based samples prepared using as-received TiC (Grade TiC-2012) powder, sourced from Pacific Particulate Materials (Vancouver, BC), with a mean particle size of ~1.3 μm. The as received TiC powder was uniaxially compressed to ~45 MPa in a steel die, giving pellets ~31.75 mm in diameter x ~4 mm thick. The pressed discs were vacuum-sealed in plastic and cold isostatically pressed (CIPed) at 220 MPa. Finally, each sample was placed on a bed of bubble alumina (Al_2O_3) within an Al_2O_3 crucible. An appropriate amount of Ni_3Al powder (alloy IC-50; -325 mesh; Ametek, Eighty Four, PA, USA) was then placed on the top surface of each respective sample to give Ni_3Al contents between 10 and 40 vol. %. The samples were loaded into a vacuum furnace, which was subsequently evacuated to ~20 milliTorr and maintained at this pressure throughout the duration of the melt infiltration stage. The furnace was then ramped to 1500°C, at 10°C/min, held at temperature for 1 h, and then cooled to room temperature at a nominal rate of 25°C/min.

The post-infiltration density was measured following Archimedes' principle in water. Each sample was subsequently ground flat using a surface grinder with a diamond peripheral wheel. The samples were then ground and polished using a series of increasingly finer grades of diamond pads and pastes, ranging from 125 μm down to 1/4 μm. The microstructure of the polished samples was assessed using a scanning electron microscope (SEM; Model S-4700, Hitachi High Technologies, Tokyo, Japan), with the

chemical composition determined using energy dispersive X-ray spectroscopy (EDS). The mean grain size was subsequently was determined using the lineal intercept method.

6.3 Electrochemical Testing

Prior to any electrochemical analysis, each sample was immersed in acetone and placed in an ultrasonic bath to ensure the surface was clean and free of any oil or grease. Electrochemical testing was performed using a simple three-electrode analysis cell, containing a platinum electrode as the counter electrode, and a saturated calomel electrode (-0.241 V versus a standard hydrogen electrode) as the reference. Cermet samples were attached to the testing cell, which was then filled with 3.5 wt% NaCl in solution. Readings are obtained firstly for an open-circuit potential (OCP) test, whereby no current is applied to the cell and equilibrium is established between the sample surface and immersion solution for a period of 2 h. Subsequently, a cathodic potential is applied to the cell, scanning from -0.5V to 3V at a rate of 0.1667 mV/s, and a reading of the associated current is taken for analysis.

Following the electrochemical testing, each sample is examined using the SEM to observe the resulting influence on both the core and binder phases. Additionally, remaining solution contained within the cell is examined using an ICP analyzer to determined quantities of various metals now present in solution.

6.4 Results and Discussion

6.4.1 Sample Analysis

Each sample was analyzed following the melt-infiltration and sintering (MIS) processes. Figure 6–1 demonstrates the successful achievement of densification and melt infiltration of Ni_3Al into the pressed TiC samples. There is clear indication of the angular, faceted TiC grains distributed throughout the Ni_3Al binder. A significant observation can also be made with regards to the increasing mean binder intercept length and diminishing contiguity with increasing binder content.

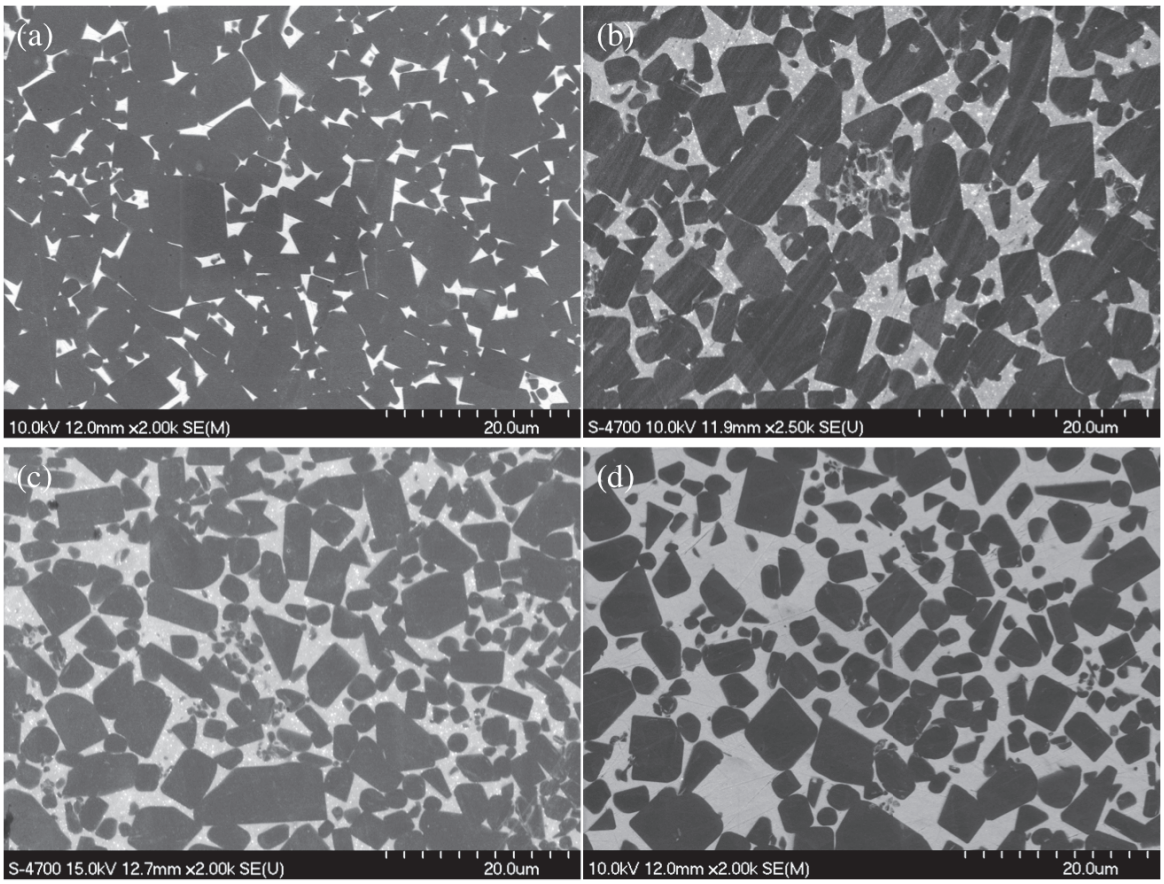

Figure 6–1 SEM micrographs of polished TiC samples: (a) TiC + 10 vol.% Ni_3Al, (b) TiC + 20 vol.% Ni_3Al, (c) TiC + 30 vol.% Ni_3Al, (d) TiC + 40 vol.% Ni_3Al

Mean grain size was calculated using the linear intercept method, demonstrated in Table 6–1, showing an increase in mean grain size with increasing binder content.

Table 6–1 Mean grain size of TiC cermets

Sample	Mean Grain Size (μm)
TiC + 10 vol.% Ni_3Al	4.36 ± 0.74
TiC + 20 vol.% Ni_3Al	4.37 ± 0.71
TiC + 30 vol.% Ni_3Al	5.02 ± 0.93
TiC + 40 vol.% Ni_3Al	5.65 ± 1.25

All samples achieved greater than 100% theoretical density caused by the as-received Ni_3Al powder containing greater stoichiometric quantities of Ni and B than those listed.

6.4.2 Electrochemical Testing

Prior to potentiometric tests a measurement of each sample's open circuit potential (OCP) is evaluated. This test allows for equilibrium to be achieved between the sample and the 3.5 wt% NaCl solution in which it is immersed, before a cathodic potential is applied to the cell. The test runs for 2 h and is measured by taking the potential of the cell between a platinum electrode and the working electrode through the use of a saturated calomel electrode (SCE; -0.241 V versus a standard hydrogen electrode) as the stable electrode. This is used to indicate that any changes in potential thereafter are directly linked to reactions between the sample and solution. Results of this test are indicated in Table 6–2.

Table 6–2 Open circuit potentials for TiC 10-40 wt.% samples

Sample	OCP *(V vs. SCE)*
TiC + 10 vol.% Ni_3Al	-0.0485 (0.0445)
TiC + 20 vol.% Ni_3Al	-0.163 (0.0381)
TiC + 30 vol.% Ni_3Al	-0.112 (0.0295)
TiC + 40 vol.% Ni_3Al	-0.0478 (0.0489)
**Values are mean (standard deviation)	

A cathodic potential is applied to the cell following the OCP test and is set to range from -0.5V to 3V at a scan rate of 0.1667 mV/s. The results are demonstrated below in Figure 6–2 showing reproducibility between samples.

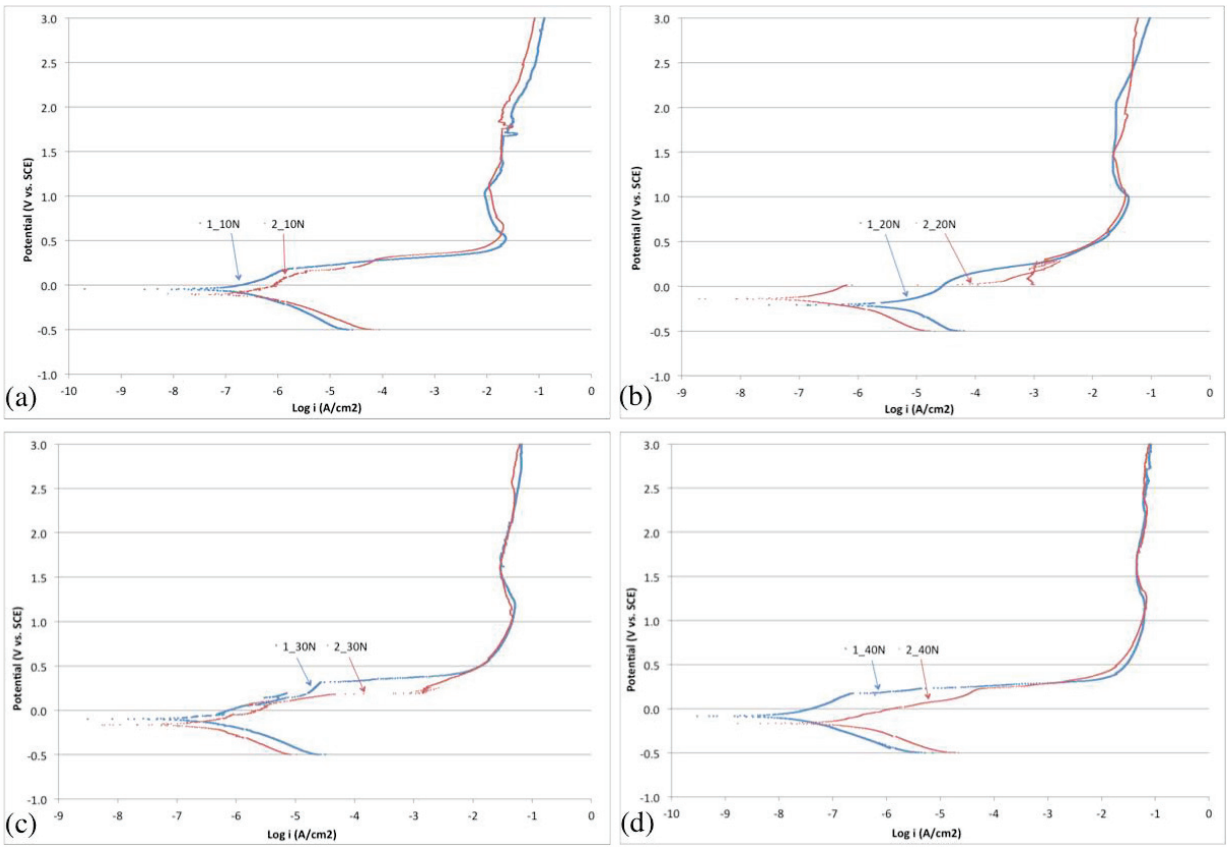

Figure 6–2 Comparative results varying from TiC with 10-40 vol.% Ni_3Al, showing reproducibility

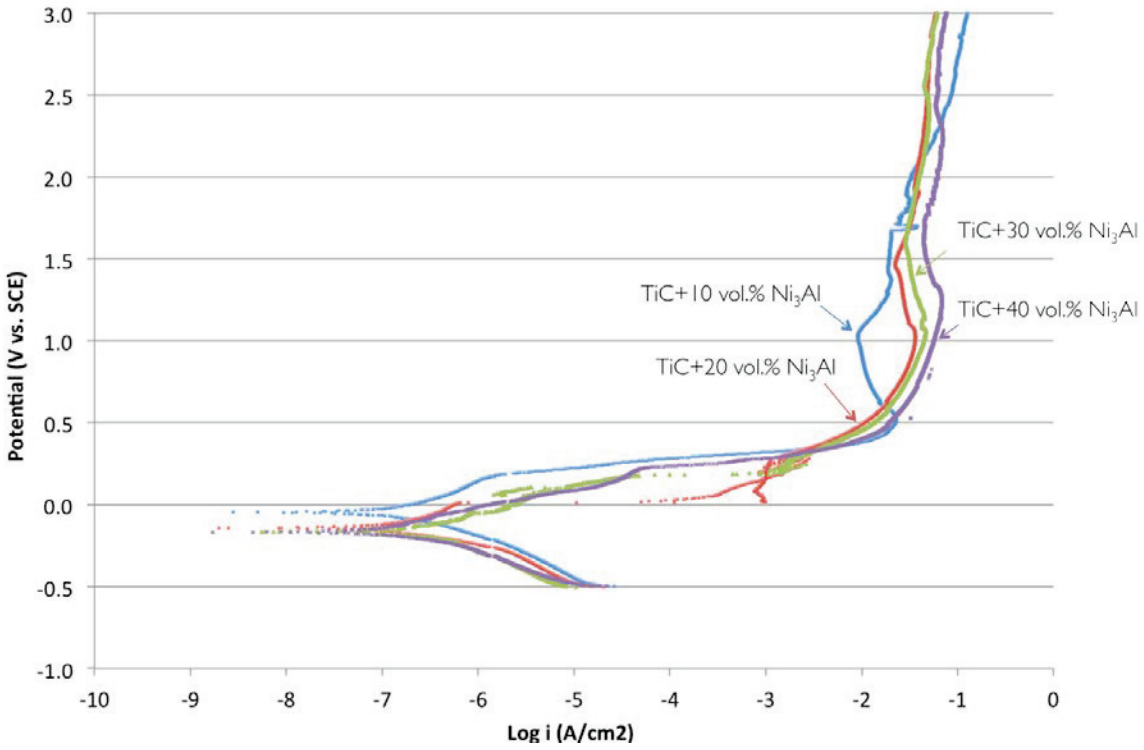

Figure 6–3 Combined potentiodynamic polarization plots for each TiC 10-40 wt.% Ni_3Al sample

Figure 6–3 demonstrates decreasing values of i_{corr} with increasing Ni_3Al content. Generally, as E_{corr} decrease and i_{corr} increase, there is an accelerated susceptibility to corrosion. The sample with the least amount of Ni_3Al demonstrates a decreased initial susceptibility to corrosion, having both a significantly higher value for E_{corr} as well as the highest corrosion current density. Based on the extrapolated data, the samples with the lowest Ni_3Al content demonstrate an increased initial susceptibility to corrosion, having a significantly higher value for E_{corr}. However, the extrapolated data demonstrates a slightly higher value for i_{corr} with this sample. The reasoning for this is based on a preferential attack of the Ni_3Al binder; this sample, containing only 10 vol. % Ni_3Al is less prone to preferential attack, allowing for a greater response by titanium's naturally forming protective oxide layer to withstand further corrosion. This summarized information can also be seen in Table 6–3, showing pertinent information drawn from the potentiodynamic testing.

Table 6–3 Results of electrochemical corrosion testing

Sample	OCP (V vs. SCE)	E_{corr} (mV vs. SCE)	i_{corr} ($\mu A/cm^2$)
TiC + 10 wt% Ni_3Al	-0.0485 (0.0445)	-72.00 (36.77)	0.2215
TiC + 20 wt% Ni_3Al	-0.163 (0.0381)	-175.00 (48.08)	0.0975
TiC + 30 wt% Ni_3Al	-0.112 (0.0295)	-159.33 (58.71)	0.1496
TiC + 40 wt% Ni_3Al	-0.0478 (0.0489)	-126.00 (59.40)	0.0470
** Values are mean (standard deviation), N = 3			

It is evident from Figure 6–3 that there is an increasing shift towards higher breakdown potentials with increasing Ni_3Al content. This implies that the higher binder content cermet undergoes a broader range of passivation. This is a result of the corrosion protection of the TiO_2 layer failing to adequately withstand further attack on the metal matrix, causing breakdown at a slightly faster rate than other samples with increased Ni_3Al content. However, it appears as though the TiC + 40 vol.% Ni_3Al sample has a larger overall range of passivity, as demonstrated in Figure 6–3, which may be due to the active-passive nature of nickel.[16]

6.4.3 Sample Characterization

Each sample was analyzed using a SEM to identify resultant microstructural changes due to electrochemical attack. As evident in Figure 6–4 to Figure 6–7, clear degradation has occurred to each sample, showing significant crevice and pitting corrosion taking place. Notably, the sample with the lowest binder content shows the fewest regions of crevicing; however a substantial degree of deep crevice corrosion, as in Figure 6–4 (b-d), similar to the next sample, shown in Figure 6–5 (a-b), where there is clear evidence of crevice corrosion, however more regions displaying the original polished surface layer running alongside.

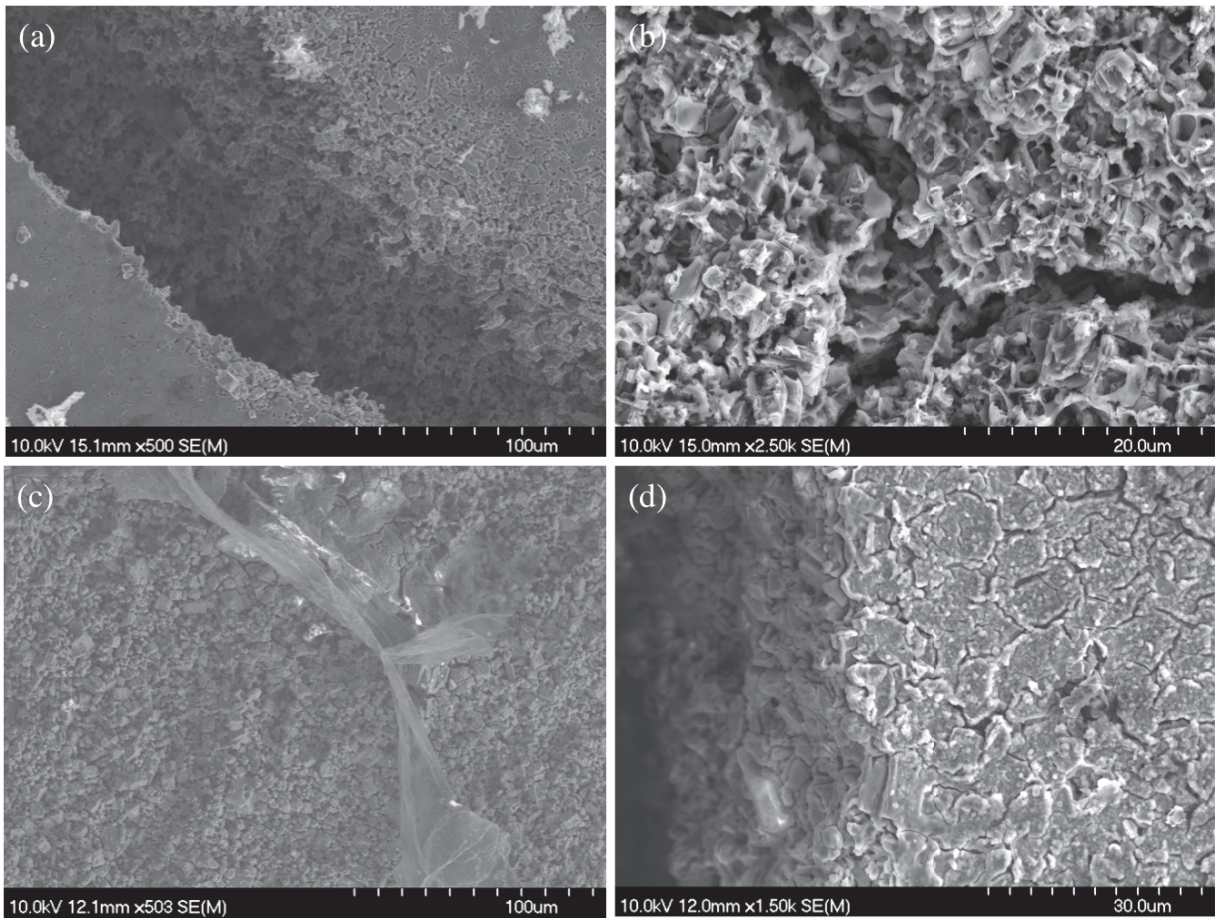

Figure 6–4 Post-corrosion testing SEM micrographs of TiC + 10 wt.% Ni_3Al

The TiC + 10 vol.% Ni_3Al sample showed an abundance of deep crevice attack, as shown in Figure 6–4. Other areas, such as in Figure 6–4 (b), showed a skeleton-like framework that indicates grain pull-out occurring, a common result observed over several regions of the sample. This grain pullout explains the EDS results, as shown in Figure 6–8, which indicate greater amounts of Ti in solution compared to the other samples. Figure 6–4 (c) was captured below a ridge, essentially the base of a creviced region, and shows the underlying grains seemingly intact, while the Ni_3Al binder is seemingly gone.

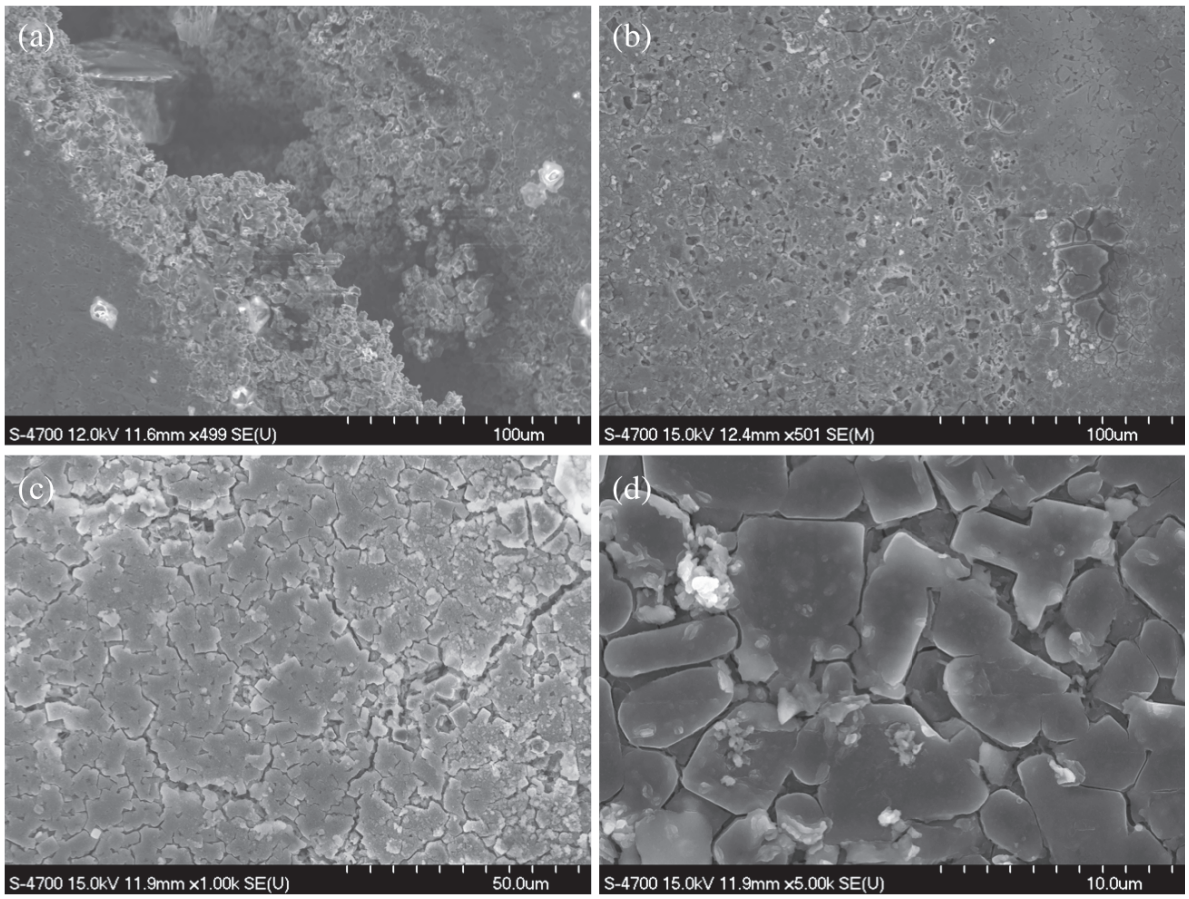

Figure 6–5 Post-corrosion testing SEM micrographs of TiC + 20 wt.% Ni_3Al

The next sample, TiC + 20 vol.% Ni_3Al, generally showed results similar to the previous sample, however more areas of the original surface structure were visible and ostensibly untouched, as in Figure 6–5 (a-d). Again, there were a variety of areas that demonstrated clear pitting and crevice corrosion, however each area observed was alongside areas that seemed unaffected, and followed the boundaries of the grains, as in Figure 6–5 (b-c). Figure 6–5 (b) showed clear pitting corrosion coupled with apparent grain pullout, resulting in pockets of void space and a skeleton structure of binder remaining. It is believed that the initial stages of the deep crevices and pitting, as apparent in Figure 6–5 (d), which shows the beginning degradation of the areas between the individual grains and as such is a result of the targeted attack first and foremost on the Ni_3Al binder.

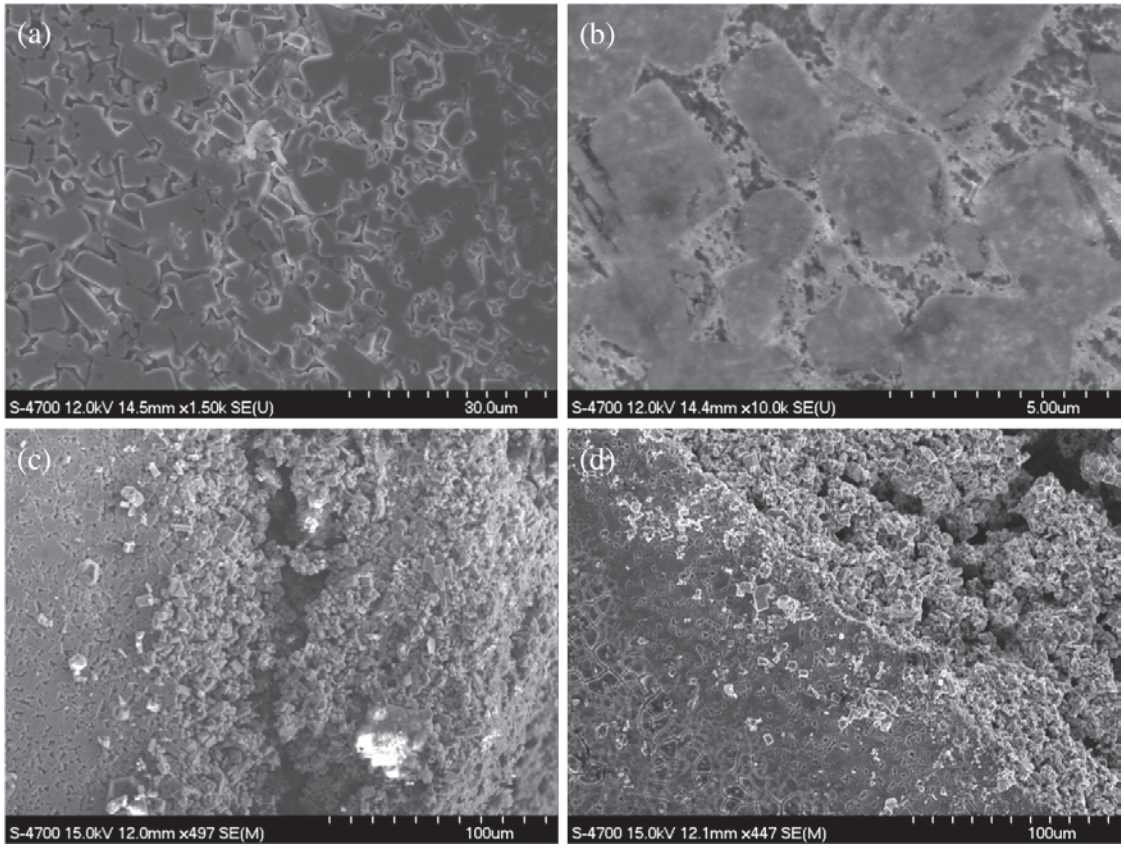

Figure 6–6 Post-corrosion testing SEM micrographs of TiC + 30 wt.% Ni_3Al

The TiC + 30 vol.% Ni_3Al sample demonstrated similar results to those previous, showing clear pitting and crevice corrosion, as well as preferential binder attack, as shown in Figure 6–6 (a-d). Figure 6–6 (a) and (b) specifically show the targeted Ni_3Al binder corrosion taking place. As a result of this, the grains are seen to disconnect from the matrix and result in the cascading grain dissolution and eventual deep crevices, as depicted in Figure 6–6 (c) and (d).

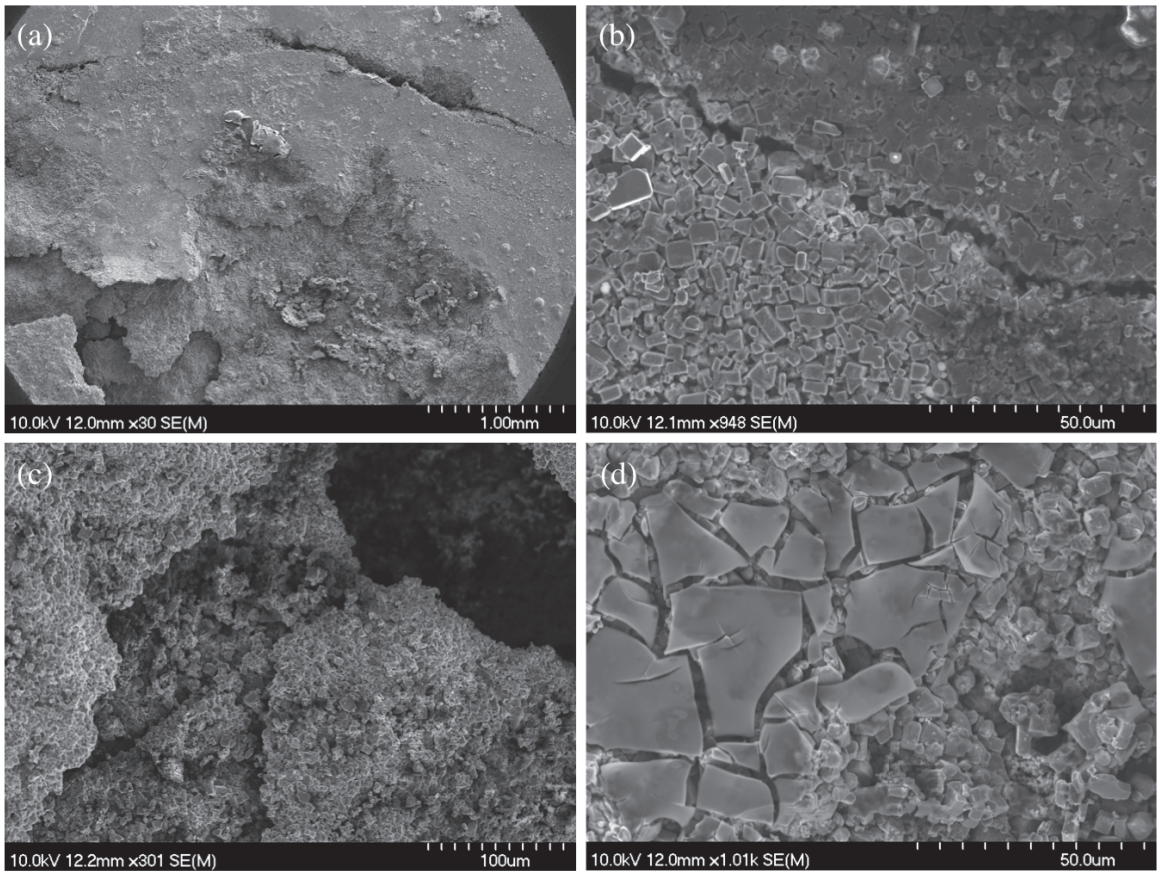

Figure 6–7 Post-corrosion testing SEM micrographs of TiC + 40 wt.%

Finally, TiC + 40 vol.% Ni_3Al appears to have the most varied results, showing deep lines of crevices, coupled with deep and wide pitting as well as removal of grains and areas that appear to resemble shifted plates of material, as depicted in Figure 6–7 (a)-(d). As discussed, this sample was shown to have the least resistance to corrosive attack, which could explain the results of the SEM imaging. However Figure 6–7 (b) shows areas of maintained polished surfaces, which are conjectured to be the result of the larger region of passivation. Although this sample showed the most susceptibility to corrosive attack, there were fewer areas of breakdown and repassivation compared with the other samples, as noted in Table 6–3. Another hypothesis is the influence of the significant active-passive behaviour of nickel, which may have provided further protection through its own oxidation layer once a certain potential was reached. This may explain the large deep crevices, while still maintaining vast regions seemingly untouched.

Remaining solution within the cell was tested using ICP analysis. Results are demonstrated in Figure 6–8. Results indicate increasing quantities of nickel and aluminum apparent in solution following corrosion testing, and inversely decreasing amounts of titanium. This is in agreement with the results given in Table 6–3, which suggest that the preferential attack of the Ni_3Al binder progressed linearly with increasing amounts of the binder within the composite.

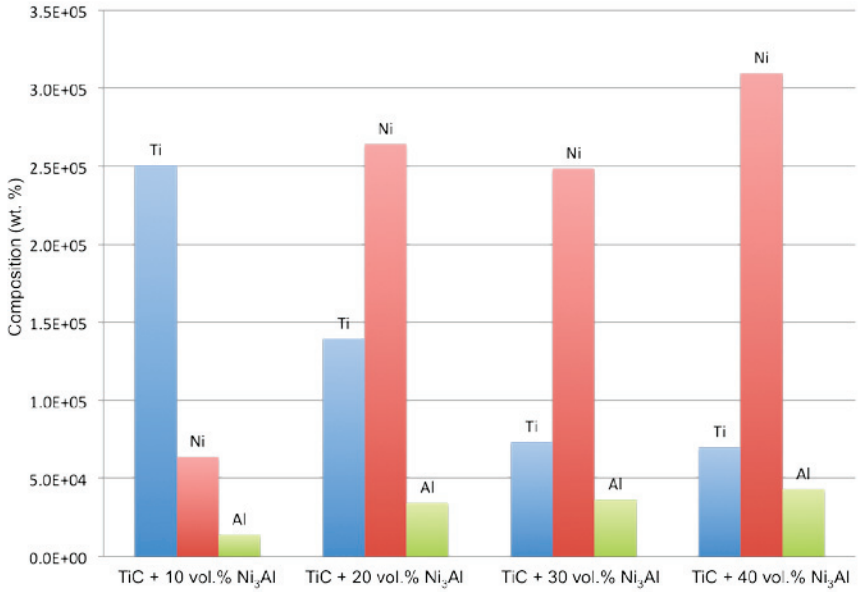

Figure 6–8 ICP results of solution remaining in flat cell upon completion of corrosion testing

EDS analysis was conducted on each sample following corrosion testing. Results, presented in Figure 6–9, indicate the 10 vol.% Ni_3Al sample to have on average more areas with greater amounts of carbon, nickel and aluminum, indicating a preferential dissolution of titanium into solution. As discussed in the previous section, the TiC + 10 vol.% Ni_3Al sample appeared to have more regions of grain pullout, which would explain the greater amount of Ti in solution. This is also in agreement with the resultant corrosion values, which indicate a much earlier breakdown potential for the lowest binder content sample. Similarly, the following three samples display an overall greater volume of titanium remaining within the sample, in agreement with ICP results that with increasing binder content comes accelerated corrosion behaviour and hence more nickel and aluminum remaining in solution while the fragmented titanium matrix remains.

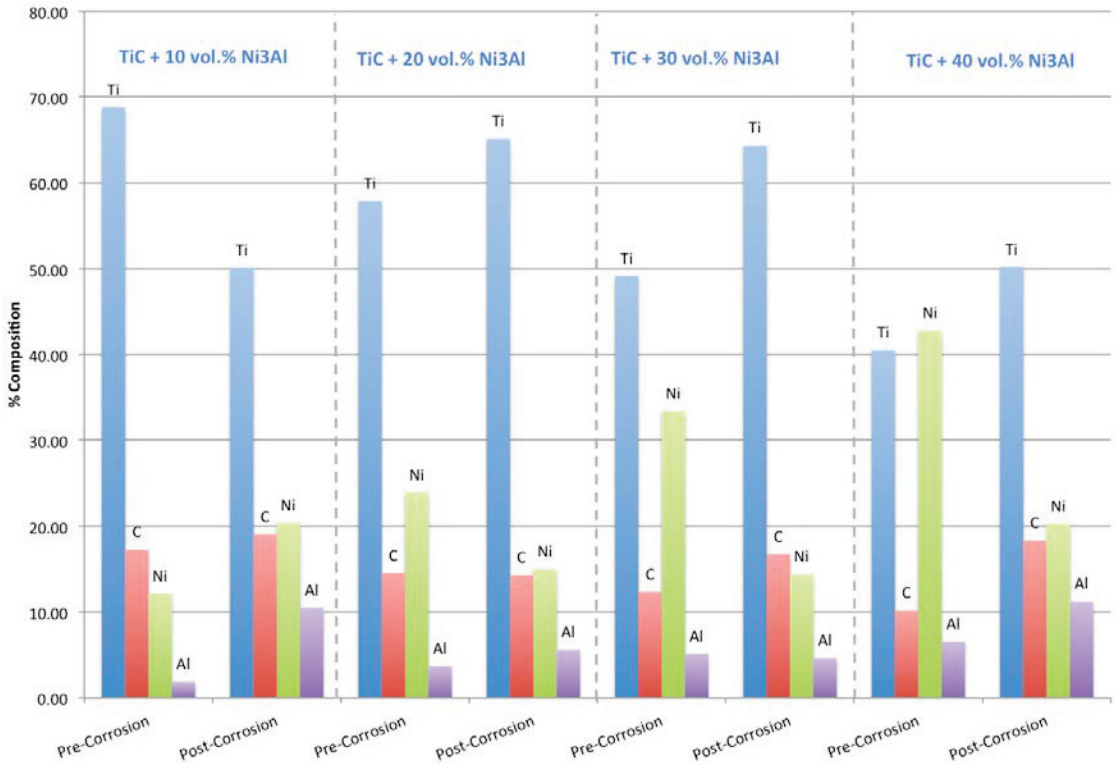

Figure 6–9 EDS analysis on remaining Ti, C, Ni and Al within the sample following corrosion testing

6.5 Conclusions

TiC preforms were successfully melt-infiltrated with varying amounts of Ni_3Al metal binder, ranging from 10 vol.% to 40 vol.%. Each sample was then subjected to electrochemical testing, to determine its susceptibility to corrosion in 3.5 wt% NaCl in ambient conditions. Results indicate that although the samples with the lowest binder content indicate an increased initial resistance to corrosion (i.e a lower value of i_{corr}), it appears as though the samples undergo more instances of passivation/repassivation, resulting in a greater number of areas demonstrating deep crevices.

Through observations from SEM, EDS and results from ICP, it has been confirmed that the lowest vulnerability to corrosion lies with the TiC + 10 vol.% Ni_3Al metal binder, which eventually succumbs to deep crevice corrosion once the protective oxide layer is broken down. However, the TiC + 40 vol.% Ni_3Al samples, in contrast, demonstrate a lower resistance to corrosion yet a greater ability to passivate/repassivate.

This demonstrates the potential for a reduced overall breakdown of the material, with focused corrosion on the metal binder in place of direct attack on the Ti(C,N) grains. The increased Ni in solution is demonstrative of a more localized attack on the metal binder, with considerably less Ti in solution between the 30 vol.% and 40 vol.% samples tested.

6.6 References

1. Kubarsepp, J., Klaasen, H., Pirso, J., *Behaviour of TiC-base cermets in different wear conditions*, Wear, 249 (2001), 229-234.

2. Becher, P., & Plucknett, K. *Properties of Ni3Al-bonded titanium carbide ceramics*, Journal of the European Ceramic Society, 18 (1997), 395-400.

3. Hussainova, I. *Effect of microstructure on the erosive wear of titanium carbide-based cermets*, Wear, 255 (2003), 121-128.

4. Zhang, S. *Titanium carbonitride-based cermets: processes and properties*. Materials Science and Engineering, A163 (1993), 141-148.

5. Zhang, S. *Material development of titanium carbonitride-based cermets for machining applications,* Key Engineering Materials, 138 (1998), 138-140.

6. Liu, N., Liu, X., Zhang, X., Zhu, L. *Effect of carbon content on the microstructure and mehcnical properties of superfine Ti(C,N)-based cermets.* Materials Characterization, 59 (2008), 1440-1446.

7. Ettmayer, P. *Hardmetals and Cermets,* Annual Reviews, 19 (1989).

8. Antonov, M., Hussainova, I., *Cermets surface transformation under erosive and abrasive wear*, Tribology International, 43 (2010), 1566-1575.

9. Mari, D., Bolognini, S., Feusier, G., Cutard, T., Verdon, C., Viatte, T. Benoit, W. *TiMoCN based cermets Part I. Morphology and phase composition*. International Journal of Refractory Metals & Hard Materials, 21 (2003), 37-46.

10. Bologini, S., Feusier, G., Mari, D., Viatte, T., Benoit, W., *High temperature mechanical behaviour of Ti(C,N)-Mo-Co cermets,* Int. J. of Ref. Metals and Hard Mater., 16 (1998), 257-268.

11. Kwon, H., Kang, S., *Microstructure and mechanical properties of TiC-WV-(Ti,W)C-Ni cermets*, Materials Science and Engineering, A 520 (2009), 75-79.

12. Han, C., & Kong, M. *Fabrication and properties of TiC-based cermet with intra/intergranular microstructure,* Materials and Design, 30 (2009), 1205-1208.

13. Cowling, R.D., Hintermann, H.E., *The corrosion of titanium carbide,* J. Electrochem. Soc.: Electrochemical Technology, 117 [11] (1970), 1447-1449.

14. Shimada, S., *Formation and mechanism of carbon-containing oxide scales by oxidation of carbides (ZrC, HfC, TiC),* Materials Science Forum, 369 [3] (2001), 377-384.

15. Abou Shabha, R.M., Ghannem, W.A., El-Sayed El-Shenawy, A., *Corrosion and inhibition of Ti-6Al-4V alloy in NaCl solution,* Int. J. Electrochem. Sci., 6 (2011), 5499-5509.

16. Keijzer, M., Hemmes, K., De Wit., J.H.W., Schoonman, J. *TiCN and metallic coatings for corrosion protection of separator plates in MCFC's*, Journal of Applied Electrochemistry, 30 (2000), 1421-1431.

7 Conclusions

This study sought to explore the behaviour of Ti(C,N) and TiC-based cermets in an aerated, aqueous corrosive environment, in 3.5 wt% NaCl solution. Ti(C,N) and TiC samples were successfully prepared through unixial and isostatic compaction, followed by melt-infiltration. Fully dense samples of $Ti(C_xN_{1-x})$ and TiC were consolidated, resulting in the following compositions: $TiC_{0.3}N_{0.7}$, $TiC_{0.5}N_{0.5}$ and $TiC_{0.7}N_{0.3}$, all with 40 vol.% Ni_3Al binder, as well as TiC with 10, 20, 30 and 40 vol.% Ni_3Al metal binder. Each sample was analyzed for its relative density, and found to be greater than 99% of the theoretical density. The chemical composition and microstructure of each sample were also investigated with the aid of SEM, EDS, ICP-OES and XRD. Following a rigorous grinding and polishing process, whereby they were polished to a final 1/4 μm finish using diamond paste, the cermets were cleaned in an ultrasonic bath using acetone. Each sample was then affixed to an electrochemical testing cell for evaluation, which allows both equilibrium and potentiodynamic tests to be conducted. Open circuit potential tests measure potential of the cell for 2 hrs while equilibrium is established between the sample and the NaCl solution within which it is immersed. Potentiodynamic testing incorporates an applied cathodic potential and measures the resultant current density of the cell. The potentiodynamic test was observed from -0.5V to 3V, scanning at a rate of 0.1667 mV/s. Each sample was analyzed to comparatively demonstrate any changes in composition or microstructure using the same analysis tools as previously mentioned. Further examination of the electrochemical response was obtained through extrapolation of data acquired by the potentiostat and associated software, Corrware, to establish direct correlation between the observable response and quantified test results. Through microstructural analysis by SEM, EDS, ICS-OES, as well as electrochemical computer software data extrapolation, it was possible to establish a pattern of susceptibility and microstructural response to electrochemical attack.

Initial observations of the microstructure indicated that the Ni_3Al was able to successfully infiltrate the $Ti(C_xN_{1-x})$ preforms, resulting in little variation from the original cubic particle shape. With increasing carbon content (or C:N ratio), SEM imaging showed slightly coarser grain sizes, as well as somewhat less of a cubic morphology.

TiC samples were also successfully fabricated through melt-infiltration and sintering, with samples produced containing 10, 20, 30 and 40 vol.% Ni_3Al metal binder. Upon examination of SEM micrographs, there appear to be clear faceted TiC grains distributed within the metal matrix. With increasing binder content, there is also an increase in mean binder intercept length, as well as significant decrease in contiguity.

Corrosion testing results of the $Ti(C_xN_{1-x})$ samples were found to have decreasing corrosion current density (i_{corr}), and hence a decreased initial susceptibility to corrosion, with increasing carbon content. This, coupled with the higher corrosion potential (E_{corr}), indicated a greater resistance to corrosion. However, it was observed that with increased carbon content where the potential for fewer consistent regions of passivation/repassivation, suggesting a potential protective oxidation layer forming with the aid of the Ni_3Al binder, contributing to the overall passivation of the sample. More frequent instances of breakdown occurred, resulting in more frequent passivation/repassivation, for higher carbon content samples, which may allow for a greater degree of pitting and for crevice corrosion. The lower carbon content samples demonstrated a greater range of passivation, which may counteract the initially higher critical current density (i_{crit}).

SEM images revealed significant degradation of each sample, with clear areas of deep pitting and crevices, originating from seemingly targeted attack on the metal binder and running alongside Ti(C,N) grains. With increasing carbon content, there also appeared to be more instances of grain pullout and the subsequent formation of a skeleton-like framework of remnant metal binder, believed to be the result of the passivation/repassivation phenomenon occurring more frequently.

ICP-OES testing revealed a lower relative amount of titanium, in conjunction with an increased amount of nickel and aluminum, in solution following the corrosion tests for samples with increasing carbon content. EDS revealed greater amounts of titanium, and correspondingly less nickel and aluminum, remaining within the sample itself. This is reflective of the observations from the SEM imaging, which revealed more occurrences of grain dissolution, which would account for the increased titanium observed in solution.

TiC cermets, prepared with 10 to 40 vol.% Ni_3Al metal binder exhibited similar results, suggesting that increased metal binder content demonstrated greater susceptibility to corrosion. Initially, the lower content metal binder samples display greater resistance to corrosion. This is in agreement with the values of E_{corr}, which increased with increasing binder content. However, the samples with higher binder contents also demonstrated a greater overall range of passivation, suggesting the influence of the nickel component may ultimately affect the overall degradation of the material. TiC cermets showed similar results in terms of the degree of degradation, pitting and crevice corrosion observed when compared to the $Ti(C_xN_{1-x})$ cermets. An increase in corrosion susceptibility with increasing metal binder content was observed, which was attributed to the preferential attack of the metal coupled with the oxidation behaviour of the Ti.

SEM imaging revealed clear areas of attack on the metal binder, demonstrating preferred breakdown of the binder phase, which ran through the matrix between grains of TiC. As with the Ti(C,N) samples, TiC with increasing binder content demonstrated a greater potential for passivation/repassivation and more instances of breakdown. This is believed to explain the notably greater instances of deep crevice formation and significant pitting within samples with a higher metal binder content.

Furthermore, with increasing binder content, ICP-OES results indicate an increased quantity of nickel and aluminum in solution following corrosion testing, and a greater amount of titanium remaining within the sample. This is in agreement with the measurable corrosion results, suggesting the higher binder content samples are the least resistant to corrosive attack.

Research into the mechanisms governing corrosion within cermets of varying stoichiometry, as well as metal binder content, remains in its infancy. As such, it is recommended that further work encompass the attributes that allow for tailored properties of the cermets, and the influence this could have on reducing susceptibility to corrosion. Results could prove to demonstrate methods of achieving a desired balance of mechanical properties and corrosion resistance, dependent upon the type of application and environment within which it may be immersed. Furthermore, it is recommended that

corrosion mechanisms be observed in a less stagnant environment (i.e. examination of combined erosion-corrosion behavior). This would aim to explore the practical application of Ti(C,N) or TiC-based cermets in an environment that may not allow for development of an oxide layer, but would rather expedite corrosion through the constant breakdown of any formed oxide layers. It is believed that this would provide great information for the use of such materials in a petro-chemical operational environment, with a focused look at the resulting response to corrosion in a more typical setting. Furthermore, study into more corrosive-resistant binders has the potential to greatly affect the cermet's overall ability to withstand corrosion. This may have great influence on reducing any instances of grain dissolution, or targeted corrosion of the metal matrix.

Works Cited

1. Zhang, S. *Material development of titanium carbonitride-based cermets for machining applications,* Key Engineering Materials, 138-140 (1998), 521-543.

2. Ettmayer, P. *Hardmetals and Cermets,* Annual Reviews, 19 (1989).

3. Monteverde, F. M. *Synthesis of ultrafine titanium carbonitride powders*. Applied Organimetallic Chemistry, 15 (2001), 421-429.

4. Ettmayer, P., Kolaska, H., & Dreyer, K. *Effect of sintering atmosphere on the properties of cermets,* Hagen Symposium, (1990).

5. Ettmayer, P., & Lengauer, W. *The Story of Cermets,* Powder Metallurgy International, 21 (1989),

6. Aronson, R. *The misunderstood cermet*. Manufacturing Engineering, 119 (2) (1997), 74-82.

7. Lavrenko, V.A., Shvets, V.A., Umanskii, A.P., Belykh, A.B., Adeev, V.M., Talash, V.N. *Electrolytic corrosion of titanium carbonitride composites*. Powder Metallurgy and Metal Ceramics, 43 (1-2) (2004), 62-66.

8. Kumar, B.V.M., Balasubramaniam, R., Basu, B. *Electrochemical behavior of TiCN-Ni-based cermets*. J. Am. Ceram. Soc*.,* 90 (1) (2007), 205-210.

9. Zhang, S. *Titanium carbonitride-based cermets: processes and properties*. Materials Science and Engineering*,* A163 (1993), 141-148.

10. Cardinal, S., Malchere, A., Gamier, V., & Fantozzi, G. *Microstructure and mechanical properties of TiC-TiN based cermets for tools application,* Int. J. of Refractory Metals & Hard Materials, 27 (2009), 521-527.

11. Zhang, X., Liu, N., & Rong, C. *Effect of molybdenum content on the microstructure and mechanical properties of ultra-fine Ti(C,N) based cermets*, Materials Characterization, 59 (2008), 1690-1696.

12. Zheng, Y., *Effect of carbon content on the microstructure and mechanical properties of Ti(C,N)-based cermets*. Ceramics International*, 30 (*2004), 2111-2115.

13. Ettmayer, P., Kolaska, H., Lengauer, W., & Dreyer, K. *Ti(C,N) Cermets - Metallurgy and Properties*, Int. J. of Refractory Metals & Hard Materials, 13 (1995), 343-351

14. Yan, Y., Zheng, Y., Yu, H., Bu, H., Cheng, X., & Zhao, N. *Effect of sintering temperature on the microstructure and mechanical properties of Ti(C,N)-based cermets*, Powder Metallurgy and Metal Ceramics, 46 (2007), 449-453.

15. Yeh, C., & Chen, Y. *Direct formation of titanium carbonitrides by SHS in nitrogen,* Ceramics International, 31 (2005), 719-729.

16. Levi, G., Kaplan, W., & Bamberger, M. *Structure refinement of titanium carbonitride (TiCN)*, Materials Letters, 35 (1998), 344-350.

17. Zheng, Y., You, M., Xiong, W., Liu, W., Wang, S. *Valence-electron structure and properties of main phases in Ti(C,N)-based cermets.* Materials Chemistry and Physics, 82 (2003), 877-881.

18. Zheng, Y., Liu, W., Wang, S., & Xiong, W. *Effect of nano additions on the microstructures and mechanical properties of Ti(C,N)-based cermets,* Ceramics International, 30 (2005), 165-170.

19. Chao, S. Liu, N., Yuan, Y., Han, C., Xu, Y., Shi, M. Feng, J. *Microstructure and mechnical properties of ultrafine Ti(CN) cermets fabricated from nano-submicron starting powders.* Ceramics International, 31 (2005), 851-862.

20. Cordoba, J.M., Sanchez-Lopez, J.C., Aviles, M.A., Alcala, M.D., Gotor, F.J. *Properties of Ti(C,N) cermets synthesized by mechanically induced self-sustaining reaction.* Journal of the European Ceramic Society, 29 (2009), 1173-1182.

21. Eslamloo-Grami, M., & Munir, Z. *The mechanism of combustion synthesis of titanium carbonitride,* Journal of Materials Research, 9 (1994), 431-435.

22. Feng, P., Xiong, W. Yu, L. Zheng, Y. Xia, Y. *Phase evolution and microstructure characteristics of ultrafine Ti(C,N)-based cermet by spark plasma sintering*. International Journal of Refractory Metals & Hard Materials, 22 (2004), 133-138.

23. Ding, J., Tsuzuki, T., McCormick, P.G., Street, R., *Ultrafine Co and Ni Particles Prepared by Mechanochemical Processing,* J. Phys. D: Appl. Phys., 29 [9] (1996) 2365–2369.

24. Pastor, H. *Titanium-carbonitride-based hard alloys for cutting tools.* Materials Science and Engineering, A105-106 (1988), 401-409.

25. Wang, C., Dai, Y., Gao, H., Ruan, X., Wang, J., & Sun, B. *Surface properties of titanium nitride: A first-principles study,* Solid State Communications, (2010), 1370-1374,

26. Cordoba, J.M., Sayagues, M.J., Alcala, M.D., Gotor, F.J. S*ynthesis of titanium carbonitride phases by reactive milling of the elemental mixed powders.* J. Am. Ceram. Soc., 88 [7] (2005), 1760-1764.

27. Mitchell, B.S. *An Introduction to Materials Engineering and Science*. Hohn Wiley & Sons Inc. (2004).

28. Schechuang, W., Shuzhu, Z., Weizhen, P., Hezhuo, M., & Wei, P. *A comparative research on the compositions and microstructure of the Ti(C,N) based cermets in different sintering atmospheres,* Engineering Materials, 368-372 (2008).

29. Xiong, W., Hu, Z., & Cui, K. *Transitional layer of phase interfaces in Ti(C,N)-based cermet*, Acta Metall. Sinica., 32 (1996).

30. Liu, N., Liu, X., Zhang, X., Zhu, L. *Effect of carbon content on the microstructure and mehcnical properties of superfine Ti(C,N)-based cermets.* Materials Characterization, 59 (2008), 1440-1446.

31. Mari, D., Bolognini, S., Feusier, G., Cutard, T., Verdon, C., Viatte, T. Benoit, W. *TiMoCN based cermets Part I. Morphology and phase composition*. International Journal of Refractory Metals & Hard Materials, 21 (2003), 37-46.

32. Fontana, M.G., *Corrosion Engineering, 3rd Edition.* Tata McGraw-Hill (2005).

33. Tomashov, N.D., Altovsky, R.M., Chernova, G.P. *Passivity and corrosion resistance of tatanium and its alloys.* Journal of the Electrochemical Society, 108 [2] (1961), 113-119.

34. Lecki, H., Shreir, L.L. *Anodic polarization of titanium in formic acid*. Defence documentation center for scientific and technical information, Alexandria, Virginia (1961), 1-28.

35. Monteverde, F. M. Microstructural evolution of titanium carbonitride based materials during oxidation. *Mikrochim. Acta. ,* 139 (2002), 97-103.

36. Komratov, G. The oxidation kinetics of titanium carbide, nitride and carbonitride powders in air. *Power Metallurgy and Metal Ceramics ,* 36 [9-10] (1997), 510-514.

37. Podchernyaeva, I. K. *Investigation of wear- and corrosion-resistant coating of the TiCN-Ni-alloy system, obtained by high-speed gas-flame spraying.* Powder Metallurgy and Metal Ceramics, 38 [7-8] (1999), 358-361.

38. Moskowitz, D., Humenik, M. Jr. *Effect of binder phase on the properties of TiC-22.5Ni-MoC_x tool materials*. The International Journal of POwder Metallurgy & Powder Technology, 14 [1] (1976), 39-45.

39. Fried Krupp AG, French Patent 715148, (1931).

40. Chen, L., Wang, S., Zhou, S., Li, J., & Zhang, Y. *Microstructure and mechanical properties of Ti(C,N) and TiN/Ti(C,N) multilayer PVD coatings*, International Journal of Refractory Metals and Hard Materials, 26 (2008), 456-460.

41. Bellosi, A., Calzavarini, M.G., Faga, F., Monteverde, C., Zancolo, G.E. *Characterisation and application of titanium carbonitride-based cutting tools*. Journal of Material Processing Technology, 143-144 (2003), 527-532.

42. El-Eskandarany, M. S., *Structure and properties of nanocrystalline TiC full-density bulk alloy consolidated from mechanically reacted powders*, Journal of Alloys and Compounds, 305 (2000), 225-238.

43. Hussainova, I. *Effect of microstructure on the erosive wear of titanium carbide-based cermets*, Wear, 255 (2003), 121-128.

44. Neumann, G., Kieffer, R., Ettmayer, P., *Ober das System TiC-TiN-TiO,* Monatshefier Chemie, 103 (1972), 1130-1137.

45. Woo, Y., Kang, H., & Kim, D. (). *Formation of TiC particle during carbothermal reduction of TiO_2*, Journal of the European Ceramic Society, 27 (2007), 719-722.

46. Qian, M., & Lim, L. (). *On the disappearance of Mo2C during low-temperature sintering of Ti(C,N)-Mo2C-Ni cermets,* Journal of Materials Science, 34 (1999), 3677-3684.

47. Zhang, X., He, X., Han, J., Qu, W., & Kvalin, V. *Combustion synthesis and densification of large-scale TiC–xNi cermets,* Materials Letters, 56 (2002), 183-187.

48. Becher, P., & Plucknett, K. *Properties of Ni3Al-bonded titanium carbide ceramics*, Journal of the European Ceramic Society, 18 (1997), 395-400.

49. Schwarzkopf, R., & Kieffer. *Refractory Hard Metals.* New York, USA: Macmillan (1953).

50. Borovinskaya, I. P., Ignat'eva, T., Emel-yanova, O. M., Vershinnikov, V. I., & Semenova, V. N. *Self-propagating high-temperature synthesis of ultrafine and nanometer-sized TiC particles,* Inorganic Materials, 43 (2007), 1343-1350.

51. Han, C., & Kong, M. *Fabrication and properties of TiC-based cermet with intra/intergranular microstructure,* Materials and Design, 30 (2009), 1205-1208.

52. Zhou, S., Wang, S., Wang, L., & Ding, Z. *Effect of sintering atmosphere on microstructure and properties of TiC based cermets,* J. Cent. South Univ. Technology, 2 (2007), 206-209.

53. Quinn, C.J., Kohlstedt, D.L. *Reactive processing of titanium carbide with titanium,* Journal of Materials Science, 19 (1984), 1229-1241.

54. Song, M., Huang, B., Zhang, M., & Li, J. *Study of formation behavior of TiC ceramic obtained by self-propagating high-temperature synthesis from Al-Ti-C elemental powders*, Int. Journal of Refractory Metals & Hard Materials, 27 (2009), 584-589.

55. Fan, Q., & Zhihao Jin, H. *Microstructural evolution in the combustion synthesis of titanium carbide,* Journal of Materials Science, 31 (1996), 2573-2577.

56. Locci, A., Cincotti, A., Delogu, F., Orru, R., & Cao, G. *Advanced modelling of self-propagating high-temperature synthesis: the case of the Ti-C system*, Chemical Engineering Society, 59 (2004), 5121-5128.

57. Deidda, C., Delogu, F., Maglia, F., Anselmi-Tamburini, U., Cocco, G., *Mechnical processing and self-sustaining high-temperature synthesis of TiC powders*, Materials Science and Engineering, A 375-377 (2004), 800-803.

58. Merzhanov, A.G., *Combustion processes that synthesize materials,* Journal of Materials Processing Technology, 56 (1996), 222-241.

59. Miracle, D.B., Lippsitt, H.A. *Mechanical properties of fine-grained substoichiometric titanium carbide,* J. Am. Ceram. Soc., 66 [8] (1983), 592.

60. Tiegs, T.N., Plucknett, K.P., Menchhofer, P.A., Becher, P.F. *Development of nickel-aluminide-bonded WC and TiC Cermets*, Proceedings of the Intl. Sym. on Nickel and Iron Aluminides: Processing, Properties and Applications, (1997), 339-357.

61. Klaasen, H, Kubarsepp, J. Sergejev, F., *Strength and failure of TiC based cermets,* Powder Metallurgy, 52 [2] (2009), 111-115.

62. Chun, D., & Kim, D. (1993). *Microstructural evolution during the sintering of TiC-Mo-Ni cermets,* J. of the American Ceramic Society, 76 [8] (1995), 2049-2052.

63. Kubarsepp, J., Klaasen, H., Pirso, J., *Behaviour of TiC-base cermets in different wear conditions*, Wear, 249 (2001), 229-234.

64. Hussainova, I., Kubarsepp, J., Pirso, J., *Mechanical properties and features of erosion of cermets,* Wear, 250 (2001), 818-825.

65. Plucknett, K.P., Becher, P.F., Alexander, K.B., *In-situ SEM observation of the fracture behaviour of titanium carbide/nickel aluminide composites*, Journal of Microscopy, 185 [2] (1997), 206-216.

66. Storms, E., *The Refractory Carbides.* New York: Academic Press, (1967).

67. Shimada, S. K. *Oxidation of TiC at low temperatures*, Journal of Materials Science, 27 (1992), 1869-1875.

68. Shimada, S. O., *Oxidation of HIPed TiC Ceramics in Dry O2, Wet O2, and H2O atmospheres*, J. Am. Ceram. Soc*., 89* [4] (2006), 1218-1225.

69. Shabalin, I. V., *Initial stages of oxidation of near-stoichiometric titanium carbide at low oxygen pressures*, Journal of Alloys and Compounds , 472 (2009), 373-377.

70. Shimada, S. M., T*he oxidation of TiC in dry oxygen, wet oxygen, and water vapor,* Journal of Materials Science*,* 39 (2004), 581-586.

71. Onuma, A., Kiyono, H., Shimada, S., Desmaison, M., *High temperature oxidation of sintered TiC in an H_2O-containing atmosphere*, Solid State Ionics, 172 (2004), 417-419.

72. Price, J. B., Borland, J. O., & Selbrede, S. *Properties of chemical-vapor-deposited titanium nitride*, Thin Solid Films, 236 (1993), 311-318.

73. Amar, M., Ahmed, W., & Taylor, H., *Titanium based nitride and carbide coatings for diamond deposition.* St Paul, MN, USA: Surface Engineering, Proceedings, (2006).

74. Munz, W-D., *Titanium aluminide films: A new alternative to TiN coatings*, J. Vac. Sci. Technol., A 4 [6] (1986), 2717-2725.

75. Helmersson, U., Johansson, B., & Sundgren, J., *Adhesion of titanium nitride coatings on high-speed steels,* Journal of vacuum science & technology, 3 (1985).

76. Russias, J., Cardinal, S., Esnouf, C., Fantozzi, G., & Bienvenu, K., *Hot pressed titanium nitride obtained from SHS starting powders: Influence of a pre-sintering heat-treatment of the starting powders on the densification process*, J. of the European Ceramic Society, 27 (2007), 327-335.

77. Carole, D., Frety, N., Etinenne-Calas, S., Merlet, C., & Marin-Ayral, R., *Microstructural and mechnical characterization of titanium nitride produced by S.H.S.*, Materials Science & Engineering, 419 (2006), 365-371.

78. Eslamloo-Grami, M., & Munir, Z. A., *Effect of porosity on the combustion synthesis of titanium nitride*, Journal of American Ceramic Society, 73 (1990), 1235-1239.

79. Kuo, D-H, Huang, K-W., *Kinetics and microstructure of TiN coatings by CVD*, Surface and Coatings Technology, 135 (2001), 150-157.

80. Sundgren, J., *Structure and properties of TiN coatings,* Thin Solid Films, 128 (1985), 21-44.

81. Pollard, F. W. *The stability and chemical reactivity of titanium nitride and titanium carbide*. Transactions of the Faraday Society*, 46* [3] (1950), 190-199.

82. Gogotsi, Y. P., *Oxidation behavior of monolithic TiN and TiN dispersed in ceramic matrices,* Oxidation of Metals*, 39* [1-2] (1993), 69-91.

83. Desmaison, J. L., *Oxidation Mechanism of Titanium Nitride in Oxygen,* Oxidation of Metals*,* 13 [6] (1979), 505-517.

84. Keijzer, M. H., *TiCN and metallic coatings for corrosion protection of separator plates in MCFCs,* Journal of Applied Electrochemistry*,* 30 (2000), 1421-1431.

85. Kaidash, O. M., *Corrosion resistance of cermets based on titanium nitride*, Powder Metallurgy and Metal Ceramics, 30 [1] (1991), 69-73.

86. German, R.M., *Liquid Phase Sintering*, Plenum Publishing, New York, (1985).